15

Soil Colloidal Behavior

Sabine Goldberg
United States Department of Agriculture

Inmaculada Lebron
Centre for Ecology & Hydrology

John C. Seaman
University of Georgia

Donald L. Suarez
United States Department of Agriculture

15.1 Nature of Soil Colloids

15.1.1 Significance of Colloidal Phenomena

The importance of colloids in soil science has been appreciated for many years. However, recent understanding that organic and inorganic contaminants are often transported via colloidal particles has increased interest in colloid science. Essentially, all chemicals and individual species are to some extent reactive with soils, including species such as chloride ions, which undergo repulsion from negatively charged surfaces. With few exceptions, soil chemistry is primarily the chemistry of colloids and surfaces. The primary importance of colloids in soil science stems from their surface reactivity and charge characteristics. The overwhelming majority of surface area and electrostatic charge in a soil resides in the less than 1 μm size fraction with particles with radii between 20 and 1000 nm constituting the major part of the soil surface area (Borkovec et al., 1993). A significant fraction of reactive soil colloidal material falls within the <100 nm size range and thus is relevant to the growing interest in the properties and behavior of nanoparticles. Furthermore, soil is often the ultimate repository for anthropogenic nanomaterials of environmental concern (Hochella, 2008; Theng and Yuan, 2008; Waychunas and Zhang, 2008). The unique aspects of "nanoscience" as a discipline separate from colloid science reflect deviations in material properties in the nanoparticle size range, especially for materials <10 nm, and in many cases the lack of a natural bulk analog in the larger size fractions, for example, ferrihydrite (Hochella, 2008; Waychunas and Zhang, 2008).

Characterizations of size, shape, surface area, surface charge density, and changes in surface charge are required for understanding the processes of adsorption, flocculation, dispersion, and transport in soils and the resultant changes in soil hydraulic properties, as well as chemical migration. Since the major part of the surface area is in the colloidal fraction of the soil, almost all surface-controlled processes including adsorption reactions, nucleation, precipitation, and dissolution involve colloids. Colloids are reactive not only because of their total surface area but also because of enhanced reactivity related to rough surfaces and highly energetic sites, as well as the effects of electrostatic charge. Colloid charge is associated with substitution of lower charge cations for those of higher charge in the mineral lattice (which results in a net permanent charge) as well as surface charge associated with broken bonds. The charge associated with broken bonds is characterized as variable charge in as much as the solution influences the surface speciation (Chapter 16). In addition to these chemical processes, colloids are mobile in soils and thus not only affect the chemical transport of otherwise immobile chemicals but also exert a strong influence on soil hydraulic properties.

15.1.2 Types of Soil Colloids

Colloidal particles are defined as having an equivalent spherical radius smaller than 1 μm (van Olphen, 1977). A homogeneous dispersion of colloidal particles in a liquid is called a colloidal dispersion. If the particles are large and settle rapidly, the dispersion is called a suspension. A colloidal dispersion is defined as a system where particles of colloidal dimensions are dispersed in a continuous phase of a different composition (van Olphen, 1977).

15.1.2.1 Oxides

Oxides, including hydroxides and oxyhydroxides, are ubiquitous constituents of soils, occurring as both discrete particles and as coatings on other soil surfaces. Oxide minerals that are commonly found in the soil clay fraction are discussed in Chapter 22.

Hydroxylation of oxide minerals can either be structural and/or occur by chemisorption of water in an aqueous medium (Schwertmann and Taylor, 1977). Edge hydroxyl groups on oxides and clay minerals represent the most abundant and reactive surface functional groups in soils (Sposito, 1984). Any one type of oxide mineral contains various groups of surface hydroxyls that are distinguishable by crystal plane location and/or extent of coordination to the cations of the bulk structure. However, as a simplification, it is often assumed that each oxide mineral has a single set of homogeneous reactive functional groups. Surface hydroxyl groups on most oxide minerals are amphoteric, exhibiting positive charge at low pH and negative charge at high pH. For this reason, oxide minerals are often referred to as variable charge soil minerals. Table 15.1 provides densities of surface hydroxyl groups for some common oxide minerals in soils.

Boehmite and gibbsite are the only crystalline Al oxides common in soils. Aluminum oxides are the products of intense weathering of aluminosilicate minerals and are most abundant in tropical soils. Gibbsite can also be found in volcanic ash soils of humid regions (Brown et al., 1978). Noncrystalline Al oxides, which have similar structure and chemical characteristics but smaller particle size than crystalline varieties, often dominate the chemical reactions with anions in soils (Hsu, 1977). Aluminum oxides play an important role in ion adsorption, stabilization of soil aggregates, and flocculation of soil particles.

Iron oxides are found in most soils and provide soil horizons with their red, yellow, and brown colors (Brown et al., 1978). Most iron oxides are the weathering products of iron-containing silicates. Goethite, which is the most common Fe oxide in temperate, subtropical, and tropical soils, is usually thermodynamically the most stable (Schwertmann and Taylor, 1977). Soil goethites are usually fine grained and contain appreciable substituted Al. Lepidocrocite is a minor constituent of waterlogged temperate soils undergoing alternating oxidizing and reducing conditions, whereas hematite is a common soil mineral that can be inherited from parent materials or formed pedogenically in warm climatic regions (Brown et al., 1978). The two magnetic Fe minerals, magnetite and maghemite, occur in soils; the former is inherited from parent rock, while the latter is formed pedogenically in highly weathered soils (Brown et al., 1978). Ferrihydrites are poorly crystalline, have indefinite composition, and occur as very small particles with high surface area (Schwertmann and Taylor, 1977). Ilmenite is an uncommon mineral usually inherited from igneous or metamorphic parent rocks (Brown et al., 1978). Iron oxides play an important role in ion adsorption and in aggregation and cementation of soil particles.

TABLE 15.1 Densities of Surface Hydroxyl Groups on Oxide Minerals

Solid	Site Density Range (Sites nm^{-2})
Gibbsite	2–12
Goethite	2.6–16.8
Hematite	5–22
Ferrihydrite	1.1–10.1
MnO_2	6.2
TiO_2	2–12
Amorphous SiO_2	4.5–12

Source: Adapted from Davis, J.A., and D.B. Kent. 1990. Surface complexation modeling in aqueous geochemistry. Rev. Mineral. Geochem. 23:177–260.

Manganese oxides occur widely in soils as minor constituents, mainly as dark coatings on particle surfaces. Manganese oxides are chemically complex, existing as a continuous range of compositions between MnO and MnO_2 (Brown et al., 1978). Birnessite, vernadite, lithiophorite, and hollandite are the most common crystalline manganese minerals in soils (McKenzie, 1989). Birnessite occurs in both acid and alkaline soils, while lithiophorite occurs mainly in neutral to acid soils (Brown et al., 1978). These oxides supply Mn for plant nutrition. Manganese oxides exhibit a strong adsorption capacity for metal cations, especially copper, due to their pH-dependent charge, small particle size, and large surface area (McKenzie, 1989).

Rutile and anatase are the common titanium oxides occurring in soils. Rutile is a high-temperature form occurring in igneous and metamorphic rocks (Hutton, 1977). Anatase is a low-temperature form occurring as an alteration product of titanium containing minerals such as ilmenite and is much less abundant than rutile (Brown et al., 1978). Titanium oxides are present in both the coarse and fine fractions of soils and are very insoluble (Hutton, 1977).

Quartz is not only the most abundant silicon oxide but also the most abundant mineral in most soils. Most quartz is found predominantly in the sand, silt, and coarse clay fractions of soils (Wilding et al., 1977). Silicon oxides are generally considered inert having a small surface area and little surface charge.

15.1.2.2 Clay Minerals

The clay fraction of most soils is dominated by various layer silicate clay minerals. Layer silicate clay minerals are classified as 1:1 where each layer consists of one tetrahedral silica sheet and one octahedral alumina sheet, 2:1 where each layer consists of one octahedral sheet sandwiched between two tetrahedral sheets, or 2:1:1 where a metal hydroxide sheet is sandwiched between the 2:1 layers. Layer silicate minerals common in soils are discussed in Chapter 21. A discussion of silicate structures is provided by Schulze (2002).

Layer silicate clay minerals are characterized by isomorphic substitution of lower valence cations in either or both the tetrahedral and the octahedral sheets. This excess of negative charge is balanced by other cations, either inside the crystal or on the external surfaces (McBride, 1994). Layer charge is an electrostatic charge balanced outside of the structural unit and determines the strength and type of bonding occurring between the basal planes. Charge arising from isomorphic substitution is

TABLE 15.2 Charge Characteristics and Cation Exchange Capacities of Clay Minerals

Solid	Charge per Unit Half Cell		Cation Exchange Capacity ($cmol_c\ kg^{-1}$)
	Tetrahedral	Octahedral	
Kaolinite	0	0	1–10
Smectite			80–120
Montmorillonite	0	−0.33	
Beidellite	−0.5	0	
Vermiculite	−0.85	+0.23	120–150
Mica			20–40
Muscovite	−0.89	−0.05	
Chlorite			10–40

Sources: Bohn, H.L., B.L. McNeal, and G.A. O'Connor. 1985. Soil chemistry. John Wiley & Sons, New York; McBride, M.B. 1994. Environmental chemistry of soils. Oxford University Press, New York.

called permanent charge because it is independent of solution pH. Layer silicate clay minerals also possess variable charge located at the broken edges of the particles. At the edges of the octahedral sheet, hydroxyl ions attached to Al cations are called aluminol groups. Similar to the hydroxyl groups on oxide minerals, aluminol groups are amphoteric. At the edges of the tetrahedral sheet, hydroxyl groups attached to Si cations are called silanol groups. Silanol groups do not undergo protonation, but dissociate and become negatively charged at high pH. Adsorbed cations on clay minerals balance both pH dependent and permanent charges. Table 15.2 provides charge characteristics and cation exchange capacities (CEC) for some common clay minerals in soils.

Kaolinite is one of the most widespread clay minerals in soils, being most abundant in soils of warm moist climates (Dixon, 1977); while halloysite is formed through acid weathering and in soils of volcanic origin. The halloysite structure is the same as the kaolinite structure but contains a sheet of water molecules between the layers. Both minerals have low colloidal activity, low surface area, and low CEC and anion exchange capacity (AEC) (Dixon, 1977). The CEC and AEC of the 1:1 minerals are predominantly pH dependent (McBride, 1994).

Micas are abundant in soils, occurring as primary minerals inherited from soil parent materials. Micas strongly retain interlayer potassium ions, rendering them nonexchangeable and reducing the CEC of these minerals. Through weathering, micas release K and provide an important natural source of this plant nutrient (Fanning and Keramidas, 1977). Illite is a secondary mineral that is less crystalline, contains less K, and contains more water than muscovite mica (McBride, 1994). Micas and illites are nonswelling minerals.

Smectites constitute an important group of 2:1 clay minerals. Members that are important in soils include montmorillonite, beidellite, and nontronite. Smectites are most significant in moderately weathered soils and have high colloidal activity and high surface area. Smectites are responsible for a large part of the CEC and the majority of the shrink/swell properties of smectitic soils (Borchardt, 1977).

Vermiculite is an important clay mineral in soils that is formed as an alteration product of muscovite and biotite micas (Douglas, 1977). Vermiculite is widely distributed and has a wide particle size range. Vermiculites contain hydrated magnesium cations that can be readily exchanged by K and ammonium ions, resulting in collapse of the clay layers and fixation of these nutrient ions. Vermiculites have high CEC and high surface area but exhibit limited swelling.

Chlorites are 2:1:1 layer silicates that occur extensively in soils. The hydroxide interlayer sheet is usually dominated either by brucite [$Mg(OH)_2$] or by gibbsite [$Al(OH)_3$]. This interlayer sheet restricts swelling, decreases effective surface area, and decreases effective CEC (McBride, 1994). Chlorites are nonswelling silicates.

15.1.2.3 Organic Matter

Soil organic matter (SOM) refers to the mixture of products resulting from microbial and chemical transformations of organic residues and is discussed in Chapter 11. An important component of SOM is called humus, a complex and microbially resistant mixture of amorphous and colloidal substances. These substances are the result of modifications of original tissues or synthesis by soil microorganisms. Humic substances are subdivided into humic acid, fulvic acid, and humin using a separation scheme based on solubility in strong acid and base (McBride, 1994). The structure and composition of humus are complex and incompletely known. The structure contains a variety of reactive functional groups including carboxyl R–COOH, phenol C_6H_5OH, alcohol $R–CH_2OH$, enol R–CH=CH–OH, ketone R–CO–R′, quinone $O=C_6H_4=O$, ether $R–CH_2–O–CH_2–R'$, and amino $R–NH_2$ (Stevenson, 1982). Humus is amorphous and highly colloidal; its surface area, ion adsorption, and CEC are greater than those of layer silicate clay minerals (McBride, 1994). The presence of humus usually promotes aggregation of soil particles.

15.1.3 Properties of Soil Colloids

15.1.3.1 Particle Size and Shape

Colloids in natural systems are characterized by a continuous particle size distribution (PSD; polydispersivity) of extreme complexity and diversity. Organisms, organic macromolecules, minerals, clays, oxides, and combinations of any of them constitute the colloidal fraction in soils. The distribution of shapes, densities, surface chemical properties, and chemical composition vary widely with size. Some fractions of the size spectrum may be living, and all particulates are subject to diverse physical, chemical, and biological processes that can alter size distribution, shape, or chemical composition (Kavanaugh and Leckie, 1980).

Colloids are dynamic particles, subject to constant alteration; the distribution of particle sizes in natural systems is the result of a number of processes, which either bring the particles together (coagulation) or disrupt existing aggregates (dispersion) (Filella and Buffle, 1993; Buffle and Leppard, 1995a, 1995b). Particle size is an important parameter in the characterization

of colloids. Sequential gravimetric sedimentation has been the classical method for measuring PSDs in soils. However, this technique has proven to be unreliable for particle sizes in the colloidal range (1–1000 nm). The reason for the lack of reliability is the combination of Brownian motion and convection currents, which each exert a significant influence on settling at diameters below ~1 μm in water.

Awareness of the environmental importance of colloids, for example, remediation schemes using engineered nanoparticles, and studies on the ecotoxicology of the products created by the emerging nanotechnology industry have accelerated the development of analytical techniques for nanoscale research (Wilkinson and Lead, 2007). These analytical techniques provide quantification, analyses, and characterization of the size, shape, and distribution of colloids in polydisperse systems within the environment (Handy et al., 2008). Some of the techniques more commonly used in soil science for colloid characterization and determination of PSD are reviewed in the following section. These include centrifugation, particle size analysis using the Coulter principle, field flow fractionation (FFF), atomic force microscopy (AFM), electron microscopy (EM), and acoustic spectroscopy. A recent publication by the International Union of Pure and Applied Chemistry (IUPAC) Wilkinson and Lead (2007) provides more detailed information on the various techniques.

It is important to consider that each particle size measurement technique has different accuracy and precision. In other words, detection limits and detection windows, corresponding to different size ranges, are technique dependent (Table 15.3). Not all techniques are able to accurately measure the full scale of size ranges for colloids in polydisperse samples. Furthermore, most of the colloidal-sizing techniques do not measure size directly, but rather determine a physicochemical property from which the size is calculated (Lead and Wilkinson, 2007). For example, scanning and transmission electron microscopic techniques determine the physical dimensions of the projected area of the particles (Lebron et al., 1999), light scattering and flow-FFF generally determine the diffusion coefficients (Lead et al., 2000; Hassellov et al., 2007), and sedimentation-FFF (Sd-FFF) and other centrifugation-based techniques measure the buoyant mass (Hassellov et al., 2007). Although particle size can be estimated from projected areas, diffusion coefficients, and buoyant mass, the calculations are based on a number of assumptions, which if not met, will reduce the quality of the results (i.e., sphericity, homogeneous charge distribution, absence of coulombic interactions among particles). Therefore, it is not uncommon to obtain different PSDs for the same sample when using different techniques (Lead and Wilkinson, 2007). Even more direct techniques like scanning electron microscopy (SEM) and environmental scanning electron microscopy (ESEM) have their limitations. Doucet et al. (2004) observed differing colloidal morphologies in preparations obtained from the same sample with SEM and AFM. They attributed these differences to the sample preparation required for each technique. The difficulty in obtaining similar PSDs using different techniques indicates the limitation of the individual techniques. Therefore, it is good practice to use the results of several characterization techniques simultaneously (Lead and Wilkinson, 2007; Hassellov et al., 2008).

TABLE 15.3 Operational Range of Colloid Particle Size Characterization for a Variety of Analytical Techniques and the Inferred Colloidal Dimension Quantified by Each Technique

Analytical Technique	Quantified Parameter	Approximate Analysis Size Range (nm)
Filtration	Equivalent pore size diameter	100–>1000
Ultrafiltration	Equivalent molar mass	1–100
Centrifugation	Equivalent spherical volume diameter	10–>1000
Dialysis	Equivalent molar mass	0.5–100
ESEM	Projected area	40–>1000
SEM	Projected area	10–>1000
TEM	Projected area	1–>1000
AFM	Three dimensions	0.5–>1000
Fl-FFF	Hydrodynamic diameter	1–1000
Sd-FFF	Equivalent spherical volume diameter	50–1000
DLS	Hydrodynamic diameter	3–>1000
Acoustic spectroscopy	Equivalent particle diameter	5–>1000

Source: Adapted from Hassellov, M., J.W. Readman, J.F. Ranville, and K. Tiede. 2008. Nanoparticle analysis and characterization methodologies in environmental risk assessment of engineered nanoparticles. Ecotoxicology 17:344–361.

15.1.3.1.1 Measurement Methodology

Minimization of sample handling and processing is recommended when analyzing colloidal systems. Currently, no in situ technique allows direct measurement of the PSD for soils. Furthermore, measurement of colloid particles cannot be compared to standard samples to evaluate the quality of measurements made because there are no accepted standards or reference materials for natural colloids (Lead and Wilkinson, 2007).

15.1.3.1.2 Electron Microscopy

EM is one of the few techniques capable of measuring the size of particles across the entire colloidal range (Table 15.3). Both transmission electron microscopy (TEM) and SEM require deposition of aqueous suspensions, sample evacuation, and in the case of SEM, sample coating with a conducting material, typically graphite or gold, to reduce charging from the beam. Hence sample preparation can, and most likely will, alter the original particle morphology and size distribution (Buffle and Leppard, 1995a, 1995b; Chanudet and Filella, 2006). However, new sample preparation techniques are constantly being developed to counteract artifacts generated by dehydration. For example, freeze-drying techniques or the use of hydrophilic resins and multimethod TEM sample generation techniques can be used to stabilize the three-dimensional structure of colloids (Mavrocordatos et al., 2007).

ESEM can, in theory, be used to quantify colloids under ambient conditions, as can AFM that is generally used only to determine the dimensions and characteristics of individual colloids. While minimal sample manipulation is an advantage, the disadvantage is a reduction in the resolution of the techniques; both ESEM and AFM produce much better resolution at lower relative humidity. Another serious problem in AFM imaging of liquids is the alteration of the AFM-derived signal due to the uptake of nanoparticles onto the AFM cantilever (Lead et al., 2005). Applications and new sample preparation techniques for environmental colloids using AFM are discussed by Balnois et al. (2007). Force-volume mode AFM has been used to evaluate the heterogeneous distribution of charge on clay surfaces (Taboada-Serrano et al., 2005).

Microscopy, despite being a very powerful technique, is not widely used for routine particle size analysis. The reasons for its limited use are the high cost of the equipment and the small sample volumes that can be scanned at any given magnification. Image analysis software facilitates the quantification of the different particle metrics in the micrographs. However, obtaining sufficient particles to allow representative and robust statistics requires the scanning of many micrographs of the specimen. Nevertheless, the determination of morphology and particle shape factor still remains the strength of microscopic techniques. Automated instrumental analysis routines that take advantage of enhanced beam stability combined with image analysis software, and greater computing capacity have the potential to address such limitations (Seaman, 2000; Laskin and Cowin, 2001). Additionally, SEM, ESEM, and TEM coupled with energy dispersive x-ray (EDX) spectroscopy can provide valuable chemical information about individual particles. It must be recognized that the resulting x-ray signal in SEM may be generated from a sample region larger than the particle of interest (Goldstein et al., 1992; Seaman, 2000). Furthermore, TEM can also, by measuring the x-ray spectra emitted by the specimen, resolve crystal spacing. Selective area electron diffraction can be used to identify colloidal minerals and to determine their degree of colloid crystallinity.

15.1.3.1.3 Centrifugation

A particle falling through an infinite fluid will eventually travel at a terminal constant velocity determined by the size of the particle and the resistance offered by the fluid. The terminal velocity in a centrifugal field is not constant, but rather a function of distance from the axis of rotation. Measurement of this radius is necessary in order to calculate the particle size. The relationship between the movement of the particle and the movement of fluid around that particle may be reduced to the Stokes equation. For fluid moving past a particle of diameter (d_p), the ratio of the inertial transfer is described by the dimensionless parameter, the Reynolds number (R_E):

$$R_E = \frac{\rho_0 u d_p}{\eta} \tag{15.1}$$

where u is the velocity. If $R_E \leq 0.2$, the fluid conditions are described as streamlined or laminar, and the drag on the particle is due mainly to viscous force within the fluid. Particles with high densities or large particle diameters may be moving with velocities that exceed $R_E = 0.2$, and in this situation, they are likely to enter the region of turbulent flow, where velocities are more difficult to calculate. In a centrifugal field, Stokes' equation has the form:

$$u = \frac{(\rho - \rho_0)\omega^2 d_p^2}{18\eta} = \frac{\ln(r/s_0)}{t} \tag{15.2}$$

where

ω is the rotational velocity (rad s^{-1})

t is the time (s) required for a particle of diameter d_p to move from its starting point radius (s_0) to the analytical radius (r)

Application of the Stokes equation requires certain assumptions that are not always achieved. All of these assumptions are critical to the measurement of the size of the sedimenting particles. The first assumption is that the particles are spherical, smooth, and rigid. Since this assumption is almost never valid, the diameter calculated is an equivalent or Stokes diameter (d_{St}). It is assumed that the particle terminal velocity is reached instantly, although calculations show that a finite but small time is actually required before this condition is reached. The particle is assumed to be moving without interference or interaction from other particles in the system. This assumption is only true at high dilutions (<1%) that ensure considerable separation between particles. Also, it is assumed that inertial effects are not present and that the fluid exhibits only Newtonian flow properties. Since water is generally the dilution medium in soils and colloidal particles are <1 μm, these assumptions are usually valid. A more detailed analysis of the methodology as well as a description of different centrifugation methods is provided by Bunville (1984), Groves (1984), Koehler et al. (1987), Holsworth et al. (1987), and Coll and Oppenheimer (1987).

15.1.3.1.4 Coulter Effect

The increase in the resistance across a small aperture produced by a nonconducting particle in a conducting medium is called the Coulter effect. The magnitude of this increase in resistance (ΔR) for a spherical particle of diameter (d_p) suspended in an aperture of diameter (D_a) is

$$\Delta R = \frac{8P_f d_p}{3\pi D_a^4}\left[1 + \frac{4}{5}\left(\frac{d_p}{D_a}\right)^2 + \frac{24}{35}\left(\frac{d_p}{D_a}\right) + \cdots\right] \tag{15.3}$$

where P_f is the resistivity of the conducting medium. This resistance pulse (ΔR) results in a voltage pulse ($i\Delta R$) for a sphere

of diameter d_p, where i is the current across the aperture. The resulting voltage pulses are counted and scaled using a multichannel analyzer.

Instruments utilizing the resistive pulse technique require calibration using standard particles with known diameter to assign a particle size to each of the thresholds. This procedure takes into account the dimensions and electrical characteristics of the aperture and the conducting medium.

The advantage of the resistive pulse technique is that no other properties of the particle, such as refractive index or specific gravity, are required for the interpretation of the data in terms of a PSD. Developments in instrumentation for particle size analysis using the resistive pulse technique allow the analysis of particle sizes <1 μm but the range is limited (typically 0.4–<1 μm) (Bunville, 1984).

15.1.3.1.5 Dynamic Light Scattering or Photon Correlation Spectroscopy

Dynamic light scattering (DLS), also called photon correlation spectroscopy, or quasielastic light-scattering measures the fluctuation in scattered intensity of a laser beam over small-time intervals when it passes through a small volume of particles under Brownian motion. These fluctuations are dependent on the diffusion coefficient of the particles.

When the particles have a regular shape other than spherical, the depolarized component can be used to study the particle rotational diffusion coefficient. The rotational and translational diffusion coefficients obtained in conjunction with theoretical, hydrodynamic relationships contain information about the particle dimensions. For a nonspherical particle larger than the incident wavelength, light is scattered from different parts of the same particle producing interferences, which are dependent on the angle of the scattered intensity and characteristic of a particular particle shape (Pecora, 1983).

Limitations of DLS are due to the assumptions made in calculating the particle radius from the diffusion coefficients. These assumptions include sphericity, nonpenetrable spheres, and noncolumbic forces existing among the particles. A more major limitation, when applied to colloidal systems, is the strong particle size dependence of the scattered light intensity. Larger particles have a much larger influence than smaller particles, biasing size quantification toward larger particle sizes. Consequently, previous sample fractionation is advised, since small fractions of dust or other micrometer-sized particles will overshadow the signal of the particles in the colloidal range (Hassellov et al., 2008). Despite limitations, DLS is quick and easy to use, is available in most laboratories, and is very useful for monitoring changes in colloid aggregation. It has been applied successfully to measure particle sizes of colloids in natural systems (Rees, 1990; Ryan and Gschwend; 1990; Lebron et al., 1993; Ledin et al., 1993, 1994; Finsy, 1994; Perret et al., 1994; Newman et al., 1994; Filella et al., 1997).

15.1.3.1.6 Field-Flow Fractionation

FFF is a group of separation techniques capable of fractionating and characterizing the PSD of colloids in the range 0.01–1 μm. Like chromatography, FFF is an elution methodology in which constituents are differentially retained, and thus separated in a flow channel (Beckett et al., 1997). With this technique, a colloidal sample is introduced into a stream of liquid and subjected to a field (such as gravitational, centrifugal, third cross-flow, thermal gradient, electrical, or magnetic) acting perpendicular to the stream direction (Beckett and Hart, 1993). According to theory, the rate at which particles are displaced downstream, measured as emergence times, can be related exactly to particle properties such as mass, size, and density. However, since different kinds of particles move at different velocities in this system, broad particle populations are sorted into graded size (or mass) distributions along the length of the flow channel. Observation of the shape of the emerging distribution, combined with theory, yields PSD curves called fractograms.

If applied as indicated above, FFF provides highly detailed size distribution curves and is a very flexible technique that can be adapted to different particle types in almost any suspending medium. The more commonly used FFFs in environmental applications are Sd-FFF and flow-FFF (Fl-FFF). Sd-FFF uses a centrifugal field to aid the separation of the colloids, while Fl-FFF uses a cross flow. For detailed information about FFF, Giddings (1993) provides a detailed explanation of this family of techniques and Hassellov et al. (2007) highlight the latest accomplishments of FFF for aquatic colloids and macromolecules.

Detection limits for colloid chemical analyses have been limited using traditional analytical techniques because the amount of colloids collected for analysis is generally limited. Presently, with the availability of low detection limit chemical analysis instrumentation such as graphite furnace atomic absorption spectrometer (GFAAS) and inductively coupled plasma-mass spectrometry (ICP-MS), concurrent particle size determination and chemical analyses can be conducted. Instruments can be assembled either off-line (disconnected) or online (connected) to achieve a more complete description of the colloid nature. Blo et al. (1995) used GFAAS as an off-line detector for Sd-FFF, while Contado et al. (1997) coupled online GFAAS to Sd-FFF to characterize suspended particulate matter from rivers. When analyzing colloidal fractions, techniques like inductively coupled optical emission spectrometry (ICP-OES) or ICP-MS that allow the simultaneous collection of multiple element signals are preferable. Sd-FFF was coupled with ICP-MS for the first time by Beckett (1991). Since then, many scientists have produced detailed chemical information about colloidal size fractions and associated elements (Murphy et al., 1993; Ranville et al., 1999). As per Table 15.3, Sd-FFF is only capable of separating particles down to ~50 nm. Since many colloids of interest are smaller, Chittleborough et al. (2004) developed the Fl-FFF-ICP-MS technique that can operate across the entire colloidal size range.

15.1.3.1.7 Acoustic Spectroscopy

Acoustic spectroscopy methods measure the propagation velocity and attenuation of sound waves (i.e., 1–100 MHz) passing through a colloidal suspension, providing information about the PSD, rheology, and electrokinetic behavior of the suspension.

Dukhin and Goetz (2002) provide a thorough discussion of acoustic methods and the six mechanisms of acoustic attenuation associated with a colloidal suspension: viscous, thermal, scattering, intrinsic, electrokinetic, and structural signal dissipation. The application of acoustic spectroscopy to colloid characterization assumes that each attenuation process functions independently and that the overall attenuation is the summation of the independent processes.

Viscous and thermal dissipation are the most important because colloids mainly interact with sound waves hydrodynamically through the generation of oscillating shear waves and thermodynamically through temperature losses. The resulting acoustic spectra are generally insensitive to the electrical conductivity of the solution and the charge of suspended particles and provide no information concerning particle morphology (Dukhin and Goetz, 2002; Seaman et al., 2003).

Acoustic attenuation attributed to the suspension is generally determined by measuring the relative change in signal at each frequency with precise changes in gap distance or sample path length in spectroscopic terms. Thermal losses dominate in emulsions and low-density dispersions, so that viscous losses may be neglected. For rigid submicron particles (i.e., soil clays, oxides), viscous attenuation dominates and limited information regarding composition of the particles (density), the media (solution density and shear viscosity), and the relative volume fraction of the two phases is required for estimating particle size, providing a minimum detectable particle size of approximately 10 nm. For complex environmental samples, however, such information may be lacking. Acoustic scattering becomes more important with increasing particle size, and sound speed must also be considered. When characterizing "soft" particles having a limited density contrast compared to the suspending solution, such as latex particles and polymers, additional information concerning their thermal expansion properties is required for interpretation of the attenuation spectra (Dukhin and Goetz, 1996, 1998, 2002).

Acoustic methods offer several advantages compared to other instrumental techniques for evaluating colloid size and surface charge properties. Ultrasound can propagate through suspensions to a much greater degree than light. Therefore, acoustic analysis can be conducted at relatively high solid to solution ratios (up to 30% solids by volume) that are more analogous to soil conditions in the field. However, the analysis may require more colloidal material than may be readily available. Analysis may be indicative of particle interaction within the intact suspension, lessening the impact of trace artifacts, that is, dust, bubbles, suspension heterogeneity due to particle segregation, and filtration artifacts that can bias sizing methods such as SEM and DLS. The applicable sizing range is much larger than light-scattering methods, that is, ≈5 nm–1000 μm. It is also less biased with respect to larger particles, making it more suitable for complex polydisperse systems. Acoustic methods are insensitive to sample convection, allowing stirring or agitation of the sample during analysis as required for reactive titration (e.g., Sun et al., 2006) or for the characterization of low charge, inherently unstable suspensions, such as materials close to their zero point of charge (ZPC) and/or critical coagulation concentration (CCC) (Babick et al., 2000; Dukhin and Goetz, 2002; Kosmulski et al., 2002; Guerin and Seaman, 2004; Guerin et al., 2004; Delgado et al., 2005). Furthermore, the relatively large sample volume allows for the collection of subsamples throughout acoustic analysis for characterization by other analytical methods (Seaman et al., 2003).

Acoustic spectrometers for use in characterizing colloidal suspensions became commercially available in the 1990s. Despite several advantages when compared to light-scattering techniques, the application of acoustic-based methods to the study of soil colloids has generally been restricted to the characterization of mineral standards or synthesized mineral analogs, such as goethite and hematite (Gunnarsson et al., 2001; Kosmulski, 2002; Kosmulski et al., 2002, 2003; Appel et al., 2003; Guerin and Seaman, 2004; Guerin et al., 2004; Delgado et al., 2005). However, acoustic methods of suspension characterization rely on the interpretation of macroscopic sample properties, that is, the acoustic attenuation spectrum of a suspension, using idealized model algorithms with various simplifying assumptions and a few known system parameters, such as suspension concentration and particle density. The limited information can often result in systems that are "ill defined" and can be described by multiple answers, that is, PSDs (Dukhin and Goetz, 2001; Babick and Ripperger, 2002), a problem that also plagues light-scattering techniques (Schurtenberger and Newman, 1993). As such, acoustic methods are most suitable for evaluating relative changes in colloid aggregation and surface charge for suspensions in response to known changes in solution chemistry rather than for comparing subtle differences between poorly defined environmental samples.

15.1.3.1.8 Applications of Particle Size Methods

PSD is a fundamental soil property, affecting soil surface area, bulk density, porosity, water retention, and hydraulic behavior. Furthermore, precise information about colloidal size and shape is important because submicron-size colloids often act as vehicles that control the transport and fate of adsorbed pollutants (hydrophobic organic compounds, toxic trace metals, and radionuclides [de Jonge et al., 2004a]). Bacteria and viruses are part of the colloidal pool in natural environments; their characterization and transport are significant for understanding biogeochemical processes (Rockhold et al., 2004), epidemic evolution (Bertuzzo et al., 2008), and the spread of diseases in general (Khilar and Fogler, 1984; McDowell-Boyer et al., 1986; Kia et al., 1987; Ryan and Elimelech, 1996; Kretzschmar et al., 1999; de Jonge et al., 2004a; McCarthy and McKay, 2004; Tufenkji, 2007). Submicron-size colloids have been insufficiently studied in the past because methods for their isolation, detection, and characterization have been inadequate, with the exception of a few examples (Kaplan et al., 1993; Kretzschmar et al., 1993; Chanudet and Filella, 2006). However, with the new fractionation methods and the coupling with low detection limit analytical instruments (FFF-ICP-MS), a new era in the characterization of soil colloids

is commencing (Chittleborough et al., 2004; Ranville et al., 2005; Lead and Wilkinson, 2007).

Despite the new advances in the characterization and analysis of colloids, many unanswered questions exist in regard to in situ colloidal behavior in natural environments, in particular, the chemical nature of colloids present and their structure, size, and shape distributions (Filella et al., 1997; Lead and Wilkinson, 2007). New methods of in situ visualization of colloids in porous media are the research focus of several recent publications; light transmission and epifluorescent microscopy are some of the new techniques developed by Crist et al. (2004) and Baumann and Werth (2004) for the observation and modeling of colloidal transport in porous media.

15.1.3.2 Surface Area

Surface area must be regarded as a relative term, in as much as it is scale dependent, as well as often dependent on the chemical and physical conditions of a system. Determinations of surface area range from particle size calculations assuming smooth surfaces and simplified geometry, generally termed geometric surface area, to possible molecular level calculations based on the distances between surface ions in a mineral structure. Because the measurement is scale and system dependent, there is no universally accepted way to measure surface area. Determination as to which measurement system to utilize should consider the scale and chemical conditions required by the application. Kinetic reactions that are diffusion controlled should likely consider geometric surface area, while surface-controlled reactions (such as some adsorption and some dissolution/precipitation reactions) should consider surface area at the scale of the reacting molecule. In most instances, surface area is related to surface reactivity, either adsorption or surface-controlled kinetic processes.

15.1.3.2.1 Measurement Methodology

The results of surface area determinations must be interpreted within the context of the size and orientation of the adsorbate, as well as the attractive forces between the surface and the adsorbate. This distinction is particularly important for clays such as smectites, which can be considered to have internal as well as external surface area. Internal surface area is representative of the surface area of the interlayers. Inert gases such as N_2 are not able to enter the interlayer positions, and thus, measure only external surface area of clay particles. In contrast, polar molecules such as ethylene glycol, ethylene glycol monoethyl ether (EGME), and water are able to cause expansion of the layers and penetrate into interlayer positions. Use of such molecules results in measurement of internal and external surface area. Since water is the solvent in environmental systems, these total surface area measurements are appropriate for adsorption studies. Soil surface area measurements obtained using N_2, water, and EGME were highly correlated with each other and with clay content when considering soils with similar mineralogy but not for soils with differing mineralogy (de Jong, 1999).

To characterize adsorption methods of surface area determination, it is useful to distinguish between chemical and physical adsorption. Physical adsorption is characterized by low heats of adsorption without structural changes at the surface, fully reversible and rapid reactions since no activation energy is required, coverage of the entire surface rather than specific sites, little or no adsorption at elevated temperatures, and potential coverage by more than one layer of adsorbate (Lowell, 1979). Chemisorption is characterized by high heats of adsorption, localization of adsorption at specific surface sites, and irreversible reaction. The term "specific surface area" has been used to denote the surface area of a material expressed on a mass basis ($m^2\ g^{-1}$).

15.1.3.2.2 Gas Adsorption Using the BET Equation

The BET equation is commonly used in conjunction with physical gas adsorption to measure surface area. The BET equation is named after Brunauer, Emmett, and Teller (1938), who extended the Langmuir theory for monolayer gas adsorption to multilayer adsorption. The Langmuir equation (Langmuir, 1918) is given by:

$$\frac{P}{V} = \frac{1}{kV_m} + \frac{P}{V_m} \tag{15.4}$$

where

P is the pressure
V is the volume of gas adsorbed per kilogram of adsorbent at that pressure
k is a constant
V_m is the volume of gas adsorbed per kilogram of adsorbent at monolayer surface coverage

The surface area is obtained by determination of $1/V_m$, which is the slope of the P/V versus P plot. The specific surface area is then equal to $1/V_m$ multiplied by the cross-sectional area of the adsorbate and the number of molecules in volume V_m.

The BET relation assumes that there is a dynamic equilibrium between the molecules in the various layers such that the number of molecules in each layer remains constant, although different sites may or may not be occupied at any given time. Use of the equation enables calculation of the number of molecules in a monolayer despite the fact that complete monolayer coverage may not have occurred. The BET equation is written as (Lowell, 1979):

$$\frac{1}{W[P_0/P]} = \frac{1}{W_m C} + \frac{C-1}{W_m C}\frac{P}{P_0} \tag{15.5}$$

where

P is the adsorbate gas pressure
P_0 is the adsorbate pressure at saturation for the temperature of the experiment
W is the weight adsorbed in the monolayer
W_m is the weight adsorbed in the complete monolayer
C is the BET constant

Multipoint BET plots are created by plotting $1/(W(P_0/P - 1))$ on the y axis and P/P_0 on the x axis. The value of W_m is calculated from the slope and intercept. The specific surface area is determined by dividing the total surface area by the sample weight. The region of P/P_0 between 0.05 and 0.35 is usually linear and within the region of pressures corresponding to sufficient adsorption to complete monolayer coverage, and thus, best suited for determination of W_m (Lowell, 1979).

Often the BET surface area can be determined from a single pressure measurement without much loss of accuracy. For relatively high values of C, the intercept value is small relative to the slope and can be approximated by zero. The BET equation is thus reduced to (Lowell, 1979):

$$W_m = W\left(1 - \frac{P}{P_0}\right) \tag{15.6}$$

Soil and mineral surface areas are most commonly measured by N_2 adsorption, using the BET equation. The calculation is made using the N_2 cross-sectional area of 0.162 nm^2 (Gregg and Sing, 1982). Often this area is referred to as the effective or occupied area. Alternatively for surface area <1 m^2 g^{-1} the use of Kr is recommended.

Most commonly, the BET method consists of adsorption of N_2 at a fixed partial pressure P in a He–N_2 mixture and measurement of the desorbed N_2 in a pure He gas stream using gas chromatography. Alternative methods include measurement of the mass of N_2 adsorbed. In this method, the sample is evacuated to high vacuum, heated, then cooled to liquid N_2 temperature, and weighed. Quantities of N_2 are then added to the system and a series of weighings is made at various pressures. In this instance, the N_2 partial pressures are equal to the total pressure in the system.

Surface area can also be determined from the sorption of water at one or more vapor pressures (Newman, 1983). In this instance, air-dried samples are reacted in evacuated desiccators containing saline solutions with relative vapor pressures on the order of 0.2–0.4. Samples are equilibrated until there is no further weight change, then samples are dried at 105°C and weighed again. Sorbed water is taken as the difference between the oven-dry weight and the desiccator-equilibrated weight. Surface area is then calculated as with N_2, using Equation 15.5. This method gives values comparable to EGME values for nonexpanding clays but underestimates surface area for smectites due to limited water uptake in the interlayers (de Jong, 1999). For smectitic soils, de Jong (1999) recommended using the Langmuir equation (monolayer) for water sorption indicating that the reduced BET equation (Equation 15.6) is not applicable because interlayer water uptake is limited. de Jong (1999) demonstrated a correspondence close to 1:1 between surface area determined with EGME using the BET equation and with water using the Langmuir expression. It can be argued that water sorption values may be more realistic than EGME values (Pennell et al., 1995), since the interlayer spaces of smectites are not accessible to nonpolar molecules until at least two layers of water are present (Quirk and Murray, 1991).

15.1.3.2.3 Organic Molecules

15.1.3.2.3.1 Ethylene Glycol Ethylene glycol was utilized by Dyal and Hendricks (1950) for determination of total surface area of clays. The method consists of adding excess ethylene glycol to soil or clays and allowing the excess to evaporate under vacuum. It is assumed that when the rate of weight loss of the sample decreases, only a monolayer of ethylene glycol remains. Dyal and Hendricks (1950) calibrated the method assuming a bentonite surface area of 810 m^2 g^{-1} and calculated that 0.31 mg of adsorbed ethylene glycol corresponded to each square meter of surface area. The method was modified by Bower and Goertzen (1959) using $CaCl_2$-monoglycolate to maintain an ethylene glycol vapor pressure just below that of the saturation vapor pressure. In this method, the sample and the liquid are placed in separate open vessels in an evacuated system and the sample is weighed until it is in equilibrium with the vapor pressure of the ethylene glycol.

15.1.3.2.3.2 Ethylene Glycol Monoethyl Ether Ethylene glycol monoethyl ether (EGME) has replaced ethylene glycol as the polar solvent of choice for determination of surface area. Since EMGE has a higher vapor pressure than ethylene glycol, it requires a shorter reaction time to equilibrate the sample (Carter et al., 1986). A solvate of EGME and $CaCl_2$ is used in the evacuated chamber to lower the vapor pressure of EGME to just below the saturation pressure. Open vessels of EGME/$CaCl_2$ and soil are placed in the chamber and the soil is periodically weighed until no further weight gain is observed. It is assumed that the EGME surface coverage is 5.2×10^{-19} m^2 per molecule and that 0.286 mg adsorbed corresponds to 1 m^2 of surface area (Carter et al., 1986). The method is limited in that the EGME affinity for cations results in greater than monolayer coverage at those sites, the assumption that EGME covers all surfaces cannot be properly evaluated, and the large size of the molecule may prevent coverage in small surface voids. A serious reservation of the procedure is the assumption that the average EGME occupancy of smectite surface applies equally well to all soil surfaces, regardless of mineralogy (Tiller and Smith, 1990). These authors found that more EGME was retained per unit area by nonexpanding soil clays such as illites and kaolinites than by smectites resulting in an overestimation in surface area of 50%–100% when using smectite as a reference. Measurement of total surface area of soils with mixed mineralogy using EGME and a single conversion factor based on smectite leads to significant under- and overestimation of surface area of many soils, even including smectitic soils (Tiller and Smith, 1990).

15.1.3.2.3.3 Methylene Blue Methylene blue, an organic cation, is reacted at various concentrations with soil suspensions (typically with organic material removed) under pH-buffered conditions. Measurement of methylene blue concentration before and after reaction with soil is made spectrophotometrically at a wavelength of 665 nm. The adsorbed concentration of methylene

blue is used to calculate surface area assuming an area of 1.3 nm^2 per methylene blue molecule (Hang and Brindley, 1970). This surface area corresponds to the molecule attaching parallel to its long axis. This method can only be used in hydrated systems. Aringhieri et al. (1992) found surface areas determined with methylene blue to be unrealistically lower than those obtained with water adsorption and suggested that the major limitation of the method is its dependence on the soil surface charge characteristics. Alternatively, Borkovec et al. (1993) obtained relatively good agreement between methylene blue and N_2 BET surface areas for four soil samples assuming a methylene blue surface area of 0.247 nm^2, corresponding to a molecular attachment of methylene blue perpendicular to its long axis. Orientation of the organic molecules may be related to surface site characteristics, as well as concentration of adsorbing molecules. These differences illustrate one of the disadvantages of using charged molecules for surface area determination; their use is not recommended.

15.1.3.2.4 Electron Microscopy Image Analysis

Transmission electron microscopy as well as SEM can be used for determination of geometric surface area using a variety of methods, including calculation of planar surface area and assumptions regarding geometry to calculate total external surface area. With this method, only edge roughness can be measured. The SEM method, which offers the possibility of measuring the external surface roughness, consists of collecting two images at different sample tilt angles and constructing a three-dimensional representation of the surface. Surface area is calculated within a grid of fixed lines by summation of the planar surfaces in the grid. The ratio of the calculated surface to the area within the grid gives a measure of surface roughness. Measurements can also be made at different scales, providing information about the size distribution of the surface features. Since these measurements are typically made at the micrometer scale, and measure external surface area, it is not surprising that the values are intermediate between geometric surface areas based on particle size and BET values. Determination of specific surface area requires conversion of particle surface area to a mass basis using the particle density. The assumption that the particle density is equal to the density of specimen samples of the mineral is reasonable and introduces relatively minor errors in comparison to other assumptions made in the calculation. Increasing computer capacity and suitable software makes this method the most useful of the geometric methods.

15.1.3.2.5 Small Angle X-Ray Scattering

In this application, $K\alpha$ radiation from a conventional x-ray tube is scattered by freeze-dried samples in glass capillary tubes. The background-corrected x-ray-scattering intensity is plotted against the scattering vector (q) to obtain the apparent surface fractal dimension (D_s) using the relation (Borkovec et al., 1993):

$$I_q = Aq^{D_s-5} + B \tag{15.7}$$

where
- I_q is the scattering intensity
- A is a proportionality constant
- B is the background correction

Values of D_s obtained for soils using this method are in relatively good agreement with values calculated from gas adsorption surface area (a) for soil particle radii (r) using the relation (Borkovec et al., 1993):

$$a = C\lambda^{2-D_s} r^{D_s-3} \tag{15.8}$$

where
- λ is the size of the probing molecules
- C is the proportionality constant

15.1.3.2.6 Negative Adsorption

Negative adsorption refers to a deficiency in the concentration of an ion in solution adjacent to a solid surface relative to the concentration of the ion in the bulk solution. The deficit is caused by electrostatic repulsion between ions and surfaces of similar charge. Since most charged surfaces in soils are negatively charged, negative adsorption usually relates to solution anion concentrations and negative surfaces. For a 1:1 electrolyte, the diffuse double layer model produces the following approximation (Sposito, 1984):

$$d_e \approx \frac{2}{\sqrt{\beta c}} - \delta \tag{15.9}$$

where
- d_e is the exclusion distance
- c is the concentration of the bulk electrolyte
- β is a constant equal to 1.08×10^{16} m mol^{-1}
- δ is the distance between two planes

The exclusion volume and area (S_e) are related by

$$V_e = S_e d_e \tag{15.10}$$

where V_e is the exclusion volume (the hypothetical volume from which the ion is completely excluded). Substituting into Equation 15.9 yields

$$V_e \approx \frac{2S_e}{\sqrt{\beta c}} - \delta S_e \tag{15.11}$$

The exclusion volume is calculated by first removing the bulk solution, determining the remaining liquid volume, displacing the liquid, and analyzing for the bulk solution and extract concentration. The exclusion volume is then equal to the mass deficit in the extract divided by the concentration in the bulk solution.

A plot of V_e vs. $c^{-0.5}$ should yield a straight line whose slope is proportional to the exclusion specific surface area as shown by inspection of Equation 15.11.

This method was first described by Schofield (1949), who used it to determine montmorillonite surface area from reactions with NaCl, $NaNO_3$, and Na_2SO_4 solutions. Subsequent work by Edwards et al. (1965a, 1965b) demonstrated that the specific surface area determined with this method varied with cation selected. Calculated values for illites ranged from values close to the N_2 BET values with Li to 0 with Cs. In contrast, for montmorillonite, LiCl exclusion volumes were 10 times greater than N_2 BET surface areas, while Cs values were comparable to those obtained by N_2 BET. Trends in surface area values measured using anion exclusion for Li, Na, K, NH_4, Cs, and Ca-montmorillonites were in agreement with those calculated from a tactoid model (Schramm and Kwak, 1982a, 1982b).

15.1.3.2.7 Applications

Surface area measurements are required for a variety of calculations. In most soils, the bulk soil surface area is dominated by the surface area of the clay minerals. Surface charge density, which requires measurement of both surface area and particle charge, has been related to cation exchange selectivity. As expected, increasing surface charge density favors adsorption of the higher valence cation in heterovalent exchange (Maes and Cremers, 1977). Surface charge density is also required for calculation of double layer thickness and for use in a variety of adsorption relationships. Determination of specific surface area is required for chemical studies on many different minerals. In this case, bulk surface area is not appropriate. Controlled laboratory studies are often performed using addition of quantities of a well-characterized mineral having a known surface area. This method is used to study a variety of chemical reactions, such as kinetics of calcite, gypsum, and dolomite dissolution, surface area of calcite for prediction of phosphate adsorption, and addition of various Fe or Mn oxides for study of adsorption and redox processes. Among the various applications of the EGME method, Ross (1978) related shrink/swell properties of soils to surface area and Supak et al. (1978) related the specific surface area of clays to the adsorption of the pesticide aldicarb.

15.1.3.3 Surface Charge

The total net surface charge on a particle (Φ_p) is

$$\sigma_p = \sigma_s + \sigma_H + \sigma_{is} = \sigma_{os} - \sigma_d \qquad (15.12)$$

where

σ_s is the permanent structural charge

σ_H is the proton surface charge resulting from the specific adsorption of protons and hydroxyl ions

σ_{is} is the inner-sphere complex charge resulting from specific ion adsorption

σ_{os} is the outer-sphere complex charge resulting from nonspecific adsorption

σ_d is the dissociated charge

This definition is similar to the one provided by Sposito (1984) with the exception that total net surface charge results from isomorphic substitution and is generated by specifically adsorbing ions (Hunter, 1981). An inner-sphere surface complex contains no water between the adsorbing ion and the surface functional group; while an outer-sphere surface complex contains at least one water molecule between the adsorbing ion and the surface functional group (Sposito, 1984). Examples of surface functional groups are reactive surface hydroxyl groups on oxide minerals, aluminol and silanol groups on clay minerals, and carboxyl and phenol groups on SOM.

15.1.3.3.1 Measurement Methodology

The total net surface charge can be measured directly using electrokinetic experiments. The point of zero charge (p.z.c.) of a particle is the solution pH value where total net particle charge is zero. The p.z.c. can be measured directly using electrokinetic experiments or indirectly from potentiometric titrations under certain experimental conditions (Sposito, 1984).

Electrokinetic phenomena are processes where a relative velocity exists between two parts of the electrical double layer (Hiemenz, 1977; Hiemenz and Rajagopalan, 1997). In this motion, a thin layer of liquid remains with the solid and a shear plane is located between the solid and liquid phases at some distance from the solid surface (van Olphen, 1977). The electric double layer potential at the shear plane is called the zeta potential (ζ). The assumption that ζ is equal to or very close to the diffuse double layer potential (ψ_d) is supported indirectly by a large body of data on a variety of surfaces (Hunter, 1981, 1989). The principle electrokinetic phenomena that measure zeta potential are discussed later.

15.1.3.3.2 Electrophoresis

Electrophoresis measures the movement of a suspended charged particle in response to an applied electric field. This movement is called electrophoretic mobility (μ_E) and is given by the Smoluchowski equation (Hunter, 1989):

$$\mu_E = \frac{\varepsilon\zeta}{\eta} \qquad (15.13)$$

where

ε is the relative permittivity

η is the viscosity

The Smoluchowski equation applies when the particle dimensions are much greater than the double layer thickness (Hunter, 1987). The complete formula relating ζ and μ_E is derived by the theoretical evaluation of the electric force on the charged particle (f_1), the hydrodynamic frictional force on the particle by the liquid (f_2), the electrophoretic retardation force (f_3), a frictional force resulting from the movement of water with the counterions, and the relaxation force (f_4), caused by distortion of the double layer around the particle (van Olphen, 1977). Additional considerations arise

for nonspherical particles and those carrying two double layers such as clays. For these reasons, the Smoluchowski equation is, in general, only approximate and it is advisable to report electrophoresis results as electrophoretic mobility rather than to attempt to convert to zeta potential (van Olphen, 1977).

Electrophoresis is the most common method of determining zeta potential. For colloidal systems, the most appropriate technique is microelectrophoresis where the movement of individual particles is followed directly by microscopy (Hunter, 1981). Microelectrophoresis is only applicable at very low particle concentrations. Electrophoresis can also be studied using laser Doppler velocimetry and photon correlation spectroscopy. The mass transport mobility apparatus measures electrophoretic mobility from the mass of colloids transported to a suitable electrode compartment (Hunter, 1981). This apparatus can be used at much higher particle concentrations than microelectrophoresis.

15.1.3.3.3 Electroosmosis

Electroosmosis measures the movement of the liquid adjacent to a flat, charged surface in response to an electric field applied parallel to the surface. This movement is called electroosmotic velocity (v_{eo}) and is also obtained from the Smoluchowski equation (Hunter, 1987):

$$v_{eo} = \frac{-\varepsilon\zeta E}{\eta} \tag{15.14}$$

where E is the electric field strength. While it is possible to measure electroosmotic velocity directly using microscopy, it is more common to measure the volume of liquid transported per unit time (Hunter, 1981):

$$\frac{V}{i} = \frac{\varepsilon\zeta}{\eta\lambda_0} \tag{15.15}$$

where

V is volume
i is the electric current
λ_0 is the electrical conductivity

The material whose zeta potential is being measured is formed into a porous plug and the transport of liquid across a tube in response to an electric field may be obtained by measuring the movement of an air bubble in the capillary providing the return path (Adamson, 1976). It is also possible to measure the electroosmotic flow by applying a counter pressure until the flow is exactly compensated (Hunter, 1981).

15.1.3.3.4 Electroacoustic Spectroscopy

A general discussion of the application of acoustic spectroscopy for characterizing colloidal suspensions was presented earlier in this chapter (Section 15.1.3.1). Both acoustic and electroacoustic spectrometers are commercially available separately or combined in a single instrument. In electroacoustic spectroscopy, one measures either (1) the colloid vibration potential (CVP) or colloid vibration current (CVI), the induced dipole moment created by the displacement or polarization of the electrical double layer in response to an acoustic wave, or (2) the electrokinetic sonic amplitude (ESA) generated by the movement of a charged particle in response to an electrical field as indicators of colloidal zeta potential. The individual dipole moments created by the interaction of sound waves with a colloidal suspension can be measured as an alternating electrical field that varies with the amplitude of the sound wave. Conversely, the electrophoretic movement of charged particles in response to an applied electrical field gives rise to sound waves, known as the ESA effect. Although electroacoustic spectroscopy can provide PSD, such information is best derived from the conventional acoustic spectra (Dukhin and Goetz, 2002; Seaman et al., 2003).

In contrast to microelectrophoretic light-scattering methods, electroacoustic measurement of zeta potential can be conducted at much higher suspension concentrations (30%–50% solids), an obvious advantage given that sample dilution and changes in solution chemistry can impact the expression of zeta potential and apparent particle size (Dukhin et al., 2001; Dukhin and Goetz, 2002; Delgado et al., 2005). Acoustic methods have been used to evaluate shifts in the isoelectric point (IEP) of materials at high-ionic strengths as indicators of specific and nonspecific sorption mechanisms (Kosmulski, 2002; Kosmulski et al., 2002; Greenwood, 2003). Such applications are best used in combination with other surface active spectroscopic methods for determining sorption mechanisms. In comparing various techniques for evaluating the IEP and p.z.c. of Fe (hydr)oxides, Kosmulski et al. (2003) noted that electroacoustic methods produced higher IEP values than observed for potentiometric titration methods. The cause of the discrepancy was not discussed.

15.1.3.3.5 Streaming Potential

The streaming potential is an electric potential difference generated when liquid adjacent to a charged surface is set in motion by an applied pressure gradient (Hunter, 1987). The streaming potential (Φ_{st}) is also governed by the Smoluchowski equation and given by (Sposito, 1984)

$$\Phi_{st} = \frac{\varepsilon\zeta}{\lambda_0\eta}\Delta P \tag{15.16}$$

where ΔP is the applied pressure difference. The streaming potential can be measured in similar fashion as the electroosmotic velocity. Liquid is forced under pressure through a porous plug and Φ_{st} is measured by electrodes in the solution on either end (Adamson, 1976).

15.1.3.3.6 Sedimentation Potential

When particles having charged surfaces settle in a liquid under the force of gravity, a plane of shear is developed. As the particles settle, the interfacial charge is separated since a portion inside the shear plane moves with the particle and the remainder is left behind (Sposito, 1984). An electric potential difference arises

from the separation of charge called the sedimentation potential. The gradient for the sedimentation potential, $d\Phi_{sed}$, is given by (Sposito, 1984)

$$\frac{d\Phi_{sed}}{dz} = \frac{\varepsilon\zeta}{\lambda_0\eta} n\Delta\rho g \tag{15.17}$$

where
- n is the number of particles per unit volume
- $\Delta\rho$ is the difference in mass density between the particles and the liquid phase
- g is gravitational acceleration
- z is distance

The potential difference is measured by inserting reversible electrode probes at two different heights in the column of settling particles (Hunter, 1981). For low particle concentration, the sedimentation potential is also governed by the Smoluchowski equation (Hunter, 1981).

15.1.3.3.7 Potentiometric Titration

Potentiometric titration measures the surface density of proton surface charge (σ_H) defined as (Sposito, 1984)

$$\sigma_H = \frac{F}{A}(q_H - q_{OH}) \tag{15.18}$$

where
- F is the Faraday constant
- A is the specific surface area
- q_H is the complexed proton charge (mol)
- q_{OH} is the complexed hydroxyl charge (mol) per unit mass of solid

Titration data consist of pH readings obtained while known amounts of acid or base are added to a solid suspension. A net titration curve is obtained by subtracting a calibration curve obtained by titrating the equivalent supernatant solution. The values of $q_H - q_{OH}$ are given by (Sposito, 1984)

$$q_H - q_{OH} = \frac{C_A - C_B - [H^+] + [OH^-]}{C_s} \tag{15.19}$$

where
- C_A is the molar concentration of acid added
- C_B is the molar concentration of base added
- $[H^+]$ is the molar proton concentration
- $[OH^-]$ is the molar hydroxyl concentration obtained from pH measurement
- C_s is the particle concentration

In order for Equation 15.19 to be valid, added protons and hydroxyl ions must only react with surface-reactive functional groups whose charge is pH dependent. Usually, other reactions that are also pH dependent occur, such as soluble complex formation, dissolution of solid phases, or complexation with surfaces whose charge is not pH dependent (Parker et al., 1979). Without these corrections, no surface chemical significance can be provided by Equation 15.19. A detailed description of the use of potentiometric titration to determine surface charge is provided by Huang (1981).

15.1.3.3.8 Applications

One of the most important applications of electrokinetic experiments and potentiometric titrations is the determination of the p.z.c. A characteristic of variable charge minerals is the p.z.c. obtained in the presence of an inert electrolyte. This p.z.c. is determined electrokinetically as the pH value where the zeta potential is zero or indirectly from the point of zero net proton charge (p.z.n.p.c.) or from the point of zero salt effect (p.z.s.e.) obtained potentiometrically. The p.z.n.p.c. and the p.z.s.e. are discussed in detail in Chapter 16. The p.z.n.p.c. and the p.z.s.e. are equivalent to the p.z.c. in the absence of surface complex formation. Table 15.4 provides characteristic values of p.z.c. obtained using electrokinetic experiments and potentiometric titrations for a variety of variable charge minerals.

TABLE 15.4 Representative Points of Zero Charge for Various Minerals

Solid	p.z.c.
Electrophoresis	
Goethite	8.8
Hematite	8.5
Magnetite	6.9
Amorphous iron oxide	8.0
Gibbsite	9.8
Bayerite	9.2
Boehmite	9.4
Pseudoboehmite	9.2
Amorphous aluminum oxide	9.3
δ-MnO_2	2.3
Rutile	4.8
Anatase	5.9
Kaolinite	2.9
Streaming potential	
γ-Al_2O_3	9.1
α-Al_2O_3	9.2
Titration	
Goethite	8.7
Hematite	8.6
Magnetite	6.9
Gibbsite	9.8
Boehmite	8.5
Pseudoboehmite	9.3
Amorphous aluminum oxide	9.5
δ-MnO_2	3.6
SiO_2	3.0
Rutile	5.8
Anatase	6.0
Kaolinite	2.9

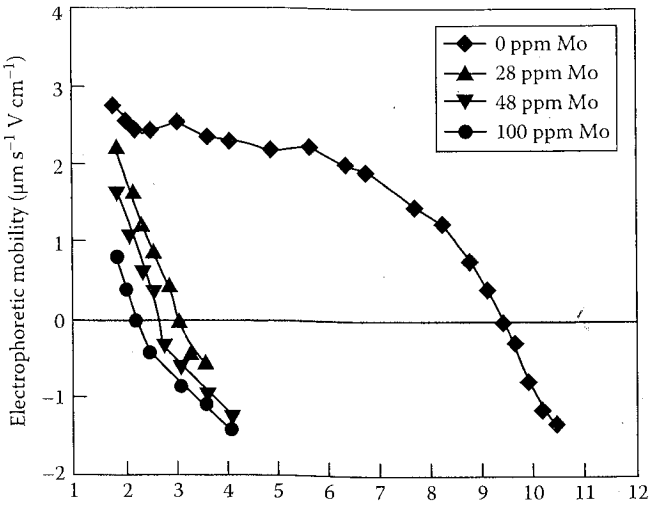

FIGURE 15.1 Shifts in p.z.c. and charge reversal of gibbsite in the presence of molybdate. (Adapted from Goldberg, S., H.S. Forster, and C.L. Godfrey. 1996. Molybdenum adsorption on oxides, clay minerals, and soils. Soil Sci. Soc. Am. J. 60:425–432.)

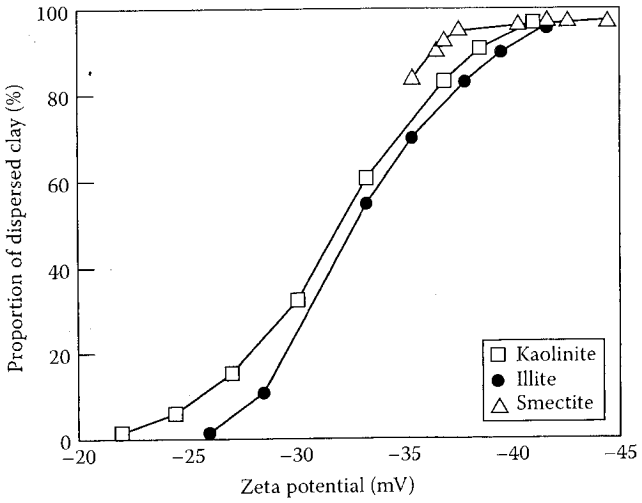

FIGURE 15.2 Relation between zeta potential and dispersible clay of Na-clay minerals obtained using electrophoresis. (Reprinted from Chorom, M., and P. Rengasamy. 1995. Dispersion and zeta potential of pure clays as related to net particle charge under varying pH, electrolyte concentration and cation type. Eur. J. Soil Sci. 46:657–665. With permission of Blackwell Science Ltd.)

Electrokinetic experiments and potentiometric titrations can be used to infer adsorption mechanisms for adsorbing ions on surfaces. Adsorption of ions that form inner-sphere surface complexes is characterized by shifts in the p.z.c. of the particles and reversals of their electrophoretic mobility with increasing ion concentration (Hunter, 1981). Adsorption of ions that form outer-sphere surface complexes does not produce p.z.c. shifts since they are assumed to lie outside the shear plane. Figure 15.1 presents the shifts in p.z.c. and charge reversals observed for gibbsite upon the specific adsorption of increasing amounts of molybdate. These results are indirect evidence for inner-sphere surface complexation of this ion.

Net particle surface charge is a primary factor in dispersion of clay minerals. Zeta potential as a measure of particle surface charge was also related to percentage of dispersible clay (Chorom and Rengasamy, 1995). Figure 15.2 indicates the relationship between zeta potential measured using electrophoresis, and dispersible clay for Na-saturated kaolinite, montmorillonite, and illite.

The plane interface technique determines the electroosmotic velocity at large plane interfaces and can be used to determine the zeta potential of two different surfaces at the same time under the same conditions (Nishimura et al., 1992). These authors used the plane interface technique to simultaneously study silica plates and muscovite mica basal planes. The zeta potential values for silica presented in Figure 15.3 indicate that the asymmetric silica–mica cell provides results comparable to those of the symmetrical silica–silica cell.

Zeta potentials of clay minerals have also been determined using a flat plate streaming potential apparatus for muscovite mica (Scales et al., 1990), saponite, and hectorite (Nishimura et al., 2002a). Zeta potential of clays becomes less negative with increasing electrolyte concentration as a result of double layer compression (Figure 15.4). The resulting charge reduction causes clay flocculation. Streaming potential measurements of sodium montmorillonite using a flexible wall permeameter were found to be dependent on the salt concentration of the permeating solution (Heister et al., 2005).

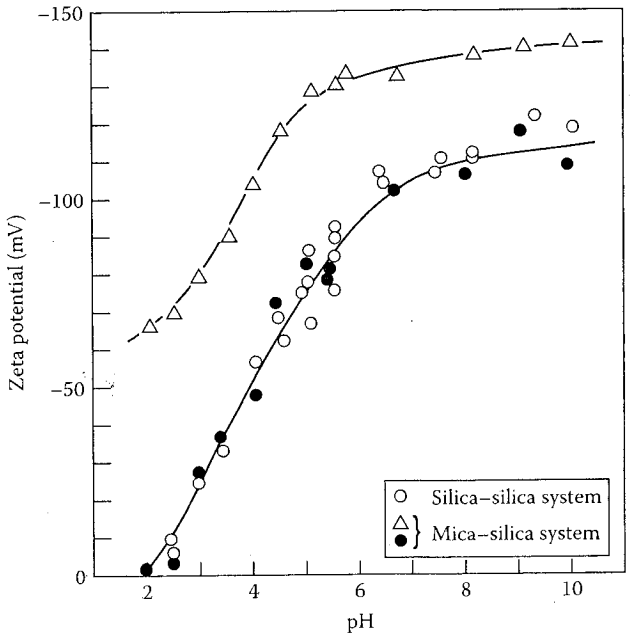

FIGURE 15.3 Zeta potentials as a function of solution pH for muscovite mica basal plane– and silica plate–aqueous solution interfaces obtained using electroosmosis. (Reprinted from Nishimura, S., H. Tateyama, K. Tsunematsu, and K. Jinnai. 1992. Zeta potential measurement of muscovite mica basal plane-aqueous solution interface by means of plane interface technique. J. Colloid Interface Sci. 152:359–367. With permission of Academic Press, Inc.)

A vastly different application of electrokinetic experiments is the application to dewatering and decontamination of soils

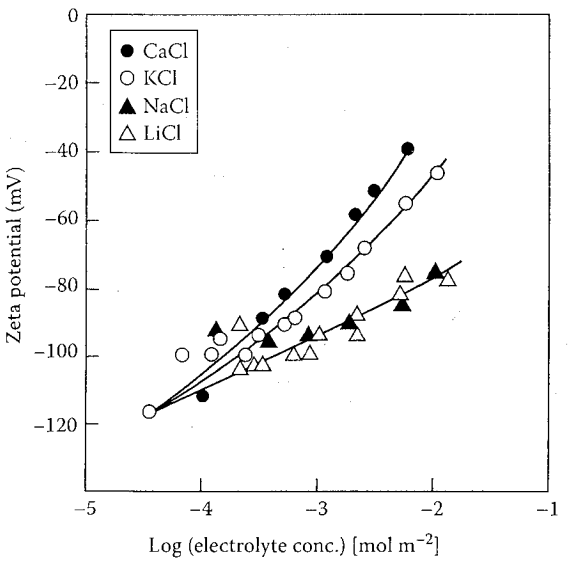

FIGURE 15.4 Relation between zeta potential and electrolyte concentration for various 1:1 electrolytes obtained from streaming potential. (Reprinted with permission from Scalés, P.J., F. Grieser, and T.W. Healy. 1990. Electrokinetics of the muscovite mica–aqueous solution interface. Langmuir 6:582–589. Copyright 1990 American Chemical Society.)

and clays. For example, electroosmosis has been used for removing organic contaminants from kaolinite and soil clays (Shapiro and Probstein, 1993; Schultz, 1997; Kim et al., 2001). These authors present applications for in situ hazardous waste remediation of soils. Economic analysis indicated that electroosmosis compared favorably with the cost of excavation and ex situ treatment (Schultz, 1997).

A potentiometric titration method has been developed to account for changes in solubility of the solid with changes in pH (Schulthess and Sparks, 1986). This is a batch method where the reference for each sample is the supernatant specific to that sample back titrated to pH 7. This method is considered to account for all sources of proton consumption (Schulthess and Sparks, 1986).

15.1.4 Thermodynamics of Colloid Surfaces

To develop the thermodynamic treatment of the surface region, a few definitions are useful. The interfacial region is a space between two adjoining phases (gas–liquid, gas–solid, liquid–liquid, liquid–solid, solid–solid), which is characterized by inhomogeneity in its properties. The Gibbs surface is a mathematical dividing surface, without volume, drawn parallel to the boundaries of the interfacial region, which is used to define the volumes of the two adjoining bulk phases. A schematic of the interfacial region and the Gibbs surface is presented in Figure 15.5. The actual values for the system as a whole will differ from the sum of the values for the bulk phases by an excess or deficiency due to the Gibbs surface (Adamson, 1976). The following relations hold for the variables of state:

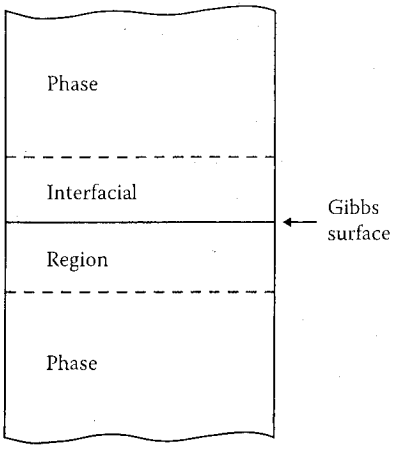

FIGURE 15.5 Representation of the interfacial region and the Gibbs surface.

$$\begin{aligned} &\textit{Volume:}\quad V = V^{\alpha} - V^{\beta} \\ &\textit{Internal Energy:}\quad E = E^{\alpha} + E^{\beta} + E^{\sigma} \\ &\textit{Entropy:}\quad S = S^{\alpha} + S^{\beta} + S^{\sigma} \\ &\textit{Moles:}\quad n_i = n_i^{\alpha} + n_i^{\beta} + n_i^{\sigma} \end{aligned} \tag{15.20}$$

where

α and β denote the bulk phases
σ denotes the Gibbs surface (Adamson, 1976)

Additional variables of state are defined as the surface tension or surface free energy (γ) and the area of the Gibbs surface (A).

The three fundamental thermodynamic relationships of surface chemistry are the Young–Laplace equation, the Kelvin equation, and the Gibbs equation (Adamson, 1976). The Young–Laplace equation is the fundamental equation of capillarity for a curved Gibbs surface:

$$P^{\beta} - P^{\alpha} = \gamma\left(\frac{1}{r_1} + \frac{1}{r_2}\right) \tag{15.21}$$

where

$P^{\beta} - P^{\alpha}$ is the capillary pressure
r_1 and r_2 are the radii of curvature

The Kelvin equation gives the effect of surface curvature on the molar free energy of a substance. The free energy of a substance can be related to its vapor pressure assuming the vapor to be ideal (Adamson, 1976). The Kelvin equation is

$$\ln\left(\frac{P}{P_0}\right) = \frac{\gamma V}{RT}\left(\frac{1}{r_1} + \frac{1}{r_2}\right) \tag{15.22}$$

where

P_0 is the normal vapor pressure of the liquid
P is the vapor pressure observed over the curved surface
R is the molar gas constant
T is temperature

For a small, reversible change dE in the energy of the system (Adamson, 1976)

$$dE = dE^{\alpha} + dE^{\beta} + dE^{\sigma}$$
$$= TdS^{\alpha} + \sum \mu_i dn_i^{\alpha} - P^{\alpha}dV^{\alpha} + TdS^{\beta}$$
$$+ \sum \mu_i dn_i^{\beta} - P^{\beta}dV^{\beta} + TdS^{\sigma} + \sum \mu_i dn_i^{\sigma} - P^{\sigma}dV^{\sigma} + \gamma dA \quad (15.23)$$

where μ_i is chemical potential. Substituting for dE^{α} and dE^{β} and manipulating the equation for dE^{σ} lead to the expression (Adamson, 1976)

$$S^{\alpha}dT = Ad\gamma + \sum n_i^{\sigma} d\mu_i = 0 \quad (15.24)$$

At constant T and A, the Gibbs equation is

$$-d\gamma = \sum \frac{n_i^{\sigma}}{A} d\mu_i = \sum \Gamma_i^{\sigma} d\mu_i \quad (15.25)$$

where Γ_i^{σ} is a surface excess concentration per unit area defined as $\Gamma_i^{\sigma} = n_i^{\sigma}/A$. The Gibbs equation can be applied to liquid–liquid and liquid–vapor interfaces where the surface tension can be measured to calculate the surface concentration of the adsorbed species causing the surface tension change. Similarly, if the surface concentration can be measured directly but the surface tension cannot, the Gibbs equation can be used to calculate the lowering of γ from the measured adsorption in solid–gas and solid–liquid systems (Hunter, 1987).

15.2 Interparticle Forces

15.2.1 Electrical Double Layer

Double layer theory describes the distribution of ionic concentrations near electrostatically charged particles. The charge on the colloidal particles is due to isomorphic substitution in the particle lattices or arises from the preferential adsorption of one ionic species from the solution phase (Babcock, 1963). Such a charge requires the presence of a layer of ions of opposite charge. The double layer consists of an excess of ions of opposite sign and a deficiency of ions of the same sign that are electrostatically repelled by the particle. Double layer theory assumes that the surface of the colloidal particles is represented by an infinite flat surface having continuous and uniform electrostatic charge density immersed in an electrolyte with a uniform dielectric constant (Babcock, 1963). All electrolyte ions are assumed to be point charges. The electrical potential, ion charge, and ion distributions can be calculated from the Poisson–Boltzmann equation:

$$\frac{d^2\psi}{dx^2} = -\frac{1}{\varepsilon_0 D} \sum cFz_i \exp\left(-z_i F\psi(x)/RT\right) \quad (15.26)$$

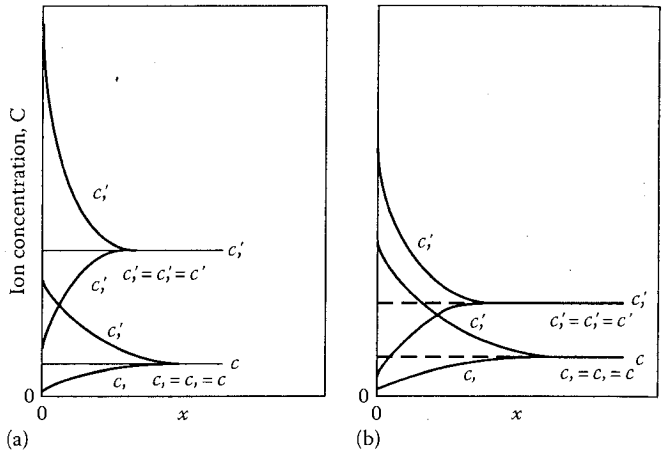

FIGURE 15.6 Distribution of ions in the electric double layer at two electrolyte concentrations ($c' > c$). (a) Constant potential surface. (b) Constant surface charge. (Adapted from van Olphen, H. 1977. An introduction to clay colloid chemistry, 2nd Ed. John Wiley & Sons, New York.)

where

- $\psi(x)$ is the inner potential at a distance x from the surface
- ε_0 is the permittivity of free space
- D is the dielectric constant of water
- c is the concentration
- R is the gas constant
- T is the temperature (K)
- F is the Faraday constant
- z_i is the valence of the charged species (Sposito, 1984)

Figures 15.6 and 15.7 present the ion distribution and the electric potential distribution, respectively, in the double layer at two electrolyte concentrations. The extent of the double layer is given by the distance ($1/\kappa$) in units of meters:

$$\frac{1}{\kappa} = \sqrt{\frac{\varepsilon_0 RT}{2000F^2 I}} \quad (15.27)$$

where I is the ionic strength $\left(=1/2\sum c_i z_i^2\right)$. Important findings of diffuse double layer theory are (1) the excess cations near the negative surface neutralize more of the charge than the anion deficit, (2) the electric potential decreases as the electrolyte concentration increases, and (3) the double layer distance ($1/\kappa$) decreases as the electrolyte concentration increases. Some important limitations of double layer theory are that it applies only to infinitely dilute suspensions and to low surface charge densities (Babcock, 1963).

15.2.2 Attractive Force

The attractive force acting on colloidal particles is called the van der Waals force and acts to bring particles closer together. The basis of the attractive force is that the fluctuating dipole of one atom polarizes another one and the two atoms attract

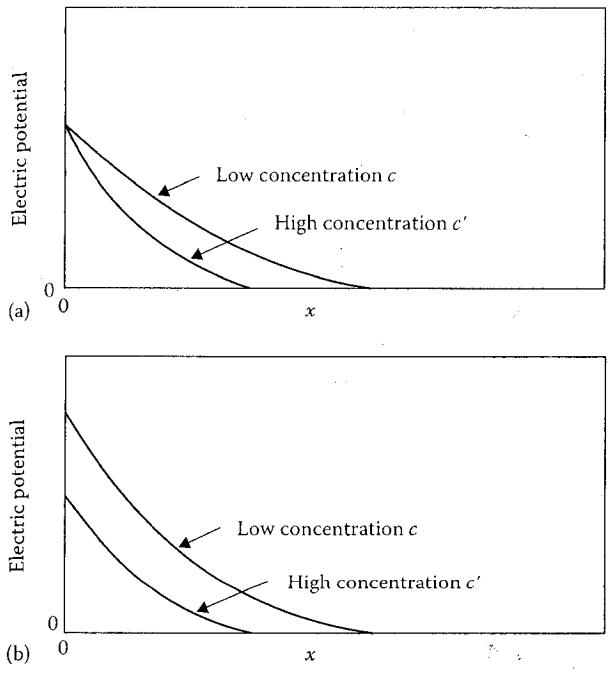

FIGURE 15.7 Electric potential distribution in the electric double layer at two electrolyte concentrations. (a) Constant potential surface. (b) Constant surface charge. (Adapted from van Olphen, H. 1977. An introduction to clay colloid chemistry, 2nd Ed. John Wiley & Sons, New York.)

each other. This attraction between atom pairs is additive, and, therefore, the energy of interaction between particles decreases much more slowly with distance than that between individual atoms (Quirk, 1994). The interaction energy per unit area between two opposing planar solids for the van der Waals force (Φ_{vdW}) is (Israelachvili, 1992)

$$\Phi_{vdW} = -\frac{A_H}{12\pi d^2} \tag{15.28}$$

where

A_H is the Hamaker constant
d is the distance separating the solid surfaces

At distances >5 nm, the correlations between the induced dipole distributions weaken and the interaction energy per unit area corresponds to the retarded van der Waals force (Φ_{RvdW}):

$$\Phi_{RvdW} = -\frac{B_{rH}}{3d^3} \tag{15.29}$$

where B_{rH} is the retarded Hamaker constant. Figure 15.8 shows values of the van der Waals force obtained experimentally between two mica surfaces. Attractive forces were observed between mica particles in the range of 0.6–2 nm in $CaCl_2$ solution both experimentally and theoretically with statistical mechanics and Monte Carlo simulations (Kjellander et al., 1990).

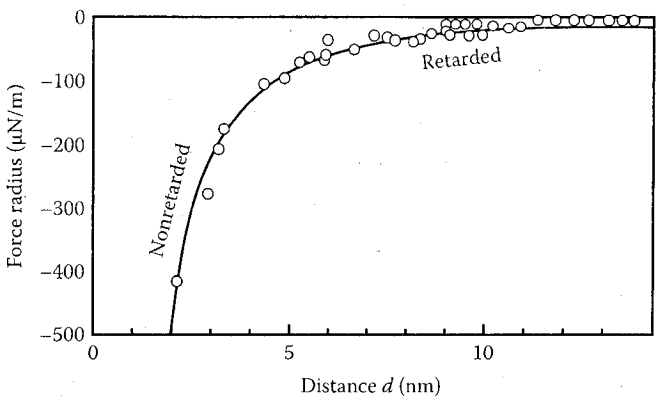

FIGURE 15.8 van der Waals forces between two mica surfaces in aqueous electrolyte solutions. The measured Hamaker constant is $A = 2.2 \times 10^{-20}$ J. Retarded van der Waals forces are observed above 5 nm. (Reprinted from Israelachvili, J.N. 1992. Intermolecular and surface forces, 2nd Ed. Academic Press, San Diego, CA. With permission of Academic Press Ltd.)

15.2.3 Repulsive Force

The electrostatic force results from the charge on the colloidal particles and acts to repel them. A force operates on charged surfaces as a result of their interacting double layers. This force is repulsive if the charges on the particles are the same. The repulsion described in terms of interaction energy per unit area (Φ_R) is given by the force times the distance through which it operates (Hiemenz, 1977; Sposito, 1984; Hiemenz and Rajagopalan, 1997):

$$\Phi_R = -\frac{64a^2}{z} cRT \exp(-z\kappa d) \tag{15.30}$$

where

$a = \tanh(z\psi_0/4RT)$
z is the charge on the electrolyte ions
c is the concentration of the electrolyte ions
κ is the inverse double layer distance
d is half of the surface separation

This equation is valid only when the surface separation $2d \gg 1/\kappa$ and $a \approx 1$. The electrostatic force between two plates for different electrolyte concentrations is presented in Figure 15.9.

When surfaces are brought closer together, an additional repulsive force becomes important. This force is called the solvation force or, when water is the medium, the hydration force. Solvation forces are of short range and oscillatory and arise whenever liquid molecules are induced to order between surfaces. Between colloid surfaces, repulsive hydration forces arise when water molecules strongly bind to hydrogen bonding surface groups such as hydrated ions or hydroxyl groups (Israelachvili, 1992). The effective range of hydration forces in clays and silicas is 3–5 nm. The interaction of mica surfaces in dilute solution obeys double layer theory, but at higher electrolyte concentration, a hydration force

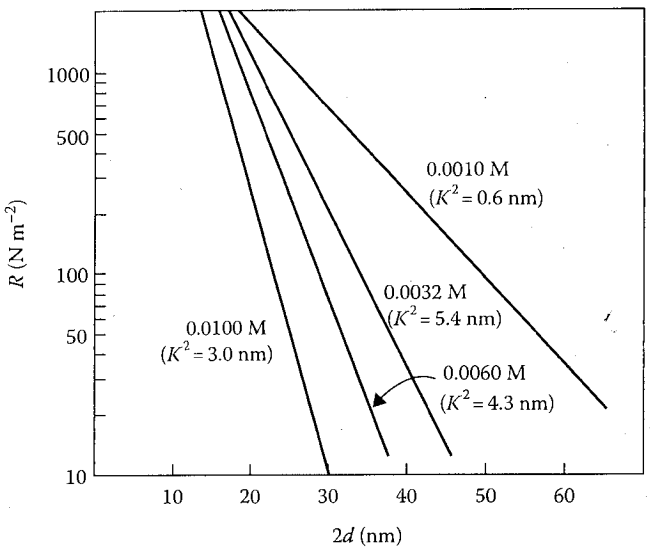

FIGURE 15.9 Repulsive force between two plates for different concentrations of a 1:1 electrolyte where κ is the inverse double layer distance. (Reprinted from Hiemenz, P.C. 1977. Principles of colloid and surface chemistry. Marcel Dekker Inc., New York. With permission of Marcel Dekker, Inc.)

develops due to the energy needed to dehydrate surface-bound cations. The strength of the hydration force, which increases with the hydration number of the cation: $Mg^{2+} > Ca^{2+} > Li^{+} \approx Na^{+} > K^{+} > Cs^{+}$ (Pashley and Quirk, 1984; Israelachvili, 1992), is illustrated for two mica surfaces in Figure 15.10.

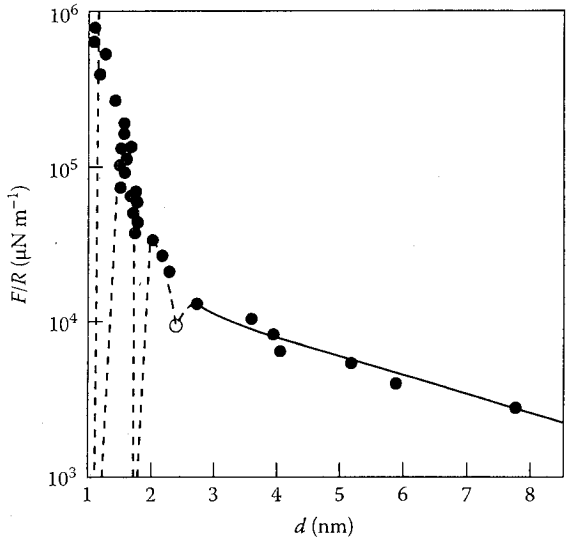

FIGURE 15.10 Forces between two mica surfaces in 7 mmol L^{-1} NaCl electrolyte. F is the total force scaled by the radius (R) of the curved surfaces. At distances > 1.5 nm, the forces are described by double layer theory. Hydration forces are observed at distances < 1.5 nm. (Reprinted with permission from Ducker, W.A., and R.M. Pashley. 1992. Forces between mica surfaces in the presence of rod-shaped divalent counterions. Langmuir 8:109–112. Copyright 1992 American Chemical Society.)

Clay swelling is the result of double layer repulsion between the surfaces of individual particles. Under confining conditions, a fluid pressure or swelling pressure is created that is a direct measure of the balance of forces between particles (van Olphen, 1977). The swelling pressure is obtained by measuring the confining force that must be applied to keep the clay layers at a given distance. The swelling pressure (Π) is

$$\Pi = P_{vdW} + P_R \tag{15.31}$$

where

P_{vdW} is the van der Waals force

P_R is the electrostatic force (Greathouse et al., 1994)

At short distances, hydration forces become significant in the swelling pressure. At greater distances, measured swelling pressures are of similar magnitude to calculated double layer repulsions (van Olphen, 1977).

Interparticle forces can be measured experimentally using the surface force apparatus (SFA), total internal reflectance microscopy, and the AFM (Israelachvili, 1992). The SFA can measure forces between surfaces at the 10^{-10} m level of resolution. This apparatus has been used to measure attractive van der Waals forces, repulsive double layer forces, and repulsive hydration forces in aqueous solutions (Israelachvili, 1992). Because of its smooth surface and ease of handling, mica has been the primary solid used in SFA studies. Total internal reflection microscopy has been used to study forces between a surface and an individual colloidal particle. AFM has been used to measure both short- and long-range forces (Ducker et al., 1991; Nishimura et al., 2002b; Zhao et al., 2008). Interactions between charged mica surfaces have been investigated using a combination of SFA and AFM experiments. Results from both methods agree with theoretical predictions (Kékicheff et al., 1993).

15.3 Colloidal Stability

15.3.1 Flocculation and Dispersion

The International Union of Pure and Applied Chemistry defines flocculation as "a process of contact and adhesion whereby the particles of a dispersion form larger-size clusters," other terms used interchangeably with flocculation are agglomeration and coagulation (IUPAC, 2009). The stability of colloidal suspensions is a balance between repulsive and attractive forces acting among the suspended particles. If net repulsive forces predominate, particles do not coagulate and remain dispersed. When the attractive forces are dominant, interacting particles coagulate and the resulting floccules settle more rapidly from the suspension than the smaller dispersed particles. Different theories in the literature attempt to describe colloid behavior (Sogami and Ise, 1984; Smalley, 1990; Ise and Smalley, 1994; McBride and Baveye, 2002). A classical continuum scale theory of the forces between particles is the DLVO theory named after Derjaguin, Landau, Verwey, and Overbeek, largely responsible

for its development (Hunter, 1987). Through the use of the SFA, it has been shown that the DLVO theory is an oversimplification of the forces acting at the mineral surface. For example, DLVO theory does not take into account short-range solvation forces (Israelachvili, 1992).

Continuum DLVO theory provides a simplified assumption of a phyllosilicate surface with permanent negative charge. Conceptually, the negative charge is developed from isomorphous substitution of lower valent cations for higher valent cations in either the tetrahedral or octahedral layers of the crystal. With regard to soils, a further complication exists in terms of mineral/organic interaction. Mounting evidence suggests that the primary reactive phases in soils are complex mineral assemblages where phyllosilicates are coated by natural organic matter and Fe-oxyhydroxide phases (Bertsch and Seaman, 1999). In this case, the theoretical models are too simplified to provide a good representation of natural colloids. Advanced computer molecular simulations must be used to begin to understand the complexities of mineral/fluid and mineral/mineral interaction, even for clean systems, for surface force behavior on the colloidal scale (Hsu, 1999). Consequently, DLVO theory, acknowledging its simplifications, will be used as a frame of reference for the discussion of flocculation dispersion.

Flocculation is a thermodynamically favorable process; however, the kinetics of coagulation determine the stability of colloidal suspensions. Generally, all colloidal suspensions will spontaneously flocculate given sufficient time, but potential energy barriers retard the rate of flocculation. These barriers are analogous to activation energies considered in chemical kinetics (Hiemenz and Rajagopalan, 1997). Particles in a primary minimum are adhesive and are not readily separated. In contrast, the dispersion/flocculation transition is the result of a secondary minimum, involves card-house type structures (Figure 15.11), and is readily reversible (Quirk, 1994).

There are many examples in the literature showing that DLVO theory can account for the observed kinetic behavior of dispersed colloidal systems (e.g., Napper and Hunter, 1974). However, this theory must be applied with caution since it treats ions exclusively as point charges ignoring their surface chemical properties and geometry, and should only be applied to dilute systems (Sogami and Ise, 1984).

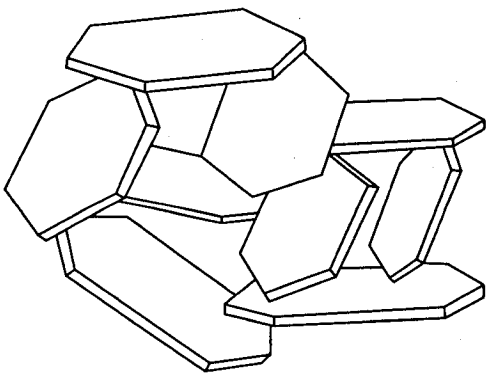

FIGURE 15.11 Representation of card-house structure. (Reprinted from Hunter, R.J. 1987. Foundations of colloid science, Vol. 1. Oxford University Press, New York by permission of Oxford University Press.)

The potential barrier preventing particles from coagulating is defined by the stability ratio (W), which is the fraction of the total number of collisions between particles that result in coagulation. The rate of coagulation in the absence of a potential barrier or rapid coagulation (R_f) is limited only by the rate of diffusion of the particles toward one another. When the particles have a potential barrier to overcome, the rate of coagulation (R_s) is slow and is related to R_f by

$$R_s = \frac{R_f}{W} \tag{15.32}$$

Rapid coagulation occurs when no significant repulsive forces act between particles and van der Waals or long-range coulombic attractions predominate. The quantification of the coagulation rate under these conditions was examined by von Smoluchowski (1916, 1917) and is discussed by Overbeek (1952).

Slow coagulation occurs over distances of the order of 1–100 nm when the approaching particles experience a barrier as their double layers overlap. Diffusion over this distance results from many individual Brownian events, some of which bring the particles closer together and some of which take them further apart. Since the rates of rapid and slow coagulation are directly proportional to the number of particles diffusing in the direction of a central particle (J), it follows from Equation 15.32 that the stability ratio is given by

$$W = \frac{R_f}{R_s} = \frac{J_f}{J_s} = 2r\int_{2r}^{\infty} \exp\left(\frac{E_T}{K_B T}\right)\frac{dr}{d^2} \tag{15.33}$$

where

r is the particle radius

$d \cong 2r$

Verwey and Overbeek (1948) showed that W was determined almost entirely by the value of the total potential energy (E_T) at the maximum (Figure 15.12). In Figure 15.12 E_R and E_A are the potential energies due to repulsive and attractive forces. A more complete analysis of the kinetics of colloid flocculation is presented in Hunter (1987).

Gravity removes suspended particles by sedimentation while inducing differential sedimentation coagulation, thereby decreasing Brownian coagulation rates. Ultimately, sedimentation limits the time of a flocculation series test. The test should be long enough to detect relative changes in suspended particle numbers, but not so long that all dispersed particles settle from a stable suspension (Hesterberg and Page, 1990a).

The reverse of flocculation is called dispersion. Ideally, the amount of energy required to separate two particles coagulated into a potential energy minimum is approximately equal to the difference between the interaction energy at the minimum and that at the adjacent maximum (van Olphen, 1977).

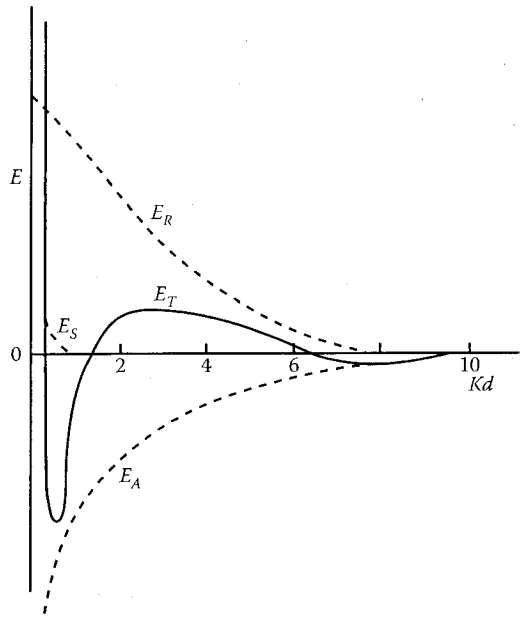

FIGURE 15.12 Total potential energy of interaction of two colloidal particles. $E_T = E_S + E_R + E_A$, where E_S is the potential energy of repulsion due to the solvent layers, E_R is the potential energy due to the repulsive forces, E_A is the potential energy due to the attractive forces, and κd is particle separation. (Reprinted from Hunter, R.J. 1987. Foundations of colloid science, Vol. 1. Oxford University Press, New York by permission of Oxford University Press.)

Under constant chemical conditions, separation of particles could presumably be induced by an input of kinetic energy (e.g., thermal or mechanical shear). Alternatively, changing the chemical conditions of the bulk solution surrounding coagulated particles could provide chemical and/or electrochemical energy to produce dispersion.

15.3.1.1 Modes of Particle Association

15.3.1.1.1 Edge–Edge, Edge–Face, Face–Face

Clay crystals have a net negative surface charge as a consequence of isomorphic substitutions of electropositive ions for ions with a lower valence. This negative charge generates an ionic reorganization in the solution medium that has been described above as the diffuse double layer. Clay particles also have edge surfaces with atomic structure different from the faces. At the edge of the platelet, the tetrahedral layer of Si and the octahedral layer of Al exhibit broken bonds, which, in turn, generate another electric double layer.

Double layer theory assumes that the surfaces of the clay minerals are of semi-infinite spatial extent and show no edge effects, a simplification that is not always satisfactory. Clay mineral particles have finite dimensions. Below the p.z.c., edge surfaces carry a positive charge due to specific adsorption of protons. Using the Poisson–Boltzmann equation, Secor and Radke (1985) calculated the effect of edge–face corners on the electrical potential distribution around an idealized, symmetrical montmorillonite disk. Spillover of the negative electrical potential from the particle faces into the edge region can result in a negative potential everywhere around the particle.

The electrical potential at the edge surface strongly depends on the electrolyte concentration and the ratio of the face to edge charge density. The extent of spillover also is a weak function of the particle shape (Secor and Radke, 1985). This study implies that attraction between positively charged edges and negatively charged faces of phyllosilicate mineral particles will depend on the extent of the edge protonation, electrolyte concentration, and shape of the particle. A phyllosilicate structure that is collapsed in the *c*-dimension, such as mica, should be able to acquire a larger edge surface charge density than a layer silicate like smectite where structural expansion increases the distance between edge surface aluminol groups (Hesterberg, 1988).

When there is a reduction in the thickness of the double layer, particles can associate among themselves in three different ways: face–face, face–edge, or edge–edge. Face–face association is also called parallel aggregation and does not produce floccules, while the other two associations do produce three-dimensional structures called card houses (see Figure 15.11).

In concentrated suspensions of clay, the edge–edge and edge–face associations form a continuum, with chains of particles in the card-house structures mentioned above. The rigidity of the gel depends on the number and strength of the bonds in the continuum structure. Some attempts to characterize the gel structure using freeze-drying techniques have been made (Norrish and Rausell-Colom, 1961). When the water is eliminated from the suspension, the volume of the system does not change and the final product is a dry clay structure with some strength that has been called aerogel (van Olphen, 1977).

15.3.1.1.2 Domains and Quasicrystals

Some colloidal systems may, under certain circumstances, show a reversible clustering among particles. The earliest reported example is the Fe-hydroxide sol described by Cotton and Mouton (1907). The term tactoid was first used by Freundlich (1932) and was more precisely defined by Overbeek (1952) as the association of particles at a certain distance affected by electrolyte concentration and pH. Quirk and Aylmore (1971) proposed the term quasicrystal to describe the regions of parallel alignment of individual aluminosilicate lamellae in montmorillonite and the term domain to describe the regions of parallel alignment of crystals for illite. This terminology is adopted in the present chapter.

The distribution model of adsorbed ions in mixed mono- and divalent systems for smectite quasicrystals was described by Shainberg and Otoh (1968) and Bar-on et al. (1970). According to this theory, called the ion demixing model, when Na is added to Ca saturated montmorillonite, most of the adsorbed Na will concentrate on the external surfaces of the quasicrystals until 10% of the adsorbed Ca has been replaced by Na. Initially, the size and shape of the particles are not altered by the addition of adsorbed Na. As further Na is added to the system, Na penetrates into the quasicrystals and brings about disintegration of the clay packets (Bar-on et al., 1970).

Lebron and Suarez (1992a) used electrophoretic mobility experiments to show that the demixing model can be applied to micaceous clays. The electrophoretic mobility of micaceous

TABLE 15.5 Critical Coagulation Concentrations of Phyllosilicates under Various Conditions

Mineral	CCC ($mol_c\ L^{-1}$)	Background Electrolyte	pH	Solids Concentration ($g\ kg^{-1}$)
Kaolinite-4	2–40	$NaNO_3$	4–10	0.025
Kaolinite-9	8, 30	$NaHCO_3$, Na_2CO_3	8.3, 9.5	0.6–0.9
Kaolinite (Georgia)	5, 245, 75	NaCl, $NaHCO_3$, Na_2CO_3	7, 8.3, 9.5	0.6–0.9
Kaolinite (KGa-1)	<0.19–54.6	NaCl	5.8–9.1	0.67
Kaolinite-4	0.1–0.3	$Ca(NO_3)_2$	4–10	0.025
Kaolinite (KGa-1)	<0.19–0.85	$CaCl_2$	5.5–9.3	0.67
Montmorillonite-23	1–10	$NaNO_3$	3.8–10	0.25
Montmorillonite-23	20, 48, 68	NaCl, $NaHCO_3$, Na_2CO_3	7, 8.3, 9.5	0.6–0.9
Montmorillonite-27	14, 47, 17	NaCl, $NaHCO_3$, Na_2CO_3	7, 8.3, 9.5	0.6–0.9
Montmorillonite (SAz-1)	14–28	NaCl	6.4–9.4	0.67
Montmorillonite (SAz-1)	1.09, 1.56	$CaCl_2$	6.1, 7.6	0.67
Montmorillonite (SAz-1)	0.93, 2.02, 0.88	$MgCl_2$	6.1, 8.4, 9.0	0.67
Vermiculite	38, 58, 30	NaCl, $NaHCO_3$, Na_2CO_3	7, 8.3, 9.5	0.6–0.9
Illite-36	9, 185, 95	NaCl, $NaHCO_3$, Na_2CO_3	7, 8.3, 9.5	0.6–0.9
Illite (Grundy)	7.24	NaCl	~6	1
Illite (Grundy)	0.2	$CaCl_2$	~6	1

Source: Adapted from Hesterberg, D.L. 1988. Critical coagulation concentrations and rheological properties of illite. Ph.D. Thesis. University of California, Riverside, CA by Oxford University Press.

domains increased when the sodium adsorption ratio (SAR) increased from 5 to approximately 10.

15.3.1.2 Critical Coagulation Concentration

The CCC, sometimes called the critical flocculation concentration (CFC), is the minimum concentration of indifferent electrolyte that induces rapid coagulation. The CCC is strongly dependent on counterion valence (Table 15.5). This observation is known as the Schulze–Hardy rule. An estimate of the CCC ($mol\ L^{-1}$) is given by (Hunter, 1987)

$$CCC = \frac{0.107\varepsilon^3(k_BT)^5Z^4}{N_AA_H^2(ze)^6} \tag{15.34}$$

where

$Z = \tanh(ze\psi_0/4k_BT)$
N_A is Avogadro's number
A_H is the Hamaker constant
ε is the relative dielectric constant
k_B is the Boltzmann constant
e is the proton charge

The variation of CCC with counterion valence depends approximately on the inverse sixth power of z. At 25°C in water, using the experimental observation that coagulation usually occurs between low-potential surfaces, the result is

$$CCC \propto \frac{\psi_0^4}{z^2} \tag{15.35}$$

where now the CCC depends on the inverse of the square of the valence. However, the CCC calculated with Equation 15.35 agrees well with experimental results if $\psi_0 \propto 1/z$. When calculating the CCC in soils, one must consider that soils consist of mixtures of permanent and variable charge minerals. The net surface charge, and consequently, the electrical potential around the mixture of particles are dependent upon variables such as pH, specifically adsorbed ions, ionic strength, and mineralogy. A more detailed evaluation of the effect of these variables on the stability of colloids is presented below.

15.3.2 Factors Affecting Colloidal Stability

15.3.2.1 Solution Composition

The magnitude of the repulsion barrier is determined by the nature of the material adsorbed on the particle surface. In the case of a charged colloid, repulsion depends on the magnitude of the surface charge and on the extent of the electrical double layer, which, in turn, depends on the total electrolyte concentration. It is necessary here to distinguish between the concentration of the potential determining ions and that of other ions that have no direct interaction with the surface. If the surface potential of the particles is determined by the concentration of potential determining ions, the magnitude of this potential is not affected by the addition of an indifferent electrolyte. For this type of double layer, when salt concentration increases, the double layer thickness decreases, the surface charge of the particles increases, and the surface potential remains constant (Figure 15.7a).

If the surface charge of the particle is determined by isomorphic substitution, the surface charge does not change with increasing electrolyte concentration. The diffuse double layer compresses, but in this case, the surface potential decreases with increasing electrolyte concentration (Figure 15.7b) (van Olphen, 1977).

15.3.2.2 Exchange Complex Composition

As explained above, clay particles are surrounded by cations as a consequence of the net negative electrical charge on the surface. Cations bonded to the surface can be exchanged for other cations in solution. Consequently, the cations on the exchange complex are dependent on the solution composition.

There is an equilibrium between the cations on the exchange complex and the cations in the solution. Not all cations are adsorbed with the same affinity. Cations with larger hydrated radii are less strongly adsorbed than those with smaller hydrated radii. In solutions with equal initial concentration of different cations, the amounts of Ca and Mg adsorbed are several times greater than the amount of Na adsorbed. In general, polyvalent cations are adsorbed more strongly than monovalent cations and are not easily displaced by other cations. The order of adsorption strength is Al > Ca > Mg > H > K > Na (Duchaufour, 1970).

The flocculation/dispersion behavior of soil colloids depends on salt concentration, exchange complex cation, cation valence, and dominant clay mineralogy. In general, divalent cations are more effective in flocculating colloids than monovalent cations. For example, Quirk and Schofield (1955) found that the flocculating power of $CaCl_2$ is 50–100 times higher than that of NaCl. For monovalent cations, there is also a difference, with KCl showing greater flocculation power than NaCl (Pashley, 1981).

15.3.2.3 pH

The pH is an important determinant of the electrical potential of the clay surface. Changes in pH affect the edge charge on clays and the surface charge of variable charge minerals such as Fe and Al oxides. There is considerable variability depending on structural composition and degree of crystallinity, but Fe and Al oxides generally undergo a surface charge reversal around pH 7–9 (positively charged below that pH and negatively charged above). This is also the region in which kaolinite exhibits its edge charge reversal as evidenced by Cl^- adsorption studies (Schofield and Samson, 1954). Soil colloids consist of a mixture of minerals, each with a different p.z.c. At low pH, edge to face bonding, as well as bonding of positive Fe and Al oxides to negative clay surfaces, is expected to occur (van Olphen, 1977; Kretzschmar et al., 1993, 1997). This type of bonding should hinder dispersion and should thus result in flocculation. With increasing pH, as the p.z.c. is approached, edge to face clay bonding decreases and Fe and Al oxide bonding to clays is also expected to decrease (Suarez et al., 1984). In variable charge systems, flocculation is at a maximum at the p.z.c.

CCC increased at high SAR values with increasing pH for three soil clays whose clay mineralogy was dominantly kaolinite, montmorillonite, or illite (Goldberg and Forster, 1990). Hesterberg and Page (1990b) also found an increase in CCC for a Na- and a K-illite with increasing pH. Similar results were found for illite and three micaceous soil clays when SAR > 15 (Lebron and Suarez, 1992a, 1992b). The electrophoretic mobility of these materials increased when the SAR was greater than 20 and the pH was above the p.z.c. No pH effect was observed at SAR < 15 for either mobility or CCC.

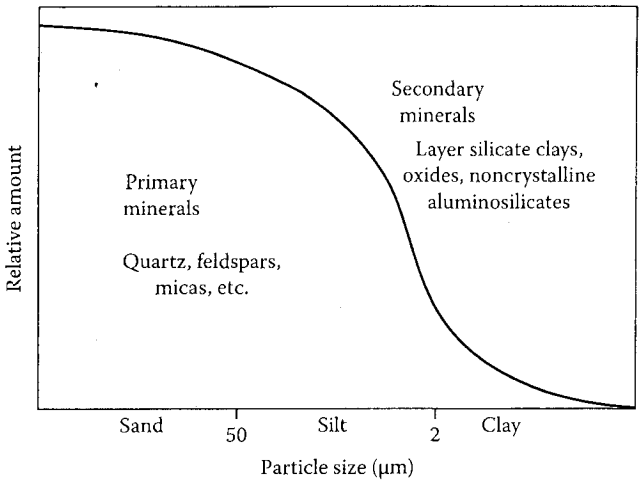

FIGURE 15.13 Typical abundance of primary and secondary minerals in different size fractions of the soil. (Reprinted from McBride, M.B. 1994. Environmental chemistry of soils. Oxford University Press, New York by permission of Oxford University Press.)

15.3.2.4 Mineralogy

The colloidal fraction of a soil consists primarily of secondary minerals (Figure 15.13). Layer silicate minerals differ in chemical composition and charge characteristics leading to different physicochemical behavior (Table 15.5). The stoichiometry of each mineral varies due to isomorphic substitutions in the crystal lattice during the formation or evolution of the mineral structure.

The siloxane (Si–O–Si) surfaces of 2:1 layer silicates without structural charge are hydrophobic. Therefore, the surface oxygens coordinated to Si show little tendency to hydrogen bond with water molecules. Smectites, such as montmorillonite, form weak hydrogen bonds between structural charge located mainly in the octahedral sheet and water. Such bonds are the result of the delocalization of some structural charge into the surface oxygens (Farmer, 1978). Smectites, such as beidellite, with a high proportion of charge in the tetrahedral sheet, form stronger hydrogen bonds. The siloxane surfaces of vermiculite are the most hydrophilic of the 2:1 layer silicate clays because they possess a large tetrahedral charge partially distributed onto surface oxygens (Farmer, 1978). Tetrahedral charge is much more localized on fewer surface oxygens than octahedral charge, explaining the stronger hydrogen bonding of adsorbed water on vermiculite (McBride, 1989). An extensive study of the structural characteristics of soil minerals can be found in Dixon and Weed (1989).

An example of how these mineral differences affect the flocculation/dispersion behavior of soil colloids is shown in Table 15.5. An overview of the data reveals that reported CCC values of kaolinite, montmorillonite, vermiculite, and illite are quite variable within and between these mineral groups.

Many of the differences in Table 15.5 are due to differences in methodology in the determination of CCC and/or differences in the stoichiometry of the silicate minerals. However, these factors do not account for all of the variability. Lebron and Suarez

(1992a) found substantial differences in CCC within samples from the same soil type. Differences in content of organic matter and other minerals can drastically change the behavior of soil colloids. Consequently, general guidelines for reclamation of agricultural land or the use of amendments to maintain colloids in a flocculated state must be implemented with caution because soils usually require higher electrolyte concentrations than the corresponding pure clay minerals to maintain a flocculated condition.

15.3.2.5 Organic Matter

Organic matter constitutes a small portion of the soil mass (0.5%–10%) but is intimately associated with inorganic particles and plays an important role in the improvement of soil structure (Nelson and Oades, 1998). Aeration, water-holding capacity, and permeability increase with increasing soil SOM content. However, adsorbed organic matter can promote dispersion of soil particles. Organic coatings, under certain conditions, maintain a dispersed state for soil colloids in suspension through a combination of electrostatic and steric mechanisms (Stevenson, 1982). Table 15.6 shows the spatial extensions for nonionic polymer molecules of different molecular weights. Like electrical double layers, macromolecules of at least a few thousand molecular weight also extend in space over distances comparable to, or greater than, the van der Waals attraction. In general, it has been shown that organic matter coatings modify the surface properties of minerals, increasing their CEC, generating hydrophobic and hydrophilic surfaces (Hunter, 1987), and significantly altering the point of zero net charge (p.z.n.c., pH at which the CEC and AEC are equal) (Heil and Sposito, 1993; Kaplan et al., 1997; Kretzschmar et al., 1997; Bertsch and Seaman, 1999).

Goldberg and Forster (1990) and Kretzschmar et al. (1993) found that the removal of SOM enhanced soil flocculation (decreased the CCC). Similarly, addition of small amounts of organic material substantially increased dispersion of Na-saturated soil or clay in the order: humic acid > soil polysaccharide ≥ anionic polysaccharide (Gu and Doner, 1993; Kretzschmar et al., 1997). Using smectite, kaolinite, and three soils whose clay fractions were dominated by one of these minerals, Frenkel et al. (1992) showed that the CCC values of Na-soils were much higher, and much more affected by organic matter than those of Ca-soils.

TABLE 15.6 Spatial Extensions of Electrical Double Layers and Polymers of Different Molecular Weight

1:1 Electrolyte Concentration (mol L^{-1})	Double-Layer Thickness, $1/\kappa$ (nm)	Polymer Molecular Weight	Spatial Extension (nm)
10^{-5}	100	1,000,000	60
10^{-4}	30	100,000	20
10^{-3}	10	10,000	6
10^{-2}	3	1000	2
10^{-1}	1		

Source: Reprinted from Hunter, R.J., *Foundations of Colloid Science*, Vol. 1, 1987 by permission of Oxford University Press.

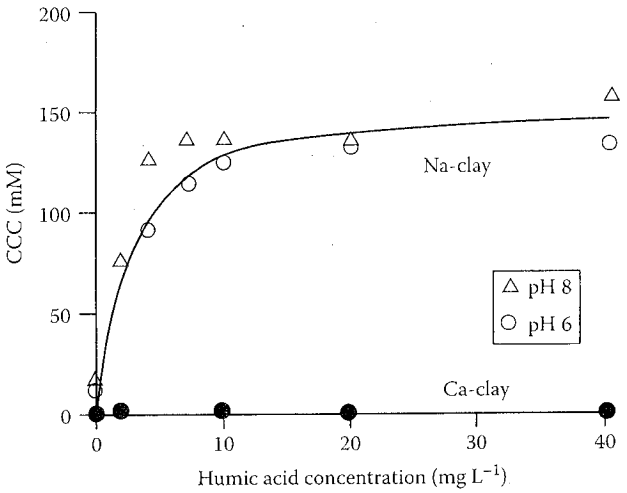

FIGURE 15.14 Effect of the humic acid concentration on the CCC of a Na-clay and a Ca-clay. (After Tarchitzky, J., Y. Chen, and A. Banin. 1993. Humic substances and pH effects on sodium and calcium-montmorillonite flocculation and dispersion. Soil Sci. Soc. Am. J. 57:367–372.)

Tarchitzky et al. (1993) showed similar comparisons between Na- and Ca-montmorillonite suspensions with varying additions of humic and fulvic acids (Figure 15.14). The effect of organic matter on stability of soil colloids is a function of its size. Large organic materials such as polysaccharides and hyphae act to bind colloid particles together. Small organic molecules such as fulvic acid and organic acids increase dispersion of soil colloids through their effect on particle charge. A more detailed review of organic matter chemistry and its effect on soils is provided in Stevenson (1982) and Nelson and Oades (1998).

15.3.3 Measurement of Colloidal Stability

15.3.3.1 Flocculation Series Test

CCC are commonly determined using the flocculation series test. The experiment can be performed by taking a series of test tubes containing the same concentration of the colloid and adding varying amounts of the coagulating electrolyte. The tubes are then shaken and allowed to stand for a given time. If the electrolyte range has been properly chosen, the CCC is defined as the concentration above which the settling material leaves behind a perfectly clear supernatant solution. Below the CCC, the supernatant retains some of the uncoagulated colloid. The concentration of colloidal particles at which the flocculation test must be performed should not exceed 10 g L^{-1}, thus avoiding interferences from different particle interactions such as gel formation.

15.3.3.2 Dispersion Indices

There are several methods (qualitative, semiquantitative, and quantitative) to determine the dispersion or flocculation status of soil colloids. Qualitative analyses of the dispersion state are those based on direct observation of small particles when the soil is immersed in water. This observation can be made with the optical microscope or with the naked eye, as is the case for

the test of Emerson (1967). Methods based on turbidity of a suspension of dispersed soil can be considered semiquantitative when comparative measurements are made. Normally, a standard curve is constructed using known amounts of dispersed clay. The soil under evaluation is assigned a dispersion value by comparison with the standard. The most commonly used quantitative method to determine soil flocculation state is the dispersion index. This index is the ratio of the amount of soil colloids in water to the amount of soil colloids in solution when the soil has been treated with a dispersant. This procedure is recommended by the Soil Conservation Service (Sherard et al., 1977). Different variations regarding particle size, dispersing agent, and manipulation of samples are found in the methods proposed by El-Swaify et al. (1970) and Dong et al. (1983), among others.

15.3.3.3 Bingham Yield Stress

Rheology is the study of the flow and deformation of colloidal systems under the influence of mechanical forces (van Olphen, 1977). A Newtonian liquid when confined between two parallel plates moves at a constant shear rate ($\dot{\gamma}$) proportional to the applied shear stress (τ):

$$\tau = \eta\dot{\gamma} \tag{15.36}$$

Non-Newtonian fluids obey different relations between shear stress and shear rate. Plastic flow is flow that occurs only above a certain finite stress (τ_0) called the yield stress. Ideal plastic flow exhibits a linear relationship between shear rate and shear stress over all rates of shear. Many colloidal dispersions exhibit Bingham flow, which is characterized by the equation

$$\tau = \tau_B - \eta_\Delta\dot{\gamma} \tag{15.37}$$

where

τ_B is the Bingham yield stress found by extrapolating Equation 15.37 to zero shear rate

η_Δ is the differential or plastic viscosity

The differential viscosity is the derivative of shear stress with respect to shear rate at a given shear rate (van Olphen, 1977). Shear rate versus shear stress relationships for Newtonian flow, ideal plastic flow, and Bingham flow are presented in Figure 15.15.

Bingham yield stress is a measure of the degree of coagulation of a colloidal suspension and the mode of particle interaction. Bingham yield stress is a function of both the number of particle–particle linkages in the coagulated structure and the energy required to break these linkages (Rand and Melton, 1977). A stable clay dispersion exhibits ideal plastic flow, while flocculated suspensions exhibit Bingham flow as can be seen in Figure 15.16 for kaolinite. Differential viscosity can also be used to assess the extent of particle flocculation, but it is a much less sensitive parameter than Bingham yield stress (Heath and Tadros, 1983).

Rheological studies have been carried out on kaolinite (Flegman et al., 1969; Rand and Melton, 1977; Yong et al., 1979; Diz and Rand, 1989; Ma and Pierre, 1999), illite (Yong et al., 1979;

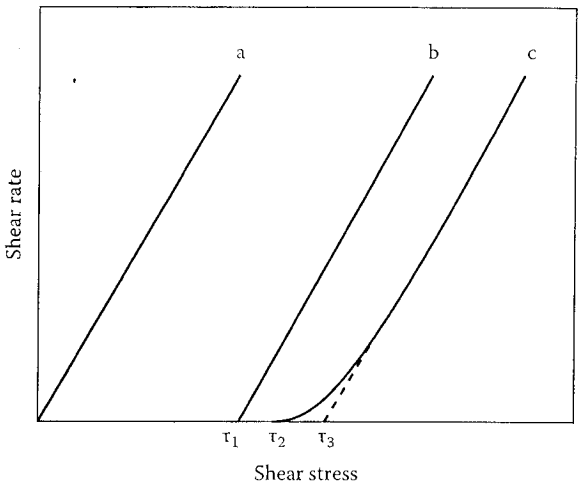

FIGURE 15.15 Shear rate versus shear stress relationships. Curve a represents Newtonian flow, curve b represents ideal plastic flow, and curve c represents Bingham flow. (Adapted from van Olphen, H. 1977. An introduction to clay colloid chemistry, 2nd Ed. John Wiley & Sons, New York.)

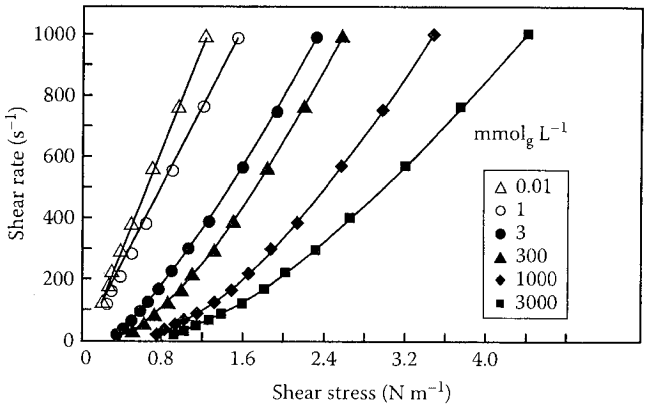

FIGURE 15.16 Shear rate versus shear stress for Na-kaolinite. The open symbols represent dispersed systems and ideal plastic flow. The closed symbols represent coagulated systems and Bingham flow. (Adapted from Yong, R.N., A.J. Sadh, H.P. Ludwig, and M.A. Jorgensen. 1979. Interparticle action and rheology of dispersive clays. J. Geotech. Eng. Div. 105:1193–1209.)

Ohtsubo et al., 1991; Hesterberg and Page, 1993), montmorillonite (Rand et al., 1980; Heath and Tadros, 1983; Keren, 1988, 1989a; Tombácz et al., 1989; Miano and Rabaioli, 1994; Benna et al., 1999; Duran et al., 2000), laponite (Laxton and Berg, 2006), clay mixtures (Yong et al., 1979; Keren, 1989b, 1991), soil clays (Zhao et al., 1991), and soils (Ghezzehei and Or, 2001; Markgraf et al., 2006). A series of curves of Bingham yield stress as a function of pH obtained at successively increasing electrolyte concentration should coincide at one point. This point is characteristic of the pH value of the edge p.z.c. of the mineral (Rand and Melton, 1977). Edge p.z.c. values have been determined in this manner for various kaolinites and range in value from pH 5.6 to 8.8 (Diz and Rand, 1989). Kaolinite particles occur in edge–face associations below the edge p.z.c. and in edge–edge associations around the edge p.z.c. (Rand and Melton, 1977).

Montmorillonite exhibits no edge–face associations over the pH range 4–11; coagulation produced by electrolyte additions is initially the result of edge–edge interactions with face–face interactions occurring at high-electrolyte concentrations (Rand et al., 1980). No edge p.z.c. could be determined on montmorillonite using this method. This is likely because the edge area is small and attraction between edges and faces is small compared to repulsion between faces (Rand et al., 1980). From yield stress and electrophoretic mobility measurements determined without electrolyte addition, Benna et al. (1999) suggested that the p.z.c. of three bentonites occurred in the pH range of 7.5–8.5.

In distilled water, Ca-montmorillonite exhibited Newtonian flow. With increasing exchangeable sodium percentage (ESP), differential viscosity, deviation from Newtonian flow, and Bingham yield stress of montmorillonite all increased (Keren, 1988). These increases are likely due to the increased number of particles in solution as tactoids break down. Differential viscosity and Bingham yield stress decreased with increasing electrostatic charge density of smectites (Keren, 1989a). This result is attributed to the reduced swelling of higher charge density smectites. Kaolinite exhibited Newtonian flow at all ESPs. The introduction of even 5% montmorillonite into the kaolinite systems resulted in deviations from Newtonian flow and increased differential viscosity (Keren, 1989b). Bingham yield stress and deviations from Newtonian flow of kaolinite–montmorillonite mixtures also increased with ESP (Keren, 1991). Bingham yield stress of kaolinite, Ca-montmorillonite, Na-montmorillonite, and two soils increased exponentially with decreasing water content (Ghezzehei and Or, 2001).

15.4 Colloid Transport

As previously discussed, colloidal materials found in soils include phyllosilicate clays, Al, Fe, and other metal oxides, carbonate minerals, microorganisms, and other biological debris, much of which falls into the "nanoparticle" size range (see Section 15.1.2). The fundamental processes involved in colloid migration in the soil environment include mobilization, transport, and deposition, representing primarily a balance between the two opposing processes of colloid mobilization and deposition. The study of colloid transport in the subsurface environment has received considerable attention in recent years because of concern that mobile colloids may enhance the mobility of strongly sorbing contaminants (i.e., facilitated transport) and alter the hydraulic properties of soil and aquifer materials. In addition, the migration of biocolloids such as bacteria and viruses has important implications to in situ bioremediation, the protection of drinking water supplies, and the spread of disease (Khilar and Fogler, 1984; McDowell-Boyer et al., 1986; Kia et al., 1987; Ryan and Elimelech, 1996; Kretzschmar et al., 1999; de Jonge et al., 2004b; McCarthy and McKay, 2004; Tufenkji, 2007). However, our ability to predict colloid movement and deposition is often confounded by the complexities of surface interactions in such heterogeneous natural systems. Understanding colloid transport requires consideration not only of the chemical and biological processes and reactions but also of the physical principles of filtration and deposition in porous media.

Several mechanisms have been identified by which colloidal materials can be mobilized in the soil environment (Figure 15.17) including clay dispersion resulting from changes in pore-water chemistry that increase electrostatic repulsion between the colloid and collector surfaces, water film expansion and air–water interface scouring during episodic wetting events (imbibition), raindrop impact at the soil surface, and increased shear forces associated with transient hydrodynamic events (i.e., precipitation, groundwater pumping, subsurface recharge injection). Mobile colloids can also be formed in situ through precipitation reactions resulting from changes in pore-water chemistry. Clearly, colloid mobilization is associated with a physical and/or chemical perturbation sufficient to overcome the energy barrier limiting particle detachment (McCarthy and Degueldre, 1993; Ryan and Elimelech, 1996; DeNovio et al., 2004).

Compared to saturated aquifer systems, chemical and physical perturbations are common within the soil environment, with the presence of air providing an additional system interface for colloid partitioning (Wan and Wilson, 1994; Sirivithayapakorn and Keller, 2003). The presence of a dynamic air–water interface and fluctuating chemical and hydrological conditions complicate our understanding of colloid transport processes in the soil and vadose environments (Bradford and Torkzaban, 2008). Preferential flow paths can increase the mobility of colloidal material in close proximity to the pathway, while limiting the reactivity of colloidal sorbents isolated from the flow path (DeNovio et al., 2004; McCarthy and McKay, 2004).

The energy barrier limiting colloid detachment is the difference between the interaction minimum and the maximum energy potential described in Figure 15.12. In terms of chemical perturbations, soil colloid mobilization can result from changes in pore-water pH, ionic strength, and/or Na^+/Ca^{2+} ratios (McDowell-Boyer, 1992; Ryan and Gschwend, 1994; Gamerdinger and Kaplan, 2001; Bunn et al., 2002; Khaleel et al., 2002; McCarthy et al., 2002; Grolimund and Borkovec, 2006), alteration of surface charge resulting from a chemical dispersing agent or dissolved organic matter (Ryan and Gschwend, 1994; Seaman and Bertsch, 2000; Johnson et al., 2001), or dissolution of carbonate or Fe cementing agents resulting in the release and transport of silicate clays (Gschwend et al., 1990; Ryan and Gschwend, 1990; Ronen et al., 1992; Swartz and Gschwend, 1998). Furthermore, potentially mobile colloids may precipitate in situ due to altered chemical gradients (Gschwend and Reynolds, 1987; Mashal et al., 2004). In many instances, more than one of the mechanisms may be operative in order to trigger significant colloid mobilization, such as a change in pore-water chemistry that reduces particle attraction combined with an increase in pore-water velocity and shear forces.

Under ideal laminar flow conditions, the hydrodynamic shear force acting on a spherical particle attached to a flat surface can be expressed as follows:

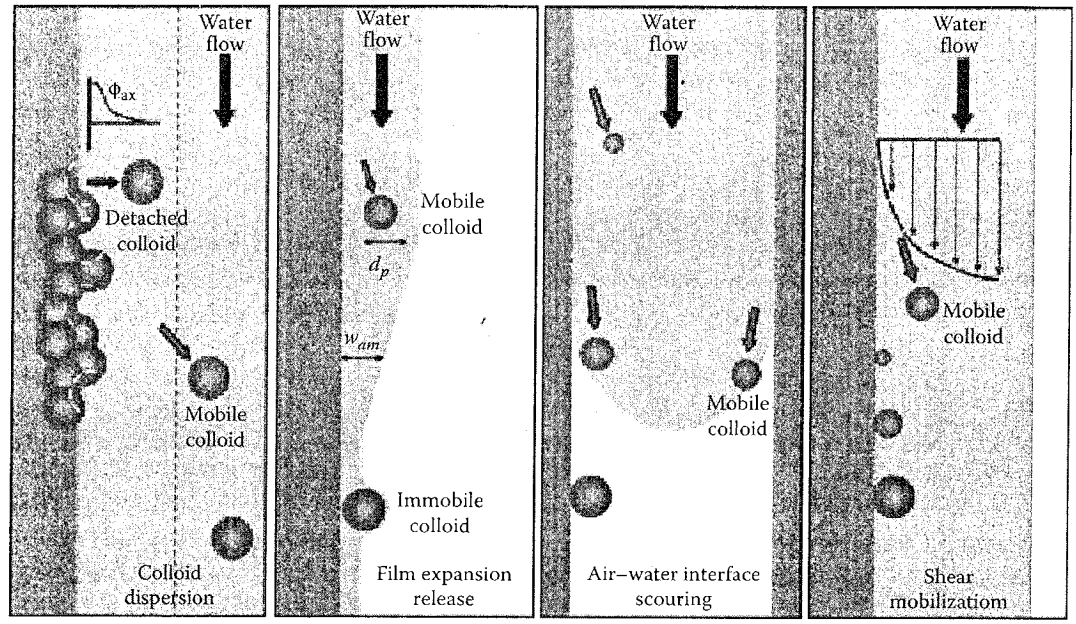

(a)

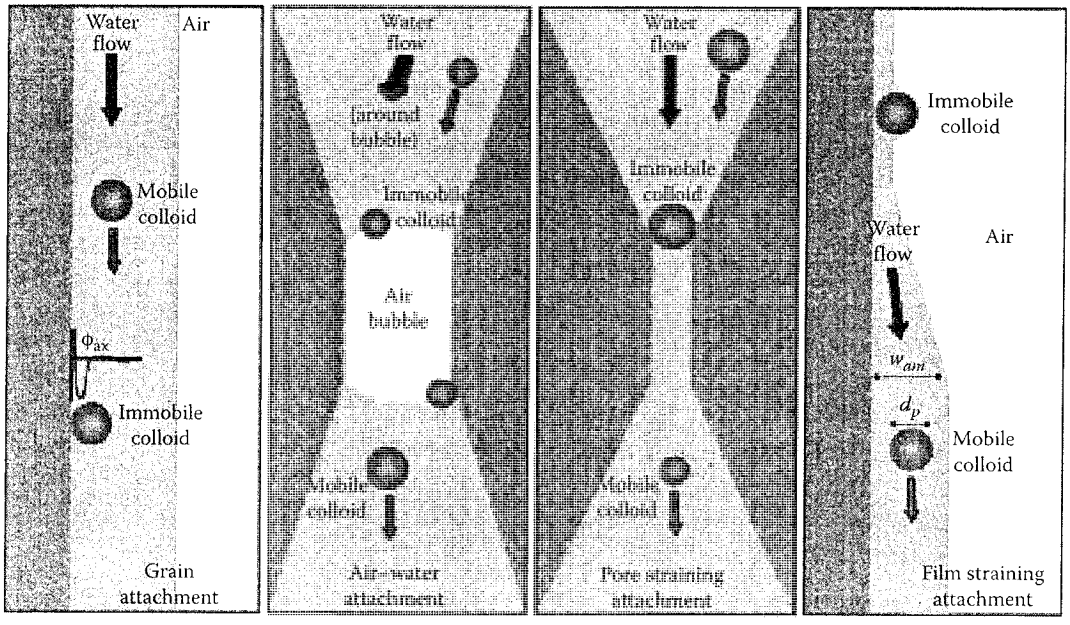

(b)

FIGURE 15.17 Colloid mobilization (a) mechanisms include dispersion due to chemical perturbation, expansion of water film during imbibition, air–water interface scouring and shear mobilization. Colloid deposition (b) mechanisms include attachment associated with physicochemical filtration, attachment to the air–water interface, physical pore straining, and water film straining. (Adapted from DeNovio, N.M., J.E. Saiers, and J.N. Ryan. 2004. Colloid movement in unsaturated porous media: Recent advances and future directions. Vadose Zone J. 3:338–351.)

$$F_{shear} = (1.7)6\pi\mu r V \tag{15.38}$$

where

V is the flow velocity at the center of the particle

μ is the fluid viscosity

r is the particle radius (Sharma et al., 1992; Ryan and Elimelech, 1996; Ryan et al., 1998; DeNovio et al., 2004)

Adhesive forces that oppose shear stress are subject to changes in solution chemistry. The critical velocity for particle release decreases with increasing particle size, even though the required hydrodynamic force increases for non-Brownian particles, that is, >1 μm in diameter (Sharma et al., 1992). As one might expect, the amount of particles mobilized should generally increase with increasing flow velocity, but greater flow velocities are required to mobilize smaller particles that extend to a lesser degree into

the advective stream. However, many assumptions inherent in applying such a physical approach to soil and aquifer systems are likely in question. In more realistic systems, interrelated factors such as contact area, adhesion strength, and surface charge heterogeneity are important in countering shear forces (Sharma et al., 1992).

In addition to the chemical factors affecting colloid stability, transport of colloids is related to soil physical factors such as pore size distribution, geometry, and continuity (Torkzaban et al., 2008; Bradford et al., 2009). Coarse-textured soils have a larger distribution of pore sizes (with larger pores) than fine-textured soils, suggesting greater potential for colloid movement. This is not generalizable since some fine-textured materials experience cracking and formation of continuous structural macropores that provide a preferential pathway for colloid transport.

15.4.1 Colloid Transport Modeling

Physical and chemical processes affect the transport of soil colloids. Colloid transport can be represented by the physical processes of molecular diffusion (Brownian movement), advective flow, and gravitational forces. Molecular diffusion, the random motion of particles caused by thermal effects, is related to temperature and viscosity. Deposition is the process whereby moving particles are attached to stationary surfaces based on the balance of attractive and repulsive forces, that is, attractive van der Waals forces and the combined influence of attractive and repulsive electrostatic forces, as described by DLVO theory of colloid stability (see Sections 15.2.2, 15.2.3, and 15.3.1).

The attachment process involves two steps: transport to the collector surface and attachment that binds the two surfaces together. The transport step reflects a combination of diffusion, convection, and gravity, with electrostatic and van der Waals forces controlling colloid binding. Models used in describing colloid transport are typically extensions of the advection dispersion equation (ADE) for describing solute movement in a homogeneous saturated porous medium:

$$\frac{\partial C}{\partial t} + \frac{\rho_b}{\theta}\frac{\partial S}{\partial t} = D\frac{\partial^2 C}{\partial x^2} - v\frac{\partial C}{\partial x} \tag{15.39}$$

where

C is the aqueous phase concentration for the solute or suspended colloidal material of interest
x is distance
t is time
D is the hydrodynamic dispersion coefficient
v is the pore-water velocity
S is the sorbed concentration of colloids or solutes
ρ_b is the matrix bulk density
θ is the volumetric water content (Grolimund and Borkovec, 2001; Bradford et al., 2003; Tufenkji, 2007)

Hydrodynamic dispersion and dispersivity appear to decrease with increasing particle size (Sinton et al., 2000; Auset and Keller, 2004). As the colloidal material moves through porous medium, it may be removed from solution by various physicochemical filtration processes, with various expressions, such as the equilibrium partitioning (K_{eq}), used to describe reversible colloid attachment processes in a manner analogous to the equilibrium partitioning of solutes. Using a numerical solution to the ADE, equilibrium partitioning can be modified to reflect any one of a variety of phenomenological equilibrium partitioning expressions, that is, Freundlich, Langmuir, etc.

In contrast to equilibrium partitioning, colloid attachment is more often viewed as a kinetically controlled process with terms accounting for both attachment (k_{att}) and detachment (k_{det}) rates:

$$\frac{\rho_b}{\theta}\frac{\partial S}{\partial t} = k_{att}C - \frac{\rho_b}{\theta}k_{det}S \tag{15.40}$$

yielding an expression that is mathematically equivalent to the reversible first-order kinetic equation for partitioning solutes. Ripening and blocking are terms that are used to describe an increase or decrease in colloid attachment efficiency (i.e., k_{att} and k_{det}) with time or distance.

Figure 15.18 illustrates colloid breakthrough behavior for irreversible (Figure 15.18a) and reversible (Figure 15.18b) attachment kinetics. Colloid attachment is commonly assumed to be irreversible (i.e., $k_{det} = 0$) as described by clean-bed colloid filtration theory (CFT) (O'Melia and Tiller, 1993; Bradford et al., 2003; Simunek et al., 2006; Tufenkji, 2007). For irreversible attachment (i.e., CFT), the kinetic rate coefficient determines the plateau level of colloid breakthrough, while more complex breakthrough behavior is observed when both attachment and detachment occur at differing rates. When $k_{att} = k_{det}$, colloid behavior becomes analogous to that of a conservative tracer, that is, $R = 1$. Colloid retention profiles for irreversible attachment (Figure 15.18c) remain unchanged after the inlet colloid source is removed and an exponential decrease in retained colloids is observed with transport distance. Again, a more complex colloid retention profile is observed for reversible attachment that depends on both the forward and reverse rate coefficients and the treatment duration (Figure 15.18d).

The irreversible colloid attachment/depositional rate constant for a clean-bed filter is

$$k_{att} = \frac{3(1-\theta)v}{2d_c}\eta_0\alpha \tag{15.41}$$

where

d_c is the average grain size of the matrix
η_0 is the collector contact efficiency for the three transport mechanisms (diffusion, gravity, convection)
α is the attachment efficiency (Yao et al., 1971; Bradford et al., 2003; Li et al., 2004)

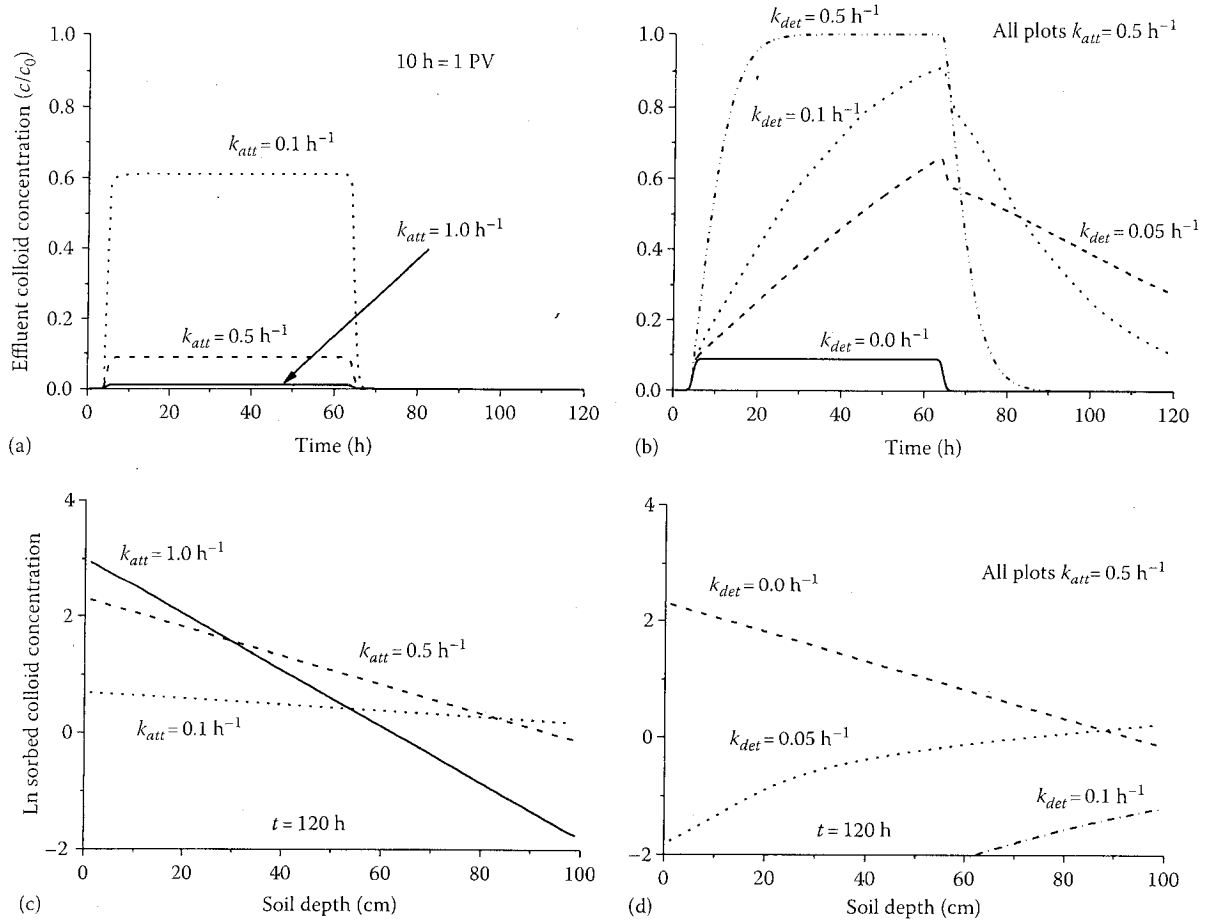

FIGURE 15.18 Simulated colloid breakthrough for a 1 m column with a saturated flow velocity of 2.4 m day^{-1} (θ = 0.5, DL = 0.01 m) exposed to a 60 h colloid pulse with kinetically controlled attachment (a = clean-bed filtration theory), and kinetically controlled attachment and detachment (b). Retained colloid profile for irreversible (c), and reversible attachment (d) after 60 h colloid pulse followed by 60 h of colloid-free inlet solution.

The collector efficiency reflects the colloid collisions with the stationary matrix resulting from diffusion, advective flow, and gravitational forces, and can be calculated (Tufenkji and Elimelech, 2004a). The attachment efficiency term (α) is generally determined experimentally by fitting colloid breakthrough results to the CFT model based on k_{att} and the calculated η (O'Melia and Tiller, 1993; Elimelech et al., 2000; Bradford et al., 2004; Tufenkji and Elimelech, 2004a; Tufenkji, 2007). Additional mechanisms of material loss, such as cell motility, growth, and inactivation, must also be considered when evaluating the transport of microbes. Furthermore, research in the last decade has demonstrated the importance of surface biomolecules, which can vary in response to the local environment, and among microbial strains and species in controlling their adhesion properties (Bolster et al., 2000; Walker et al., 2004; Tufenkji, 2007).

Studies using model colloidal systems indicate that CFT is generally applicable under conditions favoring particle attachment, that is, no significant electrostatic repulsion. However, the CFT approach fails in describing experimental data under apparently unfavorable conditions when significant electrostatic repulsion exists between the mobile colloid and matrix grain surface. For particles with the same charge, a deep primary attractive force exists at very short separation distances, known as the primary minimum (Figure 15.12). However, electrostatic repulsion supposedly limits particle approach in a manner similar to chemical activation energies. Such discrepancies in deposition studies, and in batch aggregation experiments, have been attributed to porous media heterogeneity that can be difficult to quantify experimentally (i.e., grain size, morphology, and surface charge) and a secondary energy minimum that favors colloid sorption without the necessity to overcome the full electrostatic repulsion required to enter the primary minimum (Figure 15.12), resulting in an apparent change in the attachment rate coefficient (k_{att}) with transport distance (Roy and Dzombak, 1996; Elimelech et al., 2000; Chen et al., 2001; Bradford et al., 2002, 2003; Tufenkji et al., 2003; Hahn and O'Melia, 2004; Li et al., 2004; Redman et al., 2004; Tufenkji and Elimelech, 2005; Tufenkji, 2007). The secondary minimum reflects the exponential decay in electrostatic forces with separation distance, in contrast to van der Waals forces that decrease more slowly with distance. The inability to remobilize particles trapped within the "secondary" minimum by altering solution chemistry, that is, reducing ionic strength, further demonstrates the hydrodynamic

and physicochemical complexity of colloid retention mechanisms (Bradford and Torkzaban, 2008; Torkzaban et al., 2008; Bradford et al., 2009).

Verifying the spatial distribution of retained colloids based on the attachment parameter (α_{BTC}) derived from effluent breakthrough data is a good method for testing the validity of the CFT model. In many instances, the slope of the relationship is greater than CFT predictions, indicating higher initial colloid retention that decreases with increasing transport distance (Li et al., 2004; Tufenkji, 2007). Such discrepancies have been addressed through the use of multiple deposition rate constants, that is, a fast and a slow rate, or a defined statistical distribution of randomly assigned particle deposition rates that reflect the inherent variability in colloidal surface potentials (Li et al., 2004; Tufenkji and Elimelech, 2004b; Tufenkji, 2007). It is interesting to note that the statistical distribution in observed deposition rate coefficients appears to narrow as colloid deposition becomes more favorable, for example, reduced flow velocities and increased ionic strengths (Li et al., 2004).

Attachment kinetics are highly sensitive to colloid–collector interaction potentials. Moderate changes with respect to colloid surface potentials can result in relatively large changes in collision efficiency and attachment rate (Elimelech and O'Melia, 1990; Ryan and Elimelech, 1996; Elimelech et al., 2000; Li et al., 2004). Deviation from the breakthrough plateau with time is indicative of a change in the colloid deposition efficiency during the course of injection, that is, filter ripening or blocking. In addition, surface modifiers such as Fe oxides and soil organics, often present in relatively minor amounts, can alter the expression of electrostatic repulsion on soil mineral surfaces (Goldberg and Forster, 1990; Kretzschmar et al., 1993; Kaplan et al., 1993, 1997; Bertsch and Seaman, 1999; Franchi and O'Melia, 2003; Seaman et al., 1995, 2003).

Recent studies indicate that pore structure and particle straining may also be more significant than previously recognized for intermediate colloid and matrix grain sizes. Colloid straining, trapping colloids in pore regions that are too small to permit passage, is generally considered to be an irreversible process. Within a transport model, straining can be addressed by including an additional first-order expression to the deposition equation given above. In the absence of colloid detachment, the kinetic deposition model accounting for colloid straining becomes

$$\frac{\rho_b}{\theta}\frac{\partial S}{\partial t} = k_{att}C - k_{str}\psi_{str}C \tag{15.42}$$

where

k_{str} is the straining rate constant

ψ_{str} is the depth-dependent colloid straining function (Bradford et al., 2002, 2003, 2004)

In contrast to straining, traditionally considered a physical phenomenon insensitive to solution chemistry, recent hydrodynamic modeling efforts have verified particle capture within hydrodynamically disconnected regions of the porous matrix near two collector particle surfaces where the magnitude of fluid velocity is quite small compared to the bulk solution, analogous to the "immobile" regions evident in solute transport behavior. Within the immobile regions, greater colloid/colloid and colloid/collector surface interactions lead to enhanced colloid immobilization in a manner that depends on both solution chemistry and pore geometry. Furthermore, particles weakly retained in the secondary minimum can be subsequently funneled to the immobile capture regions by hydrodynamic forces that are insufficient to induce full colloid detachment (Bradford and Torkzaban, 2008; Torkzaban et al., 2008; Bradford et al., 2009).

15.4.2 Colloid-Mediated Contaminant Transport

Numerous studies have established that organic and inorganic chemicals, which are highly sorbed onto soil nonetheless, are often transported in the subsurface to a greater degree than expected. Such anomalies have been attributed to kinetic effects associated with nonequilibrium sorption and bypass flow, as well as contaminant transport associated with a mobile colloidal fraction that enhances apparent migration beyond the levels controlled by thermodynamically based solubilities or partitioning reactions. Furthermore, colloidal materials may move at rates that are similar or faster than those of nonreactive solute tracers because of physical size or electrostatic exclusion from a fraction of the saturated pore space (Simunek et al., 2006). In general, colloid-facilitated transport is only significant when the contaminant is strongly sorbed to the mobile colloidal phase, approaching irreversible partitioning. Otherwise, the sorbed contaminant will desorb in response to the decrease in the aqueous phase contaminant concentration when the colloidal phase travels faster than the aqueous phase (Grolimund and Borkovec, 2005).

Models that include colloid-facilitated transport generally differ in the manner in which they account for the various colloid release and attachment processes described in Section 15.4.1 (i.e., reversible vs. irreversible attachment, kinetic vs. equilibrium) (Mills et al., 1991; Dunnivant et al., 1992; Corapcioglu and Jiang, 1993; Grolimund and Borkovec, 2005) with additional equilibrium or kinetic expressions used to account for contaminant–colloid interactions. Only recently have models been developed that address partially saturated conditions, colloid straining, and size exclusion (Simunek et al., 2006). The development of such a contaminant transport model, while requiring numerous simplifying assumptions (van de Weerd and Leijnse, 1997; Simunek et al., 2006), still results in a significant list of parameters required to account for both contaminant sorption and colloid attachment. For example, transport and mass balance expressions must account for the aqueous phase contaminant, contaminant sorbed to the immobile matrix, contaminant sorbed to the mobile colloids, and contaminant sorbed to colloids immobilized by various mechanisms, that is, stationary phase attachment, air–water interphase attachment, and straining. Additional expressions are required to account for colloid mass balance as well, illustrating the potential level of model

complexity. Simunek et al. (2006) recommend the use of sensitivity analysis to discern the relative importance of such variables in accurately describing contaminant fate and transport.

Although subject to numerous sampling artifacts, significant concentrations of mobile colloids have been observed in soil and groundwater systems (Ronen et al., 1992; McCarthy and Degueldre, 1993; DeNovio et al., 2004). However, contaminant transport models generally fail to account for the impact of mobile colloids in facilitating the transport of strongly sorbing contaminants. For example, colloid-facilitated transport has been implicated in the migration of organic contaminants (e.g., atrazine, prochloraz, and dichlorodiphenyltrichloroethane [DDT]) (Vinten et al., 1983; Seta and Karathanasis, 1996; Seta and Karathanasis, 1997; de Jonge et al., 1998; Roy and Dzombak, 1998), metals (e.g., Pb, Ni, Cu, and Zn) (Kaplan et al., 1994b, 1995; Grolimund et al., 1996; Roy and Dzombak, 1997; Karathanasis, 1999; Grolimund and Borkovec, 2005; Karathanasis et al., 2005), radionuclides (e.g., ^{137}Cs) (Von Gunten et al., 1988; Kaplan et al., 1994a; Kersting et al., 1999; Flury et al., 2002), and sparingly soluble nutrients, such as phosphate (de Jonge et al., 2004b). Some of the general issues concerning contaminant migration via colloid-facilitated transport are discussed by McDowell-Boyer et al. (1986), McCarthy and Zachara (1989), Ryan and Elimelech (1996), and Kretzschmar et al. (1999).

15.4.3 Effect of Colloid Transport on Hydraulic Conductivity and Soil Formation

Some degree of colloid movement is generally considered a major factor in soil profile development. However, dispersion and transport of soil colloids have been linked to soil crust formation, reduced infiltration and hydraulic conductivity, and erosion (Shainberg et al., 1981; Miller and Baharuddin, 1986; Miller and Radcliffe, 1992). Reductions in hydraulic conductivity caused by colloid transport can be divided into two groups: formation of crusts and migration and deposition within the medium. Crust formation results when the colloids are not able to enter the soil media and form a compact layer above the soil. Alternatively, the particles may enter the medium, flow with the water in a suspension, and be deposited within the medium. This process may result from either mechanical filtration of large colloids or physicochemical processes of attraction/repulsion of small colloids as discussed above (see Section 15.4.1).

Research in soil science related to the effects of colloid transport on hydraulic conductivity has focused primarily on description of the chemical process affecting clay movement, rather than on mathematical expressions for prediction of flow rates. Conditions of low ionic strength, high exchangeable Na, and elevated pH were related to both dispersion of clays (Suarez et al., 1984; Goldberg and Forster, 1990; Miller et al., 1990) and subsequent migration and reduction in soil hydraulic conductivity (Suarez et al., 1984). In highly weathered acid soils where positively charged colloids are important, Seaman et al. (1995, 1997) determined that addition of $CaCl_2$ initially enhanced colloid mobility, likely due to release of exchangeable Al and a decrease in pH.

Soil profile development is often affected by colloid movement. Among these processes are the formation of impermeable clay layers in the subsurface and movement of Fe and Al, most probably as organic metal complexes. Moderately to strongly developed soils are generally characterized by depleted clay contents in the A horizon and larger amounts of clay generally in the upper portion of the B horizon. A substantial portion of the argillic B horizon is related to migration of clays from the upper portion of the profile and subsequent deposition (Birkeland, 1974). Flocculation in the lower part of the profile is enhanced by increased electrolyte concentration relative to the surface horizons. Clay colloid migration is evident by the presence of clay films over ped surfaces and inside voids and presence of oriented clay particles. This process is also observed in aridisols where low organic matter and elevated exchangeable Na enhance colloid transport. Clay deposition is enhanced by increasing electrolyte concentration and removal of water by evapotranspiration. In general, formation of argillic horizons requires that the soil be at least partially dry during some part of the season.

Formation of Fe- and Al-rich layers by translocation (podzolization) is probably caused by transport of metal–fulvic acid complexes, rather than movement of the dissolved metals. The spodic B horizon marks the location at which these chelates either flocculate due to increases in electrolyte concentration or by decomposition of the organic matter (Birkeland, 1974).

References

Adamson, A.W. 1976. Physical chemistry of surfaces, 3rd Ed. John Wiley & Sons, New York.

Appel, C., L.Q. Ma, R.D. Rhue, and E. Kennelley. 2003. Point of zero charge determination in soils and minerals via traditional methods and detection of electroacoustic mobility. Geoderma 113:77–93.

Aringhieri, R., G. Pardini, M. Gispert, and A. Sole. 1992. Testing a simple methylene blue method for surface area estimation in soils. Agrochimica 36:224–232.

Auset, M., and A.A. Keller. 2004. Pore-scale processes that control dispersion of colloids in saturated porous media. Water Resour. Res. 40:W03503, 1–11.

Babcock, K.L. 1963. Theory of chemical properties of soil colloidal systems at equilibrium. Hilgardia 34:417–542.

Babick, F., F. Hinze, and S. Ripperger. 2000. Dependence of ultrasonic attenuation on the material properties. Colloids Surf. A 172:33–46.

Babick, F., and S. Ripperger. 2002. Information content of acoustic attenuation spectra. Part. Part. Syst. Charact. 19:176–185.

Balnois, E., G. Papastavrou, and K.J. Wilkinson. 2007. Force microscopy and force measurements of environmental colloids, p. 405–467. *In* K.J. Wilkinson and J.R. Lead (eds.) Environmental colloids and particles: Behavior, structure and characterization. IUPAC series on analytical and physical chemistry of environmental systems. John Wiley & Sons, Chichester, U.K.

Bar-on, P., I. Shainberg, and I. Michaeli. 1970. Electrophoretic mobility of montmorillonite particles saturated with Na/Ca ions. J. Colloid Interface Sci. 33:471–472.

Baumann, T., and C.J. Werth. 2004. Visualization and modeling of polystyrol colloid transport in a silicon micromodel. Vadose Zone J. 3:434–443.

Beckett, R. 1991. Field-flow fractionation-ICP-MS: A powerful new analytical tool for characterizing macromolecules and particles. Atomic Spectrosc. 12:215–246.

Beckett, R., and B.T. Hart. 1993. Use of field-flow fractionation techniques to characterize aquatic particles, colloids and macromolecules, p. 165–205. *In* J. Buffle and H.P. van Leeuwen (eds.) Environmental particles, Vol. 2. Lewis Publishers, Ann Arbor, MI.

Beckett, R., D. Murphy, S. Tadjiki, D.J. Chittleborough, J.C. Giddings. 1997. Determination of thickness, aspect ratio and size distribution for platey particles using sedimentation field-flow fractionation and electron microscopy. Colloids Surf. A 120:17–26.

Benna, M., N. Kbir-Ariguib, A. Magnin, and F. Bergaya. 1999. Effect of pH on rheological properties of purified sodium bentonite suspensions. J. Colloid Interface Sci. 218:442–455.

Bertsch, P.M., and J.C. Seaman. 1999. Characterization of complex minerals assemblages: Implications for contaminant transport and environmental remediation. PNAS 96:3350–3357.

Bertuzzo, E., S. Azaele, A. Maritan, M. Gatto, I. Rodriguez-Iturbe, and A. Rinaldo. 2008. On the space-time evolution of a cholera epidemic. Water Resour. Res. W01424, doi: 10.1029/2007WR006211.

Birkeland, P.W. 1974. Pedology, weathering, and geomorphological research. Oxford University Press, New York.

Blo, G., C. Contado, F. Fagioli, M.H. Bollain-Rodriguez, and F. Dondi. 1995. Analysis of kaolin by sedimentation field-flow fractionation and electrothermal atomic absorption spectrometry detection. Chromatographia 41:715–721.

Bohn, H.L., B.L. McNeal, and G.A. O'Connor. 1985. Soil chemistry. John Wiley & Sons, New York.

Bolster, C.H., A.L. Mills, G. Hornberger, and J. Herman. 2000. Effect of intra-population variability on the long-distance transport of bacteria. Ground Water 38:370–375.

Borchardt, G.A. 1977. Montmorillonite and other smectite minerals, p. 293–330. *In* J.B. Dixon and S.B. Weed (eds.) Minerals in soil environments. SSSA, Madison, WI.

Borkovec, M., Q. Wu, G. Degovics, P. Laggner, and H. Sticher. 1993. Surface area and size distribution of soil particles. Colloids Surf. A 73:65–76.

Bower, C.A., and J.O. Goertzen. 1959. Surface area of soils by an equilibrium ethylene glycol method. Soil Sci. 87:289–292.

Bradford, S.A., M. Bettahar, J. Simunek, and M.T. van Genuchten. 2004. Straining and attachment of colloids in physically heterogeneous porous media. Vadose Zone J. 3:384–394.

Bradford, S.A., J. Simunek, M. Bettahar, M.T. van Genuchten, and S.R. Yates. 2003. Modeling colloid attachment, straining, and exclusion in saturated porous media. Environ. Sci. Technol. 37:2242–2250.

Bradford, S.A., and S. Torkzaban. 2008. Colloid transport and retention in unsaturated porous media: A review of interface-, collector-, and pore-scale processes and models. Vadose Zone J. 7:667–681.

Bradford, S.A., S. Torkzaban, F. Leij, J. Simunek, and M.T. van Genuchten. 2009. Modeling the coupled effects of pore space geometry and velocity on colloid transport and retention. Water Resour. Res. 45:W02414, doi: 10.1029/2008WR007096.

Bradford, S.A., S.R. Yates, M. Bettahar, and J. Simunek. 2002. Physical factors affecting the transport and fate of colloids in saturated porous media. Water Resour. Res. 38:63/1–63/12.

Brown, G., A.C.D. Newman, J.H. Rayner, and A.H. Weir. 1978. The structure and chemistry of soil clay minerals, p. 29–178. *In* D.G. Greenland and M.H.B. Hayes (eds.) The chemistry of soil constituents. John Wiley & Sons, New York.

Brunauer, S., P.H. Emmett, and E. Teller. 1938. Adsorption of gases in multimolecular layers. J. Am. Chem. Soc. 60:309–319.

Buffle, J., and G.G. Leppard. 1995a. Characterization of aquatic colloids and macromolecules. 1. Structure and behavior of colloidal materials. Environ. Sci. Technol. 29:2169–2175.

Buffle, J., and G.G Leppard. 1995b. Characterization of aquatic colloids and macromolecules. 2. Key role of physical structures on analytical results. Environ. Sci. Technol. 29:2176–2184.

Bunn, R.A., R.D. Magelky, J.N. Ryan, and M. Elimelech. 2002. Mobilization of natural colloids from an iron oxide-coated sand aquifer: Effect of pH and ionic strength. Environ. Sci. Technol. 36:314–322.

Bunville, L.G. 1984. Commercial instrumentation for particle size analysis, p. 1–42. *In* H.G. Barth (ed.) Modern methods of particle size analysis. John Wiley & Sons, New York.

Carter, D.L., M.M. Mortland, and W.D. Kemper. 1986. Specific surface, p. 413–423. *In* A. Klute (ed.) Methods of soil analysis. Part 1—Physical and mineralogical methods, 2nd Ed. SSSA Publ., Madison, WI.

Chanudet, V., and M. Filella. 2006. A non-perturbing scheme for the mineralogical characterization and quantification of inorganic colloids in natural waters. Environ. Sci. Technol. 40:5045–5051.

Chen, J.Y., C. Ko, S. Bhattacharjee, and M. Elimelech. 2001. Role of spatial distribution of porous medium surface charge heterogeneity in colloid transport. Colloids Surf. A 191:3–15.

Chittleborough, D.J., S. Tadjiki, J.F. Ranville, F. Shanks, and R. Beckett. 2004. Soil colloid analysis by field-flow fractionation. Super Soil 2004, 3rd Australian N.Z. Soils Conf., December 5–9, 2004. University of Sydney, Sydney, Australia.

Chorom, M., and P. Rengasamy. 1995. Dispersion and zeta potential of pure clays as related to net particle charge under varying pH, electrolyte concentration and cation type. Eur. J. Soil Sci. 46:657–665.

Coll, H., and L.E. Oppenheimer. 1987. Improved techniques in disc centrifugation, p. 202–214. *In* T. Provder (ed.) Particle size distribution. Assessment and characterization. American Chemical Society, Washington, DC.

Contado, C., G. Blo, F. Fagioli, F. Dondi, and R. Beckett. 1997. Characterisation of river Po particles by sedimentation field-flow fractionation coupled to GFAAS and ICP-MS. Colloids Surf. A 120:47–59.

Corapcioglu, M.Y., and S.Y. Jiang. 1993. Colloid-facilitated groundwater contaminant transport. Water Resour. Res. 29:2215–2226.

Cotton, A., and H. Mouton. 1907. Magneto-optical properties of colloids and heterogeneous liquids. Ann. Chim. Phys. 11:145–203, 289–339.

Crist, J.T., J.F. McCarthy, Y. Zevi, P. Baveye, J.A. Throop, and T.S. Steenhuis. 2004. Pore-scale visualization of colloid transport and retention in partly saturated porous media. Vadose Zone J. 3:444–450.

Davis, J.A., and D.B. Kent. 1990. Surface complexation modeling in aqueous geochemistry. Rev. Mineral. Geochem. 23:177–260.

de Jong, E. 1999. Comparison of three methods of measuring surface area of soils. Can. J. Soil Sci. 79:345–351.

de Jonge, H., O.H. Jacobsen, L.W. de Jonge, and P. Moldrup. 1998. Particle-facilitated transport of prochloraz in undisturbed sandy loam soil columns. J. Environ. Qual. 27:1495–1503.

de Jonge, L.W., C. Kjaergaard, and P. Moldrup. 2004a. Colloids and colloid-facilitated transport of contaminants in soils: An introduction. Vadose Zone J. 3:321–325.

de Jonge, L.W., P. Moldrup, G.H. Rubaek, K. Schelde, and J. Djurhuus. 2004b. Particle leaching and particle-facilitated transport of phosphorus at field scale. Vadose Zone J. 3:462–470.

Delgado, A.V., S. Ahualli, F.J. Arroyo, and F. Carrique. 2005. Dynamic electrophoretic mobility of concentrated suspensions comparison between experimental data and theoretical predictions. Colloids Surf. A 267:95–102.

DeNovio, N.M., J.E. Saiers, and J.N. Ryan. 2004. Colloid movement in unsaturated porous media: Recent advances and future directions. Vadose Zone J. 3:338–351.

Dixon, J.B. 1977. Kaolinite and serpentine group minerals, p. 357–403. *In* J.B. Dixon and S.B. Weed (eds.) Minerals in soil environments. SSSA Inc., Madison, WI.

Dixon, J.B., and S.B. Weed. 1989. Minerals in soil environments. SSSA Inc., Madison, WI.

Diz, H.M.M., and B. Rand. 1989. The variable nature of the isoelectric point of the edge surface of kaolinite. Br. Ceram. Trans. 88:162–166.

Dong, A., G. Chesters, and G.V. Simsiman. 1983. Soil dispersibility. Soil Sci. 136:208–212.

Doucet, F.J., L. Maguire, and J.R. Lead. 2004. Size fractionation of aquatic colloids and particles by cross flow filtration: Analysis by scanning electron and atomic force microscopy. Anal. Chim. Acta 522:59–71.

Douglas, L.A. 1977. Vermiculites, p. 259–292. *In* J.B. Dixon and S.B. Weed (eds.) Minerals in soil environments. SSSA Inc., Madison, WI.

Ducker, W.A., and R.M. Pashley. 1992. Forces between mica surfaces in the presence of rod-shaped divalent counterions. Langmuir 8:109–112.

Ducker, W.A., T.J. Senden, and R.M. Pashley. 1991. Direct measurement of colloidal forces using an atomic force microscope. Nature 353:239–241.

Dukhin, A.S., and P.J. Goetz. 1996. Acoustic and electroacoustic spectroscopy. Langmuir 12:4336–4344.

Dukhin, A.S., and P.J. Goetz. 1998. Characterization of aggregation phenomena by means of acoustic and electroacoustic spectroscopy. Colloids Surf. A 144:49–58.

Dukhin, A.S., and P.J. Goetz. 2001. Acoustic and electroacoustic spectroscopy for characterizing concentrated dispersions and emulsions. Adv. Colloid Interface Sci. 92:71–132.

Dukhin, A.S., and P.J. Goetz. 2002. Ultrasound for characterizing colloids. Elsevier, Amsterdam, the Netherlands.

Dukhin, A.S., P.J. Goetz, and S. Truesdail. 2001. Titration of concentrated dispersions using electroacoustic potential probe. Langmuir 17:964–968.

Dunnivant, F.M., P.M. Jardine, D.L. Taylor, and J.F. McCarthy. 1992. Transport of naturally occurring dissolved organic carbon in laboratory columns containing aquifer material. Soil Sci. Soc. Am. J. 56:437–444.

Duchaufour, P. 1970. Precis de pedologie. Masson et Cie., Paris, France.

Duran, J.D.G., M.M. Ramos-Tejeda, F.J. Arroyo, and F. Gonzalez-Caballaro. 2000. Rheological and electrokinetic properties of sodium montmorillonite suspensions. I. Rheological properties and interparticle energy of interaction. J. Colloid Interface Sci. 219:107–117.

Dyal, R.S., and S.B. Hendricks. 1950. Total surface of clays in polar liquids as a characteristic index. Soil Sci. 69:421–432.

Edwards, D.G., A.M. Posner, and J.P. Quirk. 1965a. Repulsion of chloride ions by negatively charged clay surfaces. Part 1. Monovalent cation Fithian illites. Trans. Faraday Soc. 61:2808–2815.

Edwards, D.G., A.M. Posner, and J.P. Quirk. 1965b. Repulsion of chloride ions by negatively charged clay surfaces. Part 2. Monovalent montmorillonites. Trans. Faraday Soc. 61:2816–2819.

Elimelech, M., and C.R. O'Melia. 1990. Kinetics of deposition of colloidal particles in porous media. Environ. Sci. Technol. 24:1528–1536.

Elimelech, M., M. Nagai, C. Ko, and J.N. Ryan. 2000. Relative insignificance of mineral grain zeta potential to colloid transport in geochemically heterogeneous porous media. Environ. Sci. Technol. 34:2143–2148.

El-Swaify, S.A., S. Ahmed, L.D. Swindale. 1970. Effects of adsorbed cations on physical properties of tropical red and tropical black earths. II. Liquid limit, degree of dispersion, and moisture retention. J. Soil Sci. 21:188–198.

Emerson, W.W. 1967. A classification of soil aggregates based on their coherence in water. Aust. J. Soil Res. 15:255–262.

Fanning, D.S., and V.Z. Keramidas. 1977. Micas, p. 195–258. *In* J.B. Dixon and S.B. Weed (eds.) Minerals in soil environments. SSSA Inc., Madison, WI.

Farmer, V.C. 1978. Water on particle surfaces, p. 405–448. *In* D.J. Greenland and M.H.B. Hayes (eds.) The chemistry of soil constituents. John Wiley & Sons, New York.

Filella, M., and J. Buffle. 1993. Factors controlling the stability of submicron colloids in natural waters. Colloids Surf. A 73:255–273.

Filella, M., J. Zhang, M.E. Newman, and J. Buffle. 1997. Analytical applications of photon correlation spectroscopy for size distribution measurements of natural colloidal suspensions: Capabilities and limitations. Colloids Surf. A 120:27–46.

Finsy, R. 1994. Particle sizing by quasi-elastic light scattering. Adv. Colloid Interface Sci. 52:79–143.

Flegman, A.W., J.W. Goodwin, and R.H. Ottewill. 1969. Rheological studies on kaolinite suspensions. Proc. Br. Ceram. Soc. 13:31–45.

Flury, M., J.B. Mathison, and J.B. Harsh. 2002. In situ mobilization of colloids and transport of cesium in Hanford sediments. Environ. Sci. Technol. 36:5335–5341.

Franchi, A., and C.R. O'Melia. 2003. Effects of natural organic matter and solution chemistry on the deposition and reentrainment of colloids in porous media. Environ. Sci. Technol. 37:1122–1129.

Frenkel, H., G.J. Levy, and M.V. Fey. 1992. Clay dispersion and hydraulic conductivity of clay–sand mixtures as affected by the addition of various anions. Clays Clay Miner. 40:515–521.

Freundlich, H. 1932. Kapillarchemie II. Eine Darstellung der Chemie der Kolloide und verwandter Gebiete. 4. Akademische Verlagsgesellschaft, Leipzig, Germany.

Gamerdinger, A.P., and D.I. Kaplan. 2001. Colloid transport and deposition in water-saturated Yucca Mountain tuff as determined by ionic strength. Environ. Sci. Technol. 35:3326–3331.

Ghezzehei, T.A., and D. Or. 2001. Rheological properties of wet soils and clays under steady and oscillatory stresses. Soil Sci. Soc. Am. J. 65:624–637.

Giddings, J.C. 1993. Field-flow fractionation: Analysis of macromolecular, colloidal, and particulate materials. Science 260:1456–1465.

Goldberg, S., and H.S. Forster. 1990. Flocculation of reference clays and arid-zone soil clays. Soil Sci. Soc. Am. J. 54:714–718.

Goldberg, S., H.S. Forster, and C.L. Godfrey. 1996. Molybdenum adsorption on oxides, clay minerals, and soils. Soil Sci. Soc. Am. J. 60:425–432.

Goldstein, J.I., D.E. Newbury, P. Echlin, D.C. Joy, A.D. Romig, C.E. Lyman, C. Fiori, and E. Lifshin. 1992. Scanning electron microscopy and X-ray microanalysis, 2nd Ed. Plenum Press, New York.

Greathouse, J.A., S.E. Feller, and D.A. McQuarrie. 1994. The modified Gouy–Chapman theory: Comparisons between electrical double layer models of clay swelling. Langmuir 10:2125–2130.

Greenwood, R. 2003. Review of the measurement of zeta potentials in concentrated aqueous suspensions using electroacoustics. Adv. Colloid Interface Sci. 106:55–81.

Gregg, S.J., and K.S.W. Sing. 1982. Adsorption, surface area and porosity. Academic Press, New York.

Grolimund, D., and M. Borkovec. 2001. Release and transport of colloidal particles in natural porous media: 1. Modeling. Water Resour. Res. 37:559–570.

Grolimund, D., and M. Borkovec. 2005. Colloid-facilitated transport of strongly sorbing contaminants in natural porous media: Mathematical modeling and laboratory column experiments. Environ. Sci. Technol. 39:6378–6386.

Grolimund, D., and M. Borkovec. 2006. Release of colloidal particles in natural porous media by monovalent and divalent cations. J. Contam. Hydrol. 87:155–175.

Grolimund, D., M. Borkovec, K. Bartmettler, and H. Sticher. 1996. Colloid-facilitated transport of strongly sorbing contaminants in natural porous media: A laboratory column study. Environ. Sci. Technol. 30:3118–3123.

Groves, M.J. 1984. The application of particle characterization methods to submicron dispersion and emulsions, p. 43–91. *In* H.G. Barth (ed.) Modern methods of particle size analysis. John Wiley & Sons, New York.

Gschwend, P.M., D.A. Backhus, J.K. MacFarlane, and A.L. Page. 1990. Mobilization of colloids in groundwater due to infiltration of water at coal ash disposal site. J. Contam. Hydrol. 6:307–320.

Gschwend, P.M., and M.D. Reynolds. 1987. Monodisperse ferrous phosphate colloids in an anoxic groundwater plume. J. Contam. Hydrol. 1:309–327.

Gu, B., and H.E. Doner. 1993. Dispersion and aggregation of soils as influenced by organic and inorganic polymers. Soil Sci. Soc. Am. J. 57:709–716.

Guerin, M., and J.C. Seaman. 2004. Characterizing clay mineral suspensions using acoustic and electroacoustic spectroscopy. Clays Clay Miner. 52:145–157.

Guerin, M., J.C. Seaman, C. Lehmann, and A. Jurgenson. 2004. Acoustic and electroacoustic characterization of variable-charge mineral suspensions. Clays Clay Miner. 52:158–170.

Gunnarsson, M., M. Rasmusson, S. Wall, E. Ahlberg, and J. Ennis. 2001. Electroacoustic and potentiometric studies of the hematite/water interface. J. Colloid Interface Sci. 240:448–458.

Hahn, M.W., and C.R. O'Melia. 2004. Deposition and reentrainment of Brownian particles in porous media under unfavorable chemical conditions: Some concepts and applications. Environ. Sci. Technol. 38:210–220.

Handy, R.D., F. von der Kammer, J.R. Lead, M. Hassellov, R. Owen, and M. Crane. 2008. The ecotoxicology and chemistry of manufactured nanoparticles. Ecotoxicology 17:287–314.

Hang, P.T., and G.W. Brindley. 1970. Methylene blue adsorption by clay minerals: Determination of surface areas and cation exchange capacities. Clays Clay Miner. 18:203–212.

Hassellov, M., J.W. Readman, J.F. Ranville, and K. Tiede. 2008. Nanoparticle analysis and characterization methodologies in environmental risk assessment of engineered nanoparticles. Ecotoxicology 17:344–361.

Hassellov, M., F. von der Kammer, and R. Beckett. 2007. Characterisation of aquatic colloids and macromolecules by field-flow fractionation, p. 23–276. *In* K.J. Wilkinson

and J.R. Lead (eds.) Environmental colloids and particles: Behavior, structure and characterization. IUPAC series on analytical and physical chemistry of environmental systems. John Wiley & Sons, Chichester, U.K.

Heath, D., and Th.F. Tadros. 1983. Influence of pH, electrolyte and poly(vinyl alcohol) addition on the rheological characteristics of aqueous dispersions of sodium montmorillonite. J. Colloid Interface Sci. 93:307–319.

Heil, D., and G. Sposito. 1993. Organic matter role in illitic soil colloids flocculation: II. Surface charge. Soil Sci. Soc. Am. J. 57:1246–1253.

Heister, K., P.J. Kleingeld, T.J.S. Keijzer, and J.P.G. Loch. 2005. A new laboratory set-up for measurements of electrical, hydraulic, and osmotic fluxes in clays. Eng. Geol. 77:295–303.

Hesterberg, D.L. 1988. Critical coagulation concentrations and rheological properties of illite. Ph.D. Thesis. University of California, Riverside, CA.

Hesterberg, D., and A.L. Page. 1990a. Flocculation series test yielding time-invariant critical coagulation concentrations of sodium illite. Soil Sci. Soc. Am. J. 54:729–735.

Hesterberg, D., and A.L. Page. 1990b. Critical coagulation concentration of sodium and potassium illite as affected by pH. Soil Sci. Soc. Am. J. 54:735–739.

Hesterberg, D., and A.L. Page. 1993. Rheology of sodium and potassium illite suspensions in relation to colloidal stability. Soil Sci. Soc. Am. J. 57:697–704.

Hiemenz, P.C. 1977. Principles of colloid and surface chemistry. Marcel Dekker Inc., New York.

Hiemenz, P.C., and R. Rajagopalan. 1997. Principles of colloid and surface chemistry, 3rd Ed. Marcel Dekker, New York.

Hochella, M.F. 2008. Nanogeoscience: From origins to cutting-edge applications. Elements 4:373–379.

Holsworth, R.M., T. Provder, and J.J. Stansbrey. 1987. External-gradient-formation method for disc centrifuge photosedimentometric particle size distribution analysis, p. 191–201. *In* T. Provder (ed.) Particle size distribution. Assessment and characterization. American Chemical Society, Washington, DC.

Hsu, P.H. 1977. Aluminum hydroxides and oxyhydroxides, p. 99–143. *In* J.B. Dixon and S.B. Weed (eds.) Minerals in soil environments. SSSA Inc., Madison, WI.

Hsu, J.P. 1999. Interfacial forces and fields: Theory and applications. CRC Press, New York.

Huang, C.P. 1981. The surface acidity of hydrous solids, p. 183–217. *In* M.A. Anderson and A.J. Rubin (eds.) Adsorption of inorganics at solid–liquid interfaces. Ann Arbor Science, Ann Arbor, MI.

Hunter, R.J. 1981. Zeta potential in colloid science. Academic Press, London, U.K.

Hunter, R.J. 1987. Foundations of colloid science, Vol. 1. Oxford University Press, New York.

Hunter, R.J. 1989. Foundations of colloid science, Vol. 2. Oxford University Press, New York.

Hutton, J.T. 1977. Titanium and zirconium minerals, p. 673–688. *In* J.B. Dixon and S.B. Weed (eds.) Minerals in soil environments. SSSA Inc., Madison, WI.

Ise, N., and M.V. Smalley. 1994. Thermal compression of colloidal crystals: Paradox of repulsion-only assumption. Phys. Rev. B Condens. Matter. 50:16722–16725.

Israelachvili, J.N. 1992. Intermolecular and surface forces, 2nd Ed. Academic Press, San Diego, CA.

IUPAC. 2009. International Union of Pure and Applied Chemistry. http://www.iupac.org

Johnson, C.R., L.A. Hellerich, N.P. Nikolaidis, and P.M. Gschwend. 2001. Colloid mobilization in the field using citrate to remediate chromium. Ground Water 39:895–903.

Kaplan, D.I., P.M. Bertsch, and D.C. Adriano. 1995. Facilitated transport of contaminant metals through an acidified aquifer. Ground Water 33:708–717.

Kaplan, D.I., P.M. Bertsch, and D.C. Adriano. 1997. Mineralogical and physicochemical differences between mobile and nonmobile colloidal phases in reconstructed pedons. Soil Sci. Soc. Am. J. 61:641–649.

Kaplan, D.I., P.M. Bertsch, D.C. Adriano, and W.P. Miller. 1993. Soil-borne colloids as influenced by water flow and organic carbon. Environ. Sci. Technol. 27:1193–1200.

Kaplan, D.I., P.M. Bertsch, D.C. Adriano, and K.A. Orlandini. 1994a. Actinide association with groundwater colloids in a coastal plain aquifer. Radiochim. Acta 66/67:181–187.

Kaplan, D.I., D.B. Hunter, P.M. Bertsch, S. Bajt, and D.C. Adriano. 1994b. Application of synchrotron x-ray fluorescence spectroscopy and energy dispersive x-ray analysis to identify contaminant metals on groundwater colloids. Environ. Sci. Technol. 28:1186–1189.

Karathanasis, A.D. 1999. Subsurface migration of copper and zinc mediated by soil colloids. Soil Sci. Soc. Am. J. 63:830–838.

Karathanasis, A.D., D.M.C. Johnson, and C.J. Matocha. 2005. Biosolid colloid-mediated transport of copper, zinc, and lead in waste-amended soils. J. Environ. Qual. 34:1153–1164.

Kavanaugh, M.C., and J.O. Leckie. 1980. Particulates in water. Adv. Chem. Ser. No. 189. American Chemical Society, Washington, DC.

Kékicheff, P., S. Marcelja, T.J. Senden, and V.E. Shubin. 1993. Charge reversal seen in electrical double layer interaction of surfaces immersed in 2:1 calcium electrolyte. J. Chem. Phys. 99:6098–6113.

Keren, R. 1988. Rheology of aqueous suspension of sodium/calcium montmorillonite. Soil Sci. Soc. Am. J. 52:924–928.

Keren, R. 1989a. Effect of clay charge density and adsorbed ions on the rheology of montmorillonite suspension. Soil Sci. Soc. Am. J. 53:25–29.

Keren, R. 1989b. Rheology of mixed kaolinite–montmorillonite suspensions. Soil Sci. Soc. Am. J. 53:725–730.

Keren, R. 1991. Adsorbed sodium fraction's effect on rheology of montmorillonite–kaolinite suspensions. Soil Sci. Soc. Am. J. 55:376–379.

Kersting, A.B., D.W. Efurd, D.L. Finnegan, D.J. Rokop, D.K. Smith, and J.L. Thompson. 1999. Migration of plutonium in groundwater at the Nevada Test Site. Nature 397:56–59.

Khaleel, R., T.C.J. Yeh, and Z. Lu. 2002. Upscaled flow and transport properties for heterogeneous unsaturated media. Water Resour. Res. 38:11/1–11/12.

Khilar, K.C., and H.S. Fogler. 1984. The existence of a critical salt concentration for particle release. J. Colloid Interface Sci. 101:214–224.

Kia, S.F., H.S. Fogler, and M.G. Reed. 1987. Effect of pH on colloidally induced fines migration. J. Colloid Interface Sci. 118:158–168.

Kim, S.-O., S.-H. Moon, and K.-W. Kim. 2001. Removal of heavy metals from soils using enhanced electrokinetic soil processing. Water Air Soil Pollut. 125:259–272.

Kjellander, R., S. Marcelja, R.M. Pashley, and J.P. Quirk. 1990. A theoretical and experimental study of forces between charged mica surfaces in aqueous $CaCl_2$ solutions. J. Chem. Phys. 92:4399–4407.

Koehler, M.E., R.A. Zandler, T. Gill, T. Provder, and T.F. Niemann. 1987. An improved disc centrifuge photosedimentometer and data system for particle size distribution analysis, p. 180–190. *In* T. Provder (ed.) Particle size distribution. Assessment and characterization. American Chemical Society, Washington, DC.

Kosmulski, M. 2002. Confirmation of the differentiating effect of small cations in the shift of the isoelectric point of oxides at high ionic strengths. Langmuir 18:785–787.

Kosmulski, M., E. Maczka, E. Jartych, and J.B. Rosenholm. 2003. Synthesis and characterization of goethite and goethite–hematite composite: Experimental study and literature survey. Adv. Colloid Interface Sci. 103:57–76.

Kosmulski, M., E. Maczka, and J.B. Rosenholm. 2002. Isoelectric points of metal oxides at high ionic strengths. J. Phys. Chem. B 106:2918–2921.

Kretzschmar, R., M. Borkovec, D. Grolimund, and M. Elimelech. 1999. Mobile subsurface colloids and their role in contaminant transport. Adv. Agron. 66:121–193.

Kretzschmar, R., D. Hesterberg, and H. Sticher. 1997. Effects of adsorbed humic acid on surface charge and flocculation of kaolinite. Soil Sci. Soc. Am. J. 61:101–108.

Kretzschmar, R., W.P. Robarge, and S.B. Weed. 1993. Flocculation of kaolinitic soil clays: Effects of humic substances and iron oxides. Soil Sci. Soc. Am. J. 57:1277–1283.

Langmuir, I. 1918. The adsorption of gases on plane surfaces of glass, mica, and platinum. J. Am. Chem. Soc. 40:1361–1402.

Laskin, A., and J.P. Cowin. 2001. Automated single-particle SEM/EDX analysis of submicrometer particles down to 0.1 μm. Anal. Chem. 73:1023–1029.

Laxton, P.B., and J.C. Berg. 2006. Relating clay yield stress to colloidal parameters. J. Colloid Interface Sci. 296:749–755.

Lead, J.R., D. Muirhead, and C.T. Gibson. 2005. Characterization of freshwater natural aquatic colloids by atomic force microscopy (AFM). Environ. Sci. Technol. 39:6930–6936.

Lead, J.R., and K.J. Wilkinson. 2007. Environmental colloids and particles: Current knowledge and future developments, p. 1–15. *In* K.J. Wilkinson and J.R. Lead (eds.) Environmental colloids and particles: Behavior, structure and characterization. IUPAC series on analytical and physical chemistry of environmental systems. John Wiley & Sons, Chichester, U.K.

Lead, J.R., K.J. Wilkinson, E. Balnois, B. Cutak, C. Larive, S. Assemi, and R. Beckett. 2000. Diffusion coefficients and polydispersities of the Suwannee River fulvic acid: Comparison of fluorescence correlation spectroscopy, pulsed-field gradient nuclear magnetic resonance and flow field-flow fractionation. Environ. Sci. Technol. 34:3508–3513.

Lebron, I., M.G. Schaap, and D.L. Suarez. 1999. Saturated hydraulic conductivity prediction from microscopic pore geometry measurements and neural network analysis. Water Resour. Res. 35:3149–3157.

Lebron, I., and D.L. Suarez. 1992a. Electrophoretic mobility of illite and micaceous soil clays. Soil Sci. Soc. Am. J. 56:1106–1115.

Lebron, I., and D.L. Suarez. 1992b. Variations in soil stability within and among soil types. Soil Sci. Soc. Am. J. 56:1412–1421.

Lebron, I., D.L. Suarez, C. Amrhein, and J.E. Strong. 1993. Size of mica domains and distribution of the adsorbed Na–Ca ions. Clays Clay Miner. 41:380–388.

Ledin, A., S. Karlsson, A. Duker, and B. Allard. 1993. Applicability of photon correlation spectroscopy for measurement of concentration and size distribution of colloids in natural waters. Anal. Chim. Acta 281:421–428.

Ledin, A., S. Karlsson, A. Duker, and B. Allard. 1994. Measurements in-situ of concentration and size distribution of colloidal matter in deep groundwaters by photon-correlation spectroscopy. Water Res. 28:1539–1545.

Li, X., T.D. Scheibe, and W.P. Johnson. 2004. Apparent decreases in colloid deposition rate coefficients with distance of transport under unfavorable deposition conditions: A general phenomenon. Environ. Sci. Technol. 38:5616–5625.

Lowell, S. 1979. Introduction to powder surface area. John Wiley & Sons, New York.

Ma, K., and A.C. Pierre. 1999. Clay sediment-structure formation in aqueous kaolinite suspensions. Clays Clay Miner. 47:522–526.

Maes, A., and A. Cremers. 1977. Charge density effects in ion exchange. Part 1. Heterovalent exchange equilibria. J. Chem. Soc. Faraday Trans. 1. 73:1807–1814.

Markgraf, W., R. Horn, and S. Peth. 2006. An approach to rheometry in soil mechanics—Structural changes in bentonite, clayey and silty soils. Soil Till. Res. 91:1–14.

Mashal, K., J.B. Harsh, M. Flury, A.R. Felmy, and H. Zhao. 2004. Colloid formation in Hanford sediments reacted with simulated tank waste. Environ. Sci. Technol. 38: 5750–5756.

Mavrocordatos, D., D. Perret, and G.D. Leppard. 2007. Strategies and advances in the characterization of environmental colloids by electron microscopy, p. 345–404. *In* K.J. Wilkinson

and J.R. Lead (eds.) Environmental colloids and particles: Behavior, structure and characterization. IUPAC series on analytical and physical chemistry of environmental systems. John Wiley & Sons, Chichester, U.K.

McBride, M.B. 1989. Surface chemistry of soil minerals, p. 35–88. *In* J.B. Dixon and S.B. Weed (eds.) Minerals in soil environments, 2nd Ed. Soil Sci. Soc. Am. Book Ser. 1. SSSA, Madison, WI.

McBride, M.B. 1994. Environmental chemistry of soils. Oxford University Press, New York.

McBride, M.B., and P. Baveye. 2002. Diffuse double-layer models, long-range forces, and ordering in clay colloids. Soil Sci. Soc. Am. J. 66:1207–1217.

McCarthy, J.F., and C. Degueldre. 1993. Sampling and characterization of colloids and particles in groundwater for studying their role in contaminant transport, p. 247–315. *In* J. Buffle and H.P. van Leeuwen (eds.) Environmental particles, Vol. 2. Lewis Publishers, Ann Arbor, MI.

McCarthy, J.F., and L.D. McKay. 2004. Colloid transport in the subsurface: Past, present, and future challenges. Vadose Zone J. 3:326–337.

McCarthy, J.F., L.D. McKay, and D.D. Bruner. 2002. Influence of ionic strength and cation charge on transport of colloidal particles in fractured shale saprolite. Environ. Sci. Technol. 36:3735–3743.

McCarthy, J.E., and J.M. Zachara. 1989. Subsurface transport of contaminants. Environ. Sci. Technol. 23:496–502.

McDowell-Boyer, L.M. 1992. Chemical mobilization of micron-sized particles in saturated porous media under steady flow conditions. Environ. Sci. Technol. 26:586–593.

McDowell-Boyer, L.M., J.R. Hunt, and N. Sitar. 1986. Particle transport through porous media. Water Resour. Res. 22:1901–1921.

McKenzie, R.M. 1989. Manganese oxides and hydroxides, p. 439–465. *In* J.B. Dixon and S.B. Weed (eds.) Minerals in soil environments, 2nd Ed. SSSA Inc., Madison, WI.

Miano, F., and M.R. Rabaioli. 1994. Rheological scaling of montmorillonite suspensions: The effect of electrolytes and polyelectrolytes. Colloids Surf. A 84:229–237.

Miller, W.P., and M.K. Baharuddin. 1986. Relationship of soil dispersibility to infiltration and erosion of southeastern soils. Soil Sci. Soc. Am. J. 54:346–351.

Miller, W.P., H. Frenkel, and K.D. Newman. 1990. Flocculation concentration and sodium/calcium exchange of kaolinitic soil clays. Soil Sci. Soc. Am. J. 54:346–351.

Miller, W.P., and D.E. Radcliffe. 1992. Soil crusting in the southeastern United States, p. 233–266. *In* M.E. Sumner and B.A. Stewart (eds.) Soil crusting: Chemical and physical processes. Lewis Publishers, Boca Raton, FL.

Mills, W.B., S. Liu, and F.K. Fong. 1991. Literature review and model (comet) for colloid/metals transport in porous media. Ground Water 29:199–208.

Murphy, D.M., J.R. Garbarino, H.W. Taylor, B.T. Hart, R. Beckett. 1993. Determination of size and element composition distributions of complex colloids by sedimentation field-flow fractionation-inductively coupled plasma mass spectrometry. J. Chromatogr. 642:459–467.

Napper, D.H., and R.J. Hunter. 1974. Hydrosols, p. 161–213. *In* M. Kerker (ed.) M.T.P. Int. Rev. Sci. Phys. Chem. Ser. Butterworths, London, U.K.

Nelson, P.N., and J.M. Oades. 1998. Organic matter, sodicity and soil structure. p. 51–75. *In* M.E. Sumner and R. Naidu (eds.) Sodic soils: Distribution, properties, management and environmental consequences. Oxford University Press, New York.

Newman, A.C.D. 1983. The specific surface of soils determined by water sorption. Soil Sci. 34:23–32.

Newman, M.E., M. Filella, Y.W. Chen, J.C. Negre, D. Perret, and J. Buffle. 1994. Submicron particles in the Rhine river. 2. Comparison of field observations and model predictions. Water Res. 28:107–118.

Nishimura, S., M. Kodama, K. Yao, Y. Imai, and H. Tateyama. 2002b. Direct surface force measurement for synthetic smectites using the atomic force microscope. Langmuir 18:4681–4688.

Nishimura, S., H. Tateyama, K. Tsunematsu, and K. Jinnai. 1992. Zeta potential measurement of muscovite mica basal plane-aqueous solution interface by means of plane interface technique. J. Colloid Interface Sci. 152:359–367.

Nishimura, S., K. Yao, M. Kodama, Y. Imai, K. Ogino, and K. Mishima. 2002a. Electrokinetic study of synthetic smectites by flat plate streaming potential technique. Langmuir 18:188–193.

Norrish, K., and J.A. Rausell-Colom. 1961. Low-angle X-ray diffraction studies of the swelling of montmorillonite and vermiculite. Clays Clay Miner. 10:123–149.

Ohtsubo, M., A. Yoshimura, S.-I. Wada, and R.N. Yong. 1991. Particle interaction and rheology of illite-iron oxide complexes. Clays Clay Miner. 39:347–354.

O'Melia, C.R, and C.L. Tiller. 1993. Physicochemical aggregation and deposition in aquatic environments, p. 353–385. *In* J. Buffle and H. van Leeuwen (eds.) Environmental particles, Vol. 2. Lewis Publishers, Boca Raton, FL.

Overbeek, J.Th.G. 1952. Stability of hydrophobic colloids and emulsions. p. 302–341. *In* H.R. Kryt (ed.) J. Colloid Sci. Vol. 1, Elsevier, Amsterdam.

Parker, J.C., L.W. Zelazny, S. Sampath, and W.G. Harris. 1979. A critical evaluation of the extension of zero point of charge (ZPC) theory to soil systems. Soil Sci. Soc. Am. J. 43:668–674.

Pashley, R.M. 1981. DLVO and hydration forces between mica surfaces in Li^+, Na^+, K^+, and Cs^+ electrolyte solutions: A correlation of double-layer and hydration forces with surface cation. J. Colloid Interface Sci. 83:531–546.

Pashley, R.M., and J.P. Quirk. 1984. The effect of cation valency on DLVO and hydration forces between macroscopic sheets of muscovite mica in relation to clay swelling. Colloids Surf. 9:1–17.

Pecora, R. 1983. Quasi-elastic light scattering of macromolecules and particles in solution and suspension, p. 3–30. *In* B.E. Dahneke (ed.) Measurement of suspended particles by quasi-elastic light scattering. John Wiley & Sons, New York.

Perret, D., M.E. Newman, J.C. Negre, Y.W. Chen, and J. Buffle. 1994. Submicron particles in the Rhine river. 1. Physicochemical characterization. Water Res. 28:91–106.

Pennell, K.D., S.A. Boyd, and L.M. Abriola. 1995. Surface area of soil organic matter reexamined. Soil Sci. Soc. Am. J. 59:1012–1018.

Quirk, J.P. 1994. Interparticle forces: A basis for the interpretation of soil physical behavior. Adv. Agron. 53:121–183.

Quirk, J.P., and L.A.G. Aylmore. 1971. Domain and quasi-crystalline regions in clay systems. Proc. Soil Sci. Soc. Am. 35:652–654.

Quirk, J.P., and R.S. Murray. 1991. Towards a model for soil structural behavior. Aust. J. Soil Res. 29:829–867.

Quirk, J.P., and R.K. Schofield. 1955. The effect of electrolyte concentration on soil permeability. J. Soil Sci. 6:163–178.

Rand, B., and I.E. Melton. 1977. Particle interactions in aqueous kaolinite suspensions. I. Effect of pH and electrolyte upon the mode of particle interaction in homoionic sodium kaolinite suspensions. J. Colloid Interface Sci. 60:308–320.

Rand, B., E. Pekenc, J.W. Goodwin, and R.W. Smith. 1980. Investigation into the existence of edge–face coagulated structures in Na-montmorillonite suspensions. J. Chem. Soc. Faraday Trans. 1 76:225–235.

Ranville, J.F., D.J. Chittleborough, and R. Beckett. 2005. Particle-size and element distributions of soil colloids: Implications for colloid transport. Soil Sci. Soc. Am. J. 69:1173–1184.

Ranville, J.F., D.J. Chittleborough, F. Sanks, R.J.S. Morrison, T. Harris, F. Doss, et al. 1999. Development of sedimentation field-flow fractionation-inductively coupled plasma mass-spectroscopy for the characterization of environmental colloids. Anal. Chim. Acta 381:315–329.

Redman, J.A., S.L. Walker, and M. Elimelech. 2004. Bacterial adhesion and transport in porous media: Role of the secondary energy minimum. Environ. Sci. Technol. 38:1777–1785.

Rees, L.B. 1990. A Monte-Carlo approach to x-ray attenuation corrections for proton-induced x-ray-emission from particulate samples. Nucl. Instrum. Meth. Phys. Res. Sect. A 299:614–617.

Rockhold, M.L., R.R. Yarwood, and J.S. Selker. 2004. Coupled microbial and transport processes in soil. Vadose Zone J. 3:368–383.

Ronen, D., M. Magaritz, U. Weber, A.J. Amiel, and E. Klein. 1992. Characterization of suspended particles collected in groundwater under natural gradient flow conditions. Water Resour. Res. 28:1279–1291.

Ross, G. 1978. Relationships of specific surface area and clay content to shrink–swell potential of soils having different clay mineralogical compositions. Can. J. Soil Sci. 58:159–166.

Roy, S.B., and D.A. Dzombak. 1996. Colloid release and transport processes in natural and model porous media. Colloids Surf. A 107:245–262.

Roy, S.B., and D.A. Dzombak. 1997. Chemical factors influencing colloid-facilitated transport of contaminants in porous media. Environ. Sci. Technol. 37:656–664.

Roy, S.B., and D.A. Dzombak. 1998. Sorption nonequilibrium effects on colloid-enhanced transport of hydrophobic compounds in porous media. J. Contam. Hydrol. 30:179–200.

Ryan, J.N., and M. Elimelech. 1996. Colloid mobilization and transport in groundwater. Colloids Surf. A 107:1–56.

Ryan, J.N., and P.M. Gschwend. 1990. Colloid mobilization in two Atlantic Coastal Plain aquifers: Field studies. Water Resour. Res. 26:307–322.

Ryan, J.N., and P.M. Gschwend. 1994. Effect of solution chemistry on clay colloid release from an iron oxide-coated aquifer sand. Environ. Sci. Technol. 28:1717–1726.

Ryan, J.N., T.H. Illangasekare, M.I. Litaor, and R. Shannon. 1998. Particle and plutonium mobilization in macroporous soils during rainfall simulations. Environ. Sci. Technol. 32:476–482.

Scales, P.J., F. Grieser, and T.W. Healy. 1990. Electrokinetics of the muscovite mica–aqueous solution interface. Langmuir 6:582–589.

Schofield, R.K. 1949. Calculation of surface areas of clays from measurements of negative adsorption. Trans. Br. Ceram. Soc. 48:207–213.

Schofield, R.K., and H.R. Samson. 1954. Flocculation of kaolinite due to the attraction of oppositely charged crystal faces. Discuss. Faraday Soc. 18:135–145.

Schramm, L.L., and J.C.T. Kwak. 1982a. Influence of exchangeable cation composition on the size and shape of montmorillonite particles in dilute suspensions. Clays Clay Miner. 30:40–48.

Schramm, L.L., and J.C.T. Kwak. 1982b. Interactions in clay suspensions: The distribution of ions in suspension and the influence of tactoid formation. Colloids Surf. 3:43–60.

Schulthess, C.P., and D.L. Sparks. 1986. Backtitration technique for proton isotherm modeling of oxide surfaces. Soil Sci. Soc. Am. J. 50:1406–1411.

Schultz, D.S. 1997. Electroosmosis technology for soil remediation: Laboratory results, field trial, and economic modeling. J. Hazard. Mater. 55:81–91.

Schulze, D.G. 2002. An introduction to soil mineralogy, p. 1–35. *In* J.B. Dixon and D.G. Schulze (eds.) Soil mineralogy with environmental applications. SSSA, Madison, WI.

Schurtenberger, P., and M.E. Newman. 1993. Characterization of biological and environmental particles using static and dynamic light scattering, p. 37–115. *In* J. Buffle and H.P. van Leeuwen (eds.) Environmental particles, Vol. 2. Lewis Publishers, Ann Arbor, MI.

Schwertmann, U., and R.M. Taylor. 1977. Iron oxides, p. 145–180. *In* J.B. Dixon and S.B. Weed (eds.) Minerals in soil environments. SSSA Inc., Madison, WI.

Seaman, J.C. 2000. Thin-foil SEM analysis of soil and groundwater colloids: Reducing instrument and operator bias. Environ. Sci. Technol. 34:187–191.

Seaman, J.C., and P.M. Bertsch. 2000. Selective colloid mobilization through surface-charge manipulation. Environ. Sci. Technol. 34:3749–3755.

Seaman, J.C., P.M. Bertsch, and W.P. Miller. 1995. Chemical controls on colloid generation and transport in a sandy aquifer. Environ. Sci. Technol. 29:1808–1815.

Seaman, J.C., P.M. Bertsch, and R.N. Strom. 1997. Characterization of colloids mobilized from southeastern coastal plain sediments. Environ. Sci. Technol. 31:2782–2790.

Seaman, J.C., M. Guerin, B.P. Jackson, P.M. Bertsch, and J.F. Ranville. 2003. Analytical techniques for characterizing complex mineral assemblages: Mobile soil and groundwater colloids, p. 271–309. *In* H.M. Selim and W.L. Kingery (eds.) Geochemical and hydrological reactivity of heavy metals in soils. CRC Press, Washington, DC.

Secor, R.B., and C.J. Radke. 1985. Spillover of the diffuse double layer on montmorillonite particles. J. Colloid Interface Sci. 103:237–244.

Seta, A.K., and A.D. Karathanasis. 1996. Colloid-facilitated transport of metolachlor through intact soil columns. J. Environ. Sci. Health B 31:949–968.

Seta, A.K., and A.D. Karathanasis. 1997. Atrazine adsorption by soil colloids and co-transport through subsurface environments. Soil Sci. Soc. Am. J. 61:612–617.

Shainberg, I., and H. Otoh. 1968. Size and shape of montmorillonite particles saturated with Na/Ca ions (inferred from viscosity and optical measurements). Isr. J. Chem. 6:251–259.

Shainberg, I., J.D. Rhoades, and R.J. Prather. 1981. Effect of low electrolyte concentration on clay dispersion and hydraulic conductivity of a sodic soil. Soil Sci. Soc. Am. J. 45:273–277.

Shapiro, A.P., and R.F. Probstein. 1993. Removal of contaminants from saturated clay by electroosmosis. Environ. Sci. Technol. 27:283–291.

Sharma, M.M., H. Chamoun, D.H.S.S.R. Sarma, and R.S. Schecter. 1992. Factors controlling the hydrodynamic attachment of particles from surfaces. J. Colloid Interface Sci. 149:121–134.

Sherard, J.L., L.P. Dunningan, and R.S. Decker. 1977. Identification and nature of dispersive soils. J. Geotech. Eng. Am. Soc. Chem. Eng. 4:287–301.

Simunek, J., C. He, L. Pang, and S.A. Bradford. 2006. Colloid-facilitated solute transport in variably saturated porous media: Numerical model and experimental verification. Vadose Zone J. 5:1035–1047.

Sinton, L.W., M.J. Noonan, R.K. Finlay, L. Pang, and M.E. Close. 2000. Transport and attenuation of bacteria and bacteriophages in an alluvial gravel aquifer. N.Z. J. Mar. Freshwater Res. 34:175–186.

Sirivithayapakorn, S., and A. Keller. 2003. Transport of colloids in unsaturated porous media: A pore-scale observation of processes during the dissolution of air–water interface. Water Resour. Res. 39:SBH 6/1–6/10.

Smalley, M.V. 1990. Electrostatic interaction in macro-ionic solutions and gels. Mol. Phys. 71:1251–1267.

Sogami, I., and N. Ise. 1984. On the electrostatic interaction in macroionic solutions. J. Chem. Phys. 81:6320–6332.

Sposito, G. 1984. The surface chemistry of soils. Oxford University Press, New York.

Stevenson, F.J. 1982. Humus chemistry. Genesis, composition, reactions. John Wiley & Sons, New York.

Suarez, D.L., J.D. Rhoades, R. Lavado, and C.M. Grieve. 1984. Effect of pH on saturated hydraulic conductivity and soil dispersion. Soil Sci. Soc. Am. J. 48:50–55.

Sun, Y.-P., X.-Q. Li, J. Cao, W.-X. Zhang, and H.P. Wang. 2006. Characterization of zero-valent iron nanoparticles. Adv. Colloid Interface Sci. 120:47–56.

Supak, J.R., A.R. Swoboda, and J.B. Dixon. 1978. Adsorption of aldicarb by clays and soil organo-clay complexes. Soil Sci. Soc. Am. J. 42:244–248.

Swartz, C.H., and P.M. Gschwend. 1998. Mechanisms controlling release of colloids to groundwater in a southeastern coastal plain aquifer sand. Environ. Sci. Technol. 32:1779–1785.

Taboada-Serrano, P., V. Vithayaveroj, S. Yiacoumi, and C. Tsouris. 2005. Surface charge heterogeneities measured by atomic force microscopy. Environ. Sci. Technol. 39:6352–6360.

Tarchitzky, J., Y. Chen, and A. Banin. 1993. Humic substances and pH effects on sodium and calcium-montmorillonite flocculation and dispersion. Soil Sci. Soc. Am. J. 57:367–372.

Theng, B.K., and G. Yuan. 2008. Nanoparticles in the soil environment. Elements 4:395–399.

Tiller, K.G., and L.H. Smith. 1990. Limitations of EGME retention to estimate the surface area of soils. Aust. J. Soil Res. 28:1–26.

Tombácz, E., J. Balázs, J. Lakatos, and F. Szántó. 1989. Influence of the exchangeable cations on stability and rheological properties of montmorillonite suspensions. Colloid Polym. Sci. 267:1016–1025.

Torkzaban, S., S.S. Tazehkand, S.L. Walker, and S.A. Bradford. 2008. Transport and fate of bacteria in porous media: Coupled effects of chemical conditions and pore space geometry. Water Resour. Res. 44:W04403, doi: 10.1029/2007WR006541.

Tufenkji, N. 2007. Modeling microbial transport in porous media: Traditional approaches and recent developments. Adv. Water Resour. 30:1455–1469.

Tufenkji, N., and M. Elimelech. 2004a. Correlation equation for predicting single-collector efficiency in physicochemical filtration in saturated porous media. Environ. Sci. Technol. 38:529–536.

Tufenkji, N., and M. Elimelech. 2004b. Deviation from the classical colloid filtration theory in the presence of repulsive DLVO interactions. Langmuir 20:10818–10828.

Tufenkji, N., and M. Elimelech. 2005. Breakdown of colloid filtration theory: Role of the secondary energy minimum and surface charge heterogeneities. Langmuir 21:841–852.

Tufenkji, N., J.A. Redman, and M. Elimelech. 2003. Interpreting deposition patterns of microbial particles in laboratory-scale column experiments. Environ. Sci. Technol. 37:616–623.

van de Weerd, H., and A. Leijnse. 1997. Assessment of the effect of kinetics on colloid facilitated radionuclide transport in porous media. J. Contam. Hydrol. 26:245–256.

van Olphen, H. 1977. An introduction to clay colloid chemistry, 2nd Ed. John Wiley & Sons, New York.

Verwey, E.J.W., and J.Th.G. Overbeek. 1948. Theory of stability of lyophobic colloids. Elsevier, Amsterdam, the Netherlands.

Vinten, A.J.A., B. Yaron, and P.H. Nye. 1983. Vertical transport of pesticides when adsorbed on suspended particles. J. Agric. Food Chem. 31:662–664.

Von Gunten, H.R., U.E. Warber, and U. Krahenbuhl. 1988. The reactor accident at Chernobyl: A possibility to test colloid-controlled transport of radionuclides in a shallow aquifer. J. Contam. Hydrol. 2:237–247.

von Smoluchowski, M. 1916. Three discourses on diffusion, Brownian movements, and the coagulation of colloid particles. Phys. Z. 17:557–571, 585–599.

von Smoluchowski, M. 1917. Mathematical theory of the kinetics of the coagulation of colloidal suspensions. Z. Phys. Chem. 92:129–168.

Walker, S.L., J.A. Redman, and M. Elimelech. 2004. Role of cell surface lipopolysaccharides in *Escherichia coli* K12 adhesion and transport. Langmuir 20:7736–7746.

Wan, J., and J.L. Wilson. 1994. Visualization of the role of the gas–water interface on the fate and transport of colloids in porous media. Water Resour. Res. 30:11–23.

Waychunas, G.A., and H. Zhang. 2008. Structure, chemistry, and properties of mineral nanoparticles. Elements 4:381–387.

Wilding, L.P., N.E. Smeck, and L.R. Drees. 1977. Silica in soils: Quartz, cristobalite, tridymite, and opal, p. 471–552. *In* J.B. Dixon and S.B. Weed (eds.) Minerals in soil environments. SSSA Inc., Madison, WI.

Wilkinson, K.J., and J.R. Lead. 2007. Environmental colloids and particles: Behavior, structure and characterization. IUPAC series on analytical and physical chemistry of environmental systems. John Wiley & Sons, Chichester, U.K.

Yao, K.M., T. Habibian, and C.R. O'Melia. 1971. Water and waste water filtration, concepts and applications. Environ. Sci. Technol. 5:1105–1112.

Yong, R.N., A.J. Sadh, H.P. Ludwig, and M.A. Jorgensen. 1979. Interparticle action and rheology of dispersive clays. J. Geotech. Eng. Div. 105:1193–1209.

Zhao, H., S. Bhattacharjee, R. Chow, D. Wallace, J.H. Masliyah, and Z. Xu. 2008. Probing surface charge potentials of clay basal planes and edges by direct force measurements. Langmuir 24:12899–12910.

Zhao, H., P.F. Low, and J.M. Bradford. 1991. Effects of pH and electrolyte concentration on particle interaction in three homoionic sodium soil clay suspensions. Soil Sci. 151:196–207.

HANDBOOK OF SOIL SCIENCES

PROPERTIES AND PROCESSES

SECOND EDITION

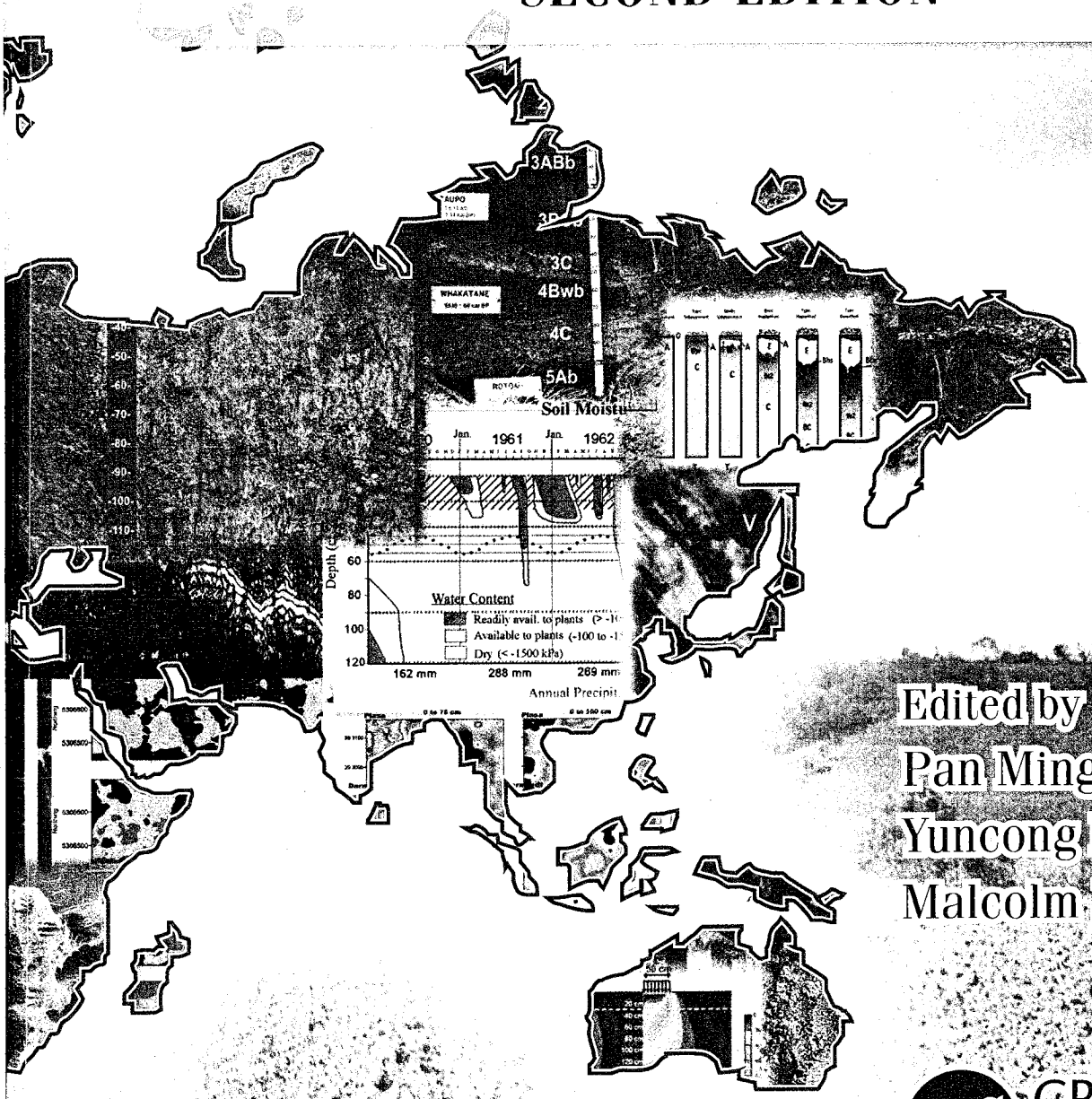

Edited by
Pan Ming Huang
Yuncong Li
Malcolm E. Sumner

CRC Press
Taylor & Francis Group
an informa business